2013

Hydrogeophysical Investigation of Contaminant Distribution at a Closed Landfill in Southwestern Ontario, Canada

Siddharth Dilip Joshi
University of Windsor

Hydrogeophysical Investigation of Contaminant Distribution at a Closed Landfill in Southwestern Ontario, Canada

By

Siddharth Dilip Joshi

A Thesis

Submitted to the Faculty of Graduate Studies

through the Department of Earth and Environmental Sciences

in Partial Fulfillment of the Requirements for

the Degree of Master of Science

at the University of Windsor

Windsor, Ontario, Canada

2013

Hydrogeophysical Investigation of Contaminant Distribution at a Closed Landfill in Southwestern Ontario, Canada

By

Siddharth Dilip Joshi

APPROVED BY:

C. Chen, External Committee Member

Electrical and Computer Engineering

M. Cioppa, Internal Committee Member

Earth and Environmental Sciences

J. Yang, Advisor

Earth and Environmental Sciences

June 19, 2013

DECLARATION OF ORIGINALITY

I hereby certify that I am the sole author of this thesis and that no part of this thesis has been published or submitted for publication.

I certify that, to the best of my knowledge, my thesis does not infringe upon anyone's copyright nor violate any proprietary rights and that any ideas, techniques, quotations, or any other material from the work of other people included in my thesis, published or otherwise, are fully acknowledged in accordance with the standard referencing practices. Furthermore, to the extent that I have included copyrighted material that surpasses the bounds of fair dealing within the meaning of the Canada Copyright Act, I certify that I have obtained a written permission from the copyright owner(s) to include such material(s) in my thesis and have included copies of such copyright clearances to my appendix.

I declare that this is a true copy of my thesis, including any final revisions, as approved by my thesis committee and the Graduate Studies office, and that this thesis has not been submitted for a higher degree to any other University or Institution.

ABSTRACT

The study looked at the application of geophysical and groundwater modeling methods to investigate the underground leachate distribution at a closed municipal landfill.

Firstly, the apparent conductivity of the landfill was mapped using two coil separations. The resulting maps displayed a high conductive zone in the western portion of the site with measurements averaging between 35mS/m to 3000mS/m. The resistivity of the same high conductive zone was measured with resistivity profiles showing the waste material occupying the upper sand aquifer as a low resistivity anomaly ranging between 1.2 – 6 Ω*m.

Results from the geophysical surveys were used to prepare two conceptual models (S-N and W-E) of the landfill. The groundwater modeling results show the contaminants occupying mainly the upper sand aquifer and most of the silt/sand aquitard after 1000 years. In most cases the lower sand aquifer remained free from contamination.

ACKNOWLEDGEMENTS

This project could not have been completed without the assistance and expert advice from a number of individuals.

Firstly, I would like to thank my supervisor Dr. Jianwen Yang for his constant support, expert advice and for providing me with the funding to successfully complete my studies. I would like to take this opportunity to thank my external committee member Dr. Chunhong Chen (Department of Electrical and Computer Engineering) and my internal committee member Dr. Maria Cioppa (Department of Earth and Environmental Sciences) for their feedback and suggestions on my study. I would also like to specially thank Mr. Beiraghdar for his advice and unconditional support during my field work. I would also like to acknowledge the assistance of Mr. Prakasan, Mr. Hoyle, Mr. Brzozowski and Mrs. Hart during my field work. I would like to take this opportunity to thank Mr. Sereres, Mr. Tamr and Mr. Cibulka (Genivar Inc.) for giving me permission to work on the site, assisting me with field work, providing me with important information about the landfill and for their comments and suggestions which helped in the overall improvement of my thesis. I would also like to thank Mrs. Horne for her advice in helping me complete all the necessary requirements for the master's program. Finally, I would like to thank my family who constantly supported me throughout my education and inspired me to be a better person.

This project was funded by the NSERC-Engage grant given to Dr. Jianwen Yang with Genivar Inc. as the industrial partner.

TABLE OF CONTENTS

LIST OF TABLES

LIST OF FIGURES

LIST OF ABBREVIATIONS

σ_a = Apparent conductivity (mS/m)

ω = Angular frequency (Hz)

μ_0 = Permeability of free space

s = Intercoil spacing (m)

H_p = Primary field

H_s = Secondary field

ρ_a = Apparent resistivity (Ω*m)

ΔV = Change in voltage (Volts)

I = Current (Ampere)

G = Geometric factor dependent on electrode arrangement

q = Specific Discharge (m/s)

K = Hydraulic conductivity (m/s)

h = Hydraulic head (m)

L = Length of area over which the hydraulic head changes

Q = Discharge (m^3/s)

ρ = Density of water (kg/m^3)

S_s = Specific Storage (m^{-1})

D = Dispersion Coefficient (m^2/s)

θ = Moisture content

C = Concentration (mg/L)

R = Source/Sink term

Chapter I

An Introduction to Waste Management/Disposal, Landfill Characteristics, Leachate Generation and Geophysical Methods

1.1 Introduction

Due to an increase in the commercial and industrial growth rate in countries around the world, proper waste management and monitoring techniques have to be developed to anticipate and avert undesirable impacts to the environment (Farquhar, 1989; Soupios et al. 2007; Renou et al. 2008).

To avoid adverse socio-economical and environmental impacts of contamination from landfills in future, government organizations have passed stringent laws which ensure that proper waste disposal/monitoring protocol are followed by individuals and other organizations. Landfilling is regarded as one of the most practical and economical methods of waste disposal, and is foreseen to have minimal environmental impacts if constructed properly. In recent years, landfills have been re-engineered to handle a large quantity and variety of waste materials (El-Fadel et al. 1997; Scott et al. 2005). Due to the ever-increasing rate of waste generation, governments are pressured to construct more landfills, which primarily rely on setting up multiple layers of expensive impermeable geo-membranes and liners to contain the effluents within the landfill and completely disregard the geological and hydrogeological parameters of the area during the planning stages (Gray et al. 1974; Tchobanoglous et al. 1993; Cossu, 1994; Cossu, 1995). This is an expedient temporary solution for the problem but uneconomical for developing countries. The problem with geo-synthetic membranes is that they are an unproven technology which has only been used for the past 30 years. Their performance beyond this time remains uncertain and this should be a cause of worry for all those nations that adopt this technology (Allen, 2001). Studies have proven that such geo-synthetic membranes have faltered under the stress of waste, temperature fluctuations due to exothermic reactions of waste degradation, type of waste buried and age-related inconsistencies (Rollin et al. 1991; Thomas and Woods-DeSchepper, 1993; Cazzuffi et al. 1995; Duquennoi et al. 1995; Surmann et al. 1995; Thomas et al. 1995; Thomas and Kolbasuk, 1995).

To make waste management sustainable and economical, new methods have to be developed that can be implemented easily and do not burden future generations with present generation waste management problems (Allen, 2001). Many naturally existing geological and hydrogeological barriers can be put to use to prevent the movement of fluids from waste cells. This can be achieved by adopting a "dilute and disperse" method (Fig. 1.0a) where one can reduce the time-frame required for waste to reach an inert state thus reducing the overall cost to maintain and monitor a landfill (Allen, 2001). A major concern with landfills is the mobilization of highly toxic fluid (liquid or gas) to areas outside the landfill boundary, which could result in groundwater, surface water, soil and air pollution (Farquhar, 1989; Kjeldsen et al. 2002). This toxic fluid could be leachate or landfill gas (CH_4, H_2S and CO_2) produced from the different stages in the decomposition of waste, and its production is

heavily dependent on the age of the landfill. Leachate can be defined as the liquid formed due to the removal of soluble contaminants from waste materials due to excess water infiltration (Fig.1.0b). The quantity and concentration of leachate produced is dependent on the amount and intensity of precipitation received by the area, the type and amount of soil and vegetation cover in the area, the thickness and integrity of the clay cap, the type of waste stored at the landfill and the influx of groundwater from outside the landfill area (Farquhar, 1989).

The idea behind modern landfills is to reduce the amount of leachate produced and, more importantly, to curtail the migration of leachate outside the landfill barrier. The leachate material is usually collected through various filtration/collection systems and is sent off to waste treatment facilities (Christensen and Kjeldsen, 1989; Farquhar, 1989; Kjeldsen et al. 2002). One of the greatest challenges faced by scientists is estimating the amount of leachate produced annually. Although there is a positive correlation between the amount of precipitation and production of leachate, there are numerous variables that are not easily understood and identifiable, such as evapotransipration rates, soil moisture, heat index and the effects of wind. Farquhar (1989) provides a good explanation about various models that can be used to estimate the amount of leachate produced.

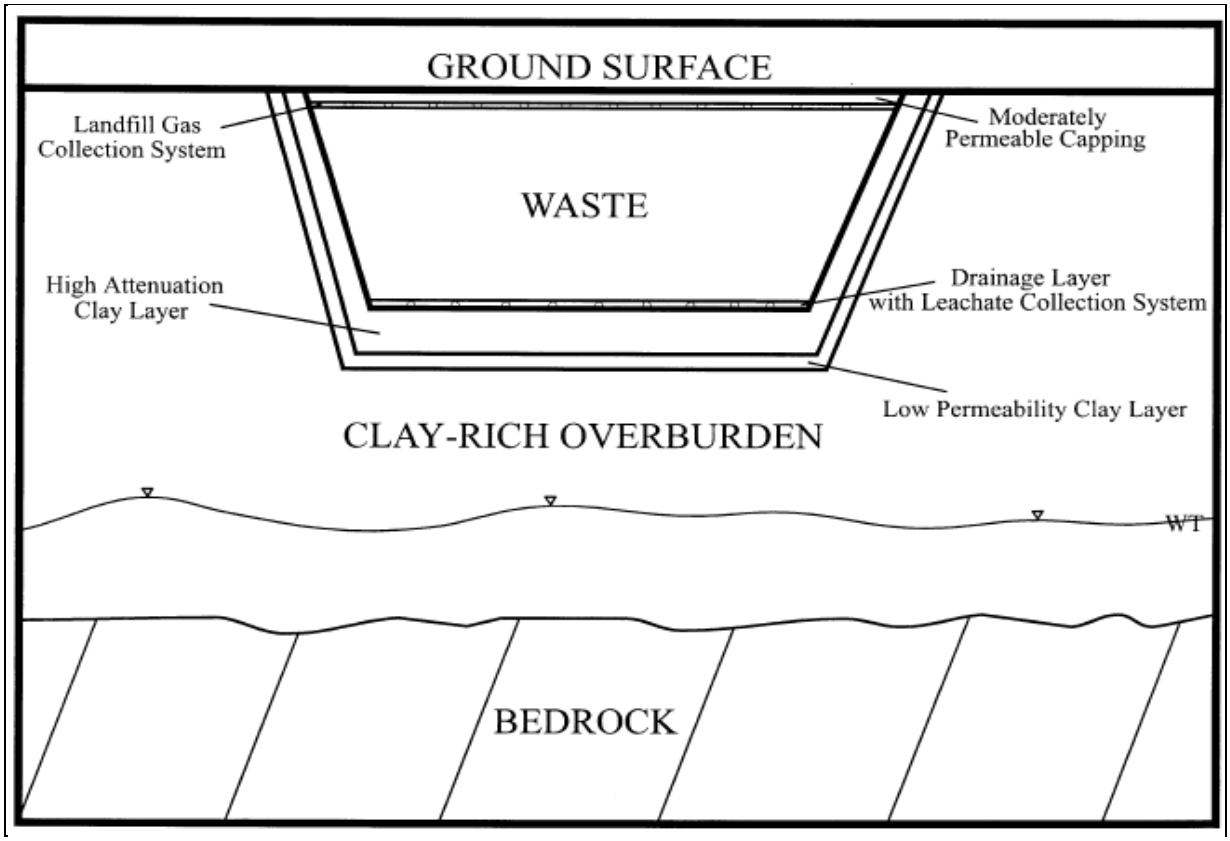

Figure 1.0a: Landfill engineered to handle the "dilute and disperse" method (Allen, 2001)

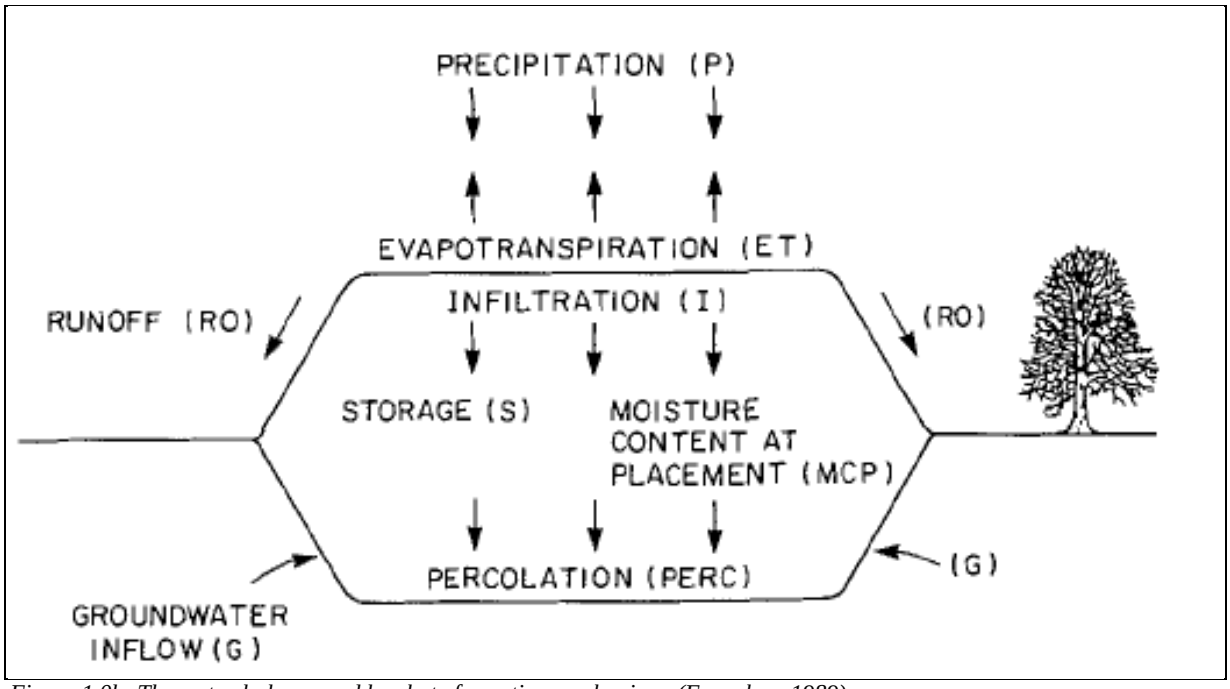

Figure 1.0b: The water-balance and leachate formation mechanisms (Farquhar, 1989)

The scrupulous examination of contaminated sites necessitates the setting up of boreholes around and within the confining areas of the site (Reichard and Evans, 1989; Freeze et al. 1990). However, boreholes offer high resolution point source information within a small area, and may not capture the areal extent of the contamination at the site (Zume et al. 2006). Non-invasive geophysical methods give a good 2D or 3D representation of subsurface geology, along with the contaminant distribution at minimal cost and labor (Whiteley and Jewell, 1992; Meju, 2000; Zume et al. 2006) and acts as a precursor in determining the exact location of boreholes within the around the periphery of the site (Bernstone and Dahlin, 1997; Butler et al. 1997; Buselli and Lu, 2001).

The success of any geophysical method relies on a strong contrast in the physical property measured between the target material and the surrounding rock/soil. If there is limited or negligible discrepancy in the physical properties being measured, false interpretations of the measurements could be produced. Therefore, before applying a specific geophysical method, it is a good idea to survey the area and study maps based on the groundwater/surface water flow regime, soil, bedrock geology and topography of the area. Pomposiello et al. (2012) states that "Geophysics should never be used as a stand-alone tool, but complementary to direct observations which provide geological/hydrogeological background information" (pg.1). Although certain geophysical methods provide a non-invasive, cheap and efficient method of collecting subsurface data, geophysicists should always be aware of the problem of "non-uniqueness". This means that, for a given set of

geophysical data, there could be a number of satisfactory models with each model providing a different interpretation to the problem. This issue can be avoided by conducting proper research on the study area and setting up assumptions or constraints in the model, thus reducing the effect of the non-uniqueness issue (Loke, 1999). Regardless of the nature of investigation, scientists should not always rely on the results of an individual method. At least two, or even three methods should be applied based on the nature of the investigation (Steeples, 2001). This will improve the accuracy of the results and ameliorate the interpretation of the resulting models. Geophysical methods such as electrical resistivity (ER), induced polarization (IP), seismic refraction tomography (SRT), gravity, ground-penetration radar (GPR), frequency-domain (FD), time-domain (TD) and very-low frequency (VLF) electromagnetic methods have been widely used and developed over the past decades. The theory of these methods are well explained and formulated in Telford et al. 1990; Lanz et al. 1994; Ulrych et al. 1994; Sharma, 1997; Reynolds, 1998; Loke, 1999; Atekwana et al. 2000; Orlando and Marchesi, 2001. From the above mentioned methods, DC resistivity and EM methods has seen tremendous success over the years and has been widely used in the field of environmental geophysics (Binley and Kemna, 2005; Bavusi et al. 2006).

The DC resistivity method relies primarily on ionic conduction that occurs through interstitial fluids under the effect of a potential voltage within pore spaces. Factors such as the water saturation, temperature of fluids within pore spaces, porosity variations of rock, lithology and ionic concentration (Sharma, 1997) will assist in the detection of a strong or a weak resistive body. The method works on galvanic contact with the ground where a pair of electrodes inject current into the ground and another pair measures the potential difference (Figure 1.1). To study the vertical variations in a set of horizontal layers, the sounding method is used, where the electrode spacing is increased systematically and the apparent resistivity is plotted on a log-log scale with electrode spacing (Sharma, 1997). An alternate method to measure apparent resistivity is to use a set of four electrodes with a specific geometric formation. This helps determine the horizontal variation of resistivity and is good for outlining vertical subsurface features such as faults and natural or man-made boundaries.

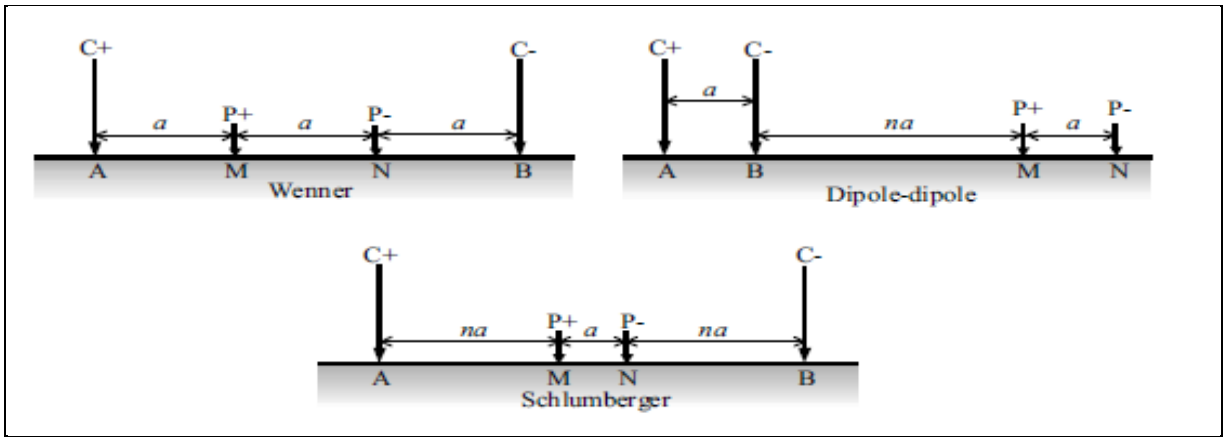

Figure 1.1: Some surface electrode configurations of DC resistivity surveys (Binley and Kemna, 2005)

EM terrain conductivity methods are in comparison faster, cheaper and easier to conduct as there is no physical contact required with the ground. The method works by sending primary EM waves into the ground and measuring the response (intensity, phase angle and amplitude variation) of the secondary wave. By comparing the ratio of the primary and secondary wave, the instrument can detect a conductive or resistive object (McNeill, 1980; DualEM User manual, 2006).

Leachate from municipal solid waste landfill sites often shows up as a low resistivity (high conductivity) anomaly, however, the detection of hydrocarbon waste such as Light Non-Aqueous Phase Liquid (LNAPL) and Dense Non-Aqueous Phase Liquid (DNAPL) by DC resistivity and EM conductivity methods is more complex (Tezkan, 1999). Studies from King and Olhoeft (1989); Daniels et al (1992); Schneider and Greenhouse (1992); de Ryck et al (1993); Endres and Redman (1993); Redman et al (1994); Grumman and Daniels (1995) Monier-Williams (1995); Campbell et al (1996); Endres and Greenhouse (1996) have shown that contaminated soils and groundwater from NAPL have lower electrical conductivity compared to the surrounding host rock/soil. Some studies such as Grumman and Daniels (1995) have reported no change in the electric conductivity of the subsurface at sites known to have hydrocarbon contaminated soils, even though water samples collected from monitoring wells suggested otherwise. However, investigations conducted by Sauck et al. (1998) suggested a temporal variation in electrical conductivity with areas contaminated with hydrocarbon pollutants. The breakdown of hydrocarbon pollutants to organic acids due to biogeochemical reactions results in the dissolution of the surrounding host rock (McMahon et al. 1995) which contributes to an increase in total dissolved solids (TDS) resulting in higher conductivity or lower resistivity readings (Benson and Stubben, 1995; Benson et al. 1997; Tezkan, 1999). Thus, when measuring the electrical resistivity/conductivity in response to hydrocarbon spills in an area, a

temporal approach should be adopted which provides the resistivity variations of contaminant plume with time.

Due to the ever-increasing rate of population growth, communities are forced to settle in close proximity to contaminated sites. This situation makes it imperative to monitor the state of surface/groundwater as accurately as possible in the vicinity of such contaminated sites. Another tool that can help in achieving the above mentioned objective is groundwater modeling. According to Anderson and Woessner, (1992) "A model is any device that represents an approximation of a field situation". Models are divided into two types: a) Physical and b) Mathematical. Physical models are those that are conducted in lab settings (e.g. sand tanks) that simulate the movement of water/solute directly. Mathematical models can be subdivided into two parts: c) Analytical models and d) Numerical models, both of which use codes to analyze the problem and perform its simulation. Analytical solutions are used for situations that are relatively simplistic and usually work for saturated and homogeneous media, however, once the model starts to get complicated where inhomogenities in the subsurface geology, changes in flow patterns and mass transport are involved, the numerical model is preferred due to its ability to handle complicated problems better than analytical models. Further information about groundwater modeling (governing equations, steady/transient models, saturated/unsaturated) will be discussed in detail in Chapter 3 of this thesis.

1.2 Objectives of Study

The study involves the application of geophysical methods and groundwater modeling techniques to assess contaminant distribution and to predict contaminant transport within the layers of the site. The specific objectives are as follows:

1) Determining the extent and depth of the contaminants along with assessing the integrity of the overlying clay cap at the site using geophysical methods.
2) Accurately mapping the sub-surface geology of the landfill site using geophysical methods.
3) Developing conceptual models of the site using results/information from the geophysical surveys and journal articles/books.
4) Simulating the flow of contaminants in aquifers through various time-scales.
5) Calibrating the model with measurements taken from monitoring/leachate wells to assess the accuracy of the model.
6) Finally, providing opportunities for future work to be done at the site.

The study utilized DC resistivity and EM conductivity methods to investigate the underground leachate distribution and the subsurface geology at the site. The results obtained from the geophysical surveys were used to create two conceptual models (S-N and W-E) of the landfill site where hydrogeological properties were assigned to each layer and the movement of contaminants through these layers was simulated using finite-element groundwater modeling software (FEFLOW). The simulation of contaminants through the aquifers was modeled for various time-scales 1, 10, 100, 1000 and in one (W-E) model up to 10,000 year(s).

Bibliography

Allen, A. (2001). Containment Landfills: the myth of sustainability. *Engineering Geology*, 60(1-4), 3-19.

Anderson, M.P. and Woessner, W.W. (1992). *Applied Groundwater Modeling*. San Diego, California, USA: Academic Press.

Atekwana, E.A., Sauck, W.A. and Werkema, D.D. (2000). Investigations of geoelectrical signatures at a hydrocarbon contaminated site. *Journal of Applied Geophysics*, 44, 167-180.

Bavusi, M., Rizzo, E. and Lapenna, V. (2006). Electromagnetic methods to characterize the Savoia di Lucania waste dump (Southern Italy), *Environmental Geology*, 51, 301-308.

Benson, A.K. and Stubben, M.A. (1995). Interval resistivities and very low frequency electromagnetic induction - An aid to detecting groundwater contamination in space and time: A case study. *Environmental Geosciences*, 2(2), 74-84.

Benson, A.K., Payne, K.L. and Stubben, M.A. (1997). Mapping groundwater contamination using dc resistivity and VLF geophysical methods - a case study. *Geophysics*, 64(1), 80-86.

Bernstone, C. and Dahlin, T. (1997). DC resistivity mapping of old landfills: two case studies. *European Journal of Engineering and Environmental Geophysics*, 2(2), 121-136.

Binley, A. and Kemna, A. (2005). DC Resistivity and Induced Polarization Methods. Rubin, Y. and Hubbard, S.S. (Eds.), *Hydrogeophysics*, 129-156.

Buselli, G. and Lu, K. (2001). Groundwater contamination monitoring with multichannel electrical and electromagnetic methods. *Journal of Applied Geophysics*, 48(1), 11-23.

Butler, D.K., Sjostrom, K.J. and Llopis, L.J. (1997). Selected short stories on novel applications of near-surface geophysics. *Leading Edge*, 16, 1593-1600.

Campbell, D.L., Lucius, J.E., Ellefsen, K.J. and Deszcz-Pan, M. (1996). Monitoring of a controlled LNAPL spill using ground penetration radar. Proceedings of the *Symposium Application of Geophysics to Engineering and Environmental Problems* (SAGEEP '96), Keystone, CO, USA, 511-517.

Cazzuffi, D., Corbett, S. and Rimoldi, P. (1995). Compressive creep test and inclined plane test for geosynthetics in landfills; in: Christensen, T.H., Cossu, R. and Stegmann, R. (Eds.), Proceedings Sardinia 95, *Fifth International Landfill Symposium*, Cagliari (1995), 2, 477-491.

Christensen, T.H. and Kjeldsen, P. (1989). Basic Biochemical processes in landfills, In: Christensen, T.H., Cossu, R. and Stegmann, R. (Eds.), *Sanitary Landfilling: Process, Technology and Environmental Impact*. Academic Press, London, UK, 1989, 29.

Cossu, R. (1994). Engineering of landfill barrier systems; in: Christensen, T.H., Cossu, R. and Stegmann, R. (Eds.), Landfilling of Waste: Barriers, E & FN Sponsors, London (1994), 11-23.

Cossu, R. (1995). The multi-barrier landfills and related engineering problems; in: Christensen, T.H., Cossu, R. and Stegmann, R. (Eds.), Proceedings Sardinia 95, *Fifth International Landfill Symposium*, 2, 3-26.

Daniels, J.J., Roberts, R. and Vendl, M. (1992). Site studies of ground penetration radar for monitoring petroleum product contaminants. Proceedings of the *Symposium on the Application of Geophysics to Engineering and Environmental Problems* (SAGEEP '92), Oakbrook, IL, USA, 597-609.

DeRyck, S.M., Redman, J.D. and Annan, A.P. (1993). Geophysical monitoring of a controlled kerosene spill. In Proceedings of the *Symposium on the Application of Geophysics to Engineering and Environmental Problems* (SAGEEP ’93), San Diego, CA, USA, 5-19.

Duquennoi, C., Bernhard, C. and Gaumet, S. (1995). Laboratory ageing of geomembranes in landfill leachate; in: Christensen, T.H., Cossu, R. and Stegmann, R. (Eds.), Proceedings Sardinia 95, *Fifth International Landfill Symposium*, Cagliari (1995), 2, 397-404.

El-Fadel, M., Findikakis, A.N. and Leckie, J.O. (1997). Modeling leachate generation and transport in solid waste landfills. *Environmental Technology*, 18(7), 669-686.

Endres, A.L. and Greenhouse, J.P. (1996). Detection and monitoring of chlorinated solvent contamination by thermal neutron logging. *Ground Water*, 34(2), 283.

Farquhar, G.J. (1989). Leachate: production and characterization. *Canadian Journal of Civil Engineering*, 16(3), 317-325.

Freeze, R.A., Massmann, J., Smith, L., Sperling, T. and James, B. (1990). Hydrogeological decision analysis: A Framework, *Groundwater*, 28(5), 738-765.

Gray, D.A., Mather, J.D. and Harrison, I.B. (1974). Review of groundwater pollution from waste disposal sites in England and Wales, with provisional guidelines for future site selection. *Quarterly Journal of Engineering Geology and Hydrogeology*, 7(2), 181-196.

Grumman, D.L. Jr. and Daniels, J.J. (1995). Experiments for the detection of organic contaminants in the vadose zone. *Journal of Environmental and Engineering Geophysics*, 0(1), 31-38.

King, T.V.V. and Olhoeft, G.R. (1989). Mapping organic contamination by detection of clay-organic processes. Proceedings AGWSE/NWWA/API Conference on *Petroleum Hydrocarbons and Organic Chemical in Ground Water - Prevention, Detection and Restoration*, 627-640.

Kjeldsen, P., Barlaz, M.A., Rooker, A.P., Baun, A., Ledin, A. and Christensen, T.H. (2002). Present and Long-Term Composition of MSW Landfill Leachate: A Review. *Critical Reviews in Environmental Science and Technology*, 32(4), 297-336.

Lanz, E., Jemmi, L., Müller, R., Green, A., Pugin, A. and Huggenburger, P. (1994). Integrated studies of Swiss waste disposal sites: results from georadar and other geophysical surveys. Proceedings of the *Fifth International Conference on Ground Penetration Radar* (GPR '94), Kitchener, Ontario, 1261-1274.

Loke, M.H. (1999). A practical guide to 2D and 3D surveys. *Electrical imaging surveys for environmental and engineering studies*, 8-10.

McMahon, P. B., Vroblesky, D.A., Bradley, P.M., Chapelle, F.H. and Gullett, C.D. (1995). Evidence for enhanced mineral dissolution in organic acid-rich shallow ground water. *Ground Water*, 33(2), 207-216

McNeill, J.D. (1980). Electromagnetic Terrain Conductivity Measurements at Low Induction Numbers, Geonics.

Meju, M.A. (2000). Geoelectrical investigations of old/abandoned, covered landfill sites in urban areas: model development with a genetic diagnosis approach. *Journal of Applied Geophysics*, 44(2-3), 115-150.

Monier-Williams, M. (1995). Properties of light non-aqueous phase liquids and detection using commonly applied shallow sensing geophysical techniques. Proceedings of the *Symposium Application of Geophysics to Engineering and Environmental Problems* (SAGEEP '95), Orlando, FL, USA.

Orlando, L. and Marchesi, E. (2001). Georadar as a tool to identify and characterize solid waste dump deposits. *Journal of Applied Geophysics*, 48, 163-174.

Pomposiello, C., Dapeña, C., Favetto, A. and Boujon, P. (2012). Application of Geophysical Methods to Waste Disposal Studies. Municipal and Industrial Waste Disposal, Dr. Xiao-Ying Yu (Ed.), InTech.

Redman, J.D., DeRyck, S.M. and Annan, A.P. (1994). Detection of LNAPL pools with GPR: Theoretical modeling and surveys of controlled spill. In Proceedings: *Fifth International Conference on Ground Penetration Radar*, Kitchener, ON, Canada, 1283-1294.

Reichard, E.G. and Evans, J.S. (1989). Assessing the value of hydrological information for risk-based remedial action decisions. *Water Resources Research*, 25(7), 1451-1460.

Renou, S., Givaudan, J.G., Poulain, S., Dirassouyan, F. and Moulin, P. (2008). Landfill leachate treatment: Review and opportunity. *Journal of Hazardous Materials*, 150(3), 468-493.

Reynolds, J.M. (1998). An Introduction to Applied and Environmental Geophysics, Wiley, Chichester.

Rollin, A., Mlynarek, J., Lafleur, J. and Zanescu, A. (1991). An Investigation of a seven year old HDPE geomembrane used in a landfill; in: Christensen, T.H., Cossu, R. and Stegmann, R. (Eds.), *Proceedings* Sardinia 91, *Third International Landfill Symposium*, CISA, Cagliari (1991), 667-678.

Sauck, W.A. (2000). A conceptual model for the geoelectrical response of LNAPL plumes in granular sediments. *Journal of Applied Geophysics*, 44, 151-165.

Sauck, W.A., Atekwana, E. and Nash, M.S. (1998). High conductivities associated with an LNAPL plume images by integrated geophysical techniques. *Journal of Environmental and Engineering Geophysics*, 2(3), 203-212.

Schneider, G.W. and Greenhouse, J.P. (1992). Geophysical detection of perchloroethylene using resistivity and nuclear logging techniques. Proceedings of the *Symposium on the Application of Geophysics to Engineering and Environmental Problems* (SAGEEP '92), Oakbrook, IL, USA, 619-628.

Scott, J., Beydoun, D., Amal, R., Low, G. and Cattle, J. (2005). Landfill Management, Leachate Generation and Leach Testing of Solid Wastes in Australia and Overseas. Critical Reviews in Environmental Science and Technology, 35(3), 239-332.

Sharma, P.V. (1997). Environmental and Engineering Geophysics, Cambridge University Press, New York, USA, 207-237.

Soupios, P., Papadopoulos, I., Kouli, M., Georgaki, I., Vallianatos, F. and Kokkinou, E. (2007). Investigation of waste disposal areas using electrical methods: a case study from Chania, Crete, Greece. *Environmental Geology*, 51, 1249-1261.

Steeples, D.W. (2001). Engineering and environmental geophysics at the millennium. *Geophysics*, 66, 31-35.

Surmann R., Pierson P. and Cottour F. (1995). Geomembrane liner performance and long term durability; in: Christensen, T.H., Cossu, R. and Stegmann R. (Eds.), *Proceedings Sardinia 95, Fifth International Landfill Symposium*, vol. 2CISA, Cagliari (1995), 405-414.

Tchobanoglous, G., Thiesen, H. and Vigil, S.A. (1993). Integrated Solid Waste Management: engineering principles and management issues. McGraw Hill, New York, 978.

Telford, W.M., Geldart, L.P. and Sherrif, R.P. (1990). Applied Geophysics, Cambridge University Press

Tezkan, B. (1999). A review of environmental applications of quasi-stationary electromagnetic techniques. *Surveys in Geophysics*, 20, 279-308.

Thomas, R.W. and Kolbasuk, G.M. (1995). Lessons learned from a cold crack in an HDPE geomembrane. In: Giroud, J.P. (Eds.), Geosynthetics: Lessons Learned from Failures, *Industrial Fabrics Association International*, 251-254.

Thomas, R.W. and Woods-DeSchepper, B. (1993). The environmental stress crack behavior of coextruded geomembranes and seams; *In Proceedings of the Fifth International Conference on Geotextiles, Geomembranes and Related Products*, Singapore (1993), 945-948.

Thomas, R.W., Kolbasuk, G.M. and Mlynarek, J. (1995). Assessing the quality of HDPE double track fusion seams; In: Christensen, T.H., Cossu, R. and Stegmann, R. (Eds.), *Proceedings Sardinia 95, Fifth International Landfill Symposium*, vol. 2CISA, Cagliari (1995), 415-427.

Ulrych, T.J., Lima, O.A.L. and Sampaio, E.E.S. (1994). In search of plumes: A GPR odyssey in Brazil. *64th Annual International Meet, Society of Exploration Geophysicist*, Los Angeles, USA, 569-572.

Whiteley, R.J. and Jewell, C. (1992). Geophysical techniques in contaminated lands assessment? Do they deliver? *Exploration Geophysics*, 23(4), 557-565.

Zume, J.T., Tarhule, A., Christenson, S. (2006). Subsurface imaging of an abandoned solid waste landfill site in Norman, Oklahoma. *Groundwater Monitoring and Remediation*, 26, 62-69.

Chapter II

Geophysical investigation of a closed municipal landfill site in southwestern Ontario

2.1 Introduction

Groundwater has been over-extracted for a number of years due to over-growing population, agriculture, and industrial purposes, especially in arid and semi-arid regions (Fried, 1975). The rate at which groundwater is withdrawn is much higher than the rate at which it is getting replenished and this makes groundwater one of the most precious and scarce resource. It is paramount that this resource is protected against contamination from waste disposal sites, salt-water intrusion and over-extraction due to excessive pumping. To reduce the adverse impact of leachate leakage on surface and groundwater from contaminated sites, government and environmental organizations have employed various methods which can help in both short and long term monitoring, keeping in mind the economical consequences (Quadrio-Curzio et al. 1994; Beede and Bloom, 1995; Fullerton and Kinnaman, 2002; Porter, 2002).

Geophysical methods, especially geo-electrical methods, have proven their credibility in environmental and engineering geophysics. These methods have enabled scientists to map out waste characteristics such as type and volume of waste, along with soil cover thickness (Bernstone et al. 2000). Application of geophysical methods to landfill-related studies have become standard over the years, as can be seen in Carpenter et al. (1990), where the authors used geophysical methods to determine the internal landfill structure, leachate levels and cap material thickness. Kobr and Linhart (1994) used Continuous Vertical Electric Sounding (CVES) and Very-Low Frequency (VLF) methods to assess both waste characteristics and local geology at a landfill. Cardarelli and Bernabini (1996) used VLF and refraction seismic methods to map the thickness and edges of a landfill. Bernstone and Dahlin (1997) used DC resistivity, magnetometry and slingram (EM) to assess metals at a closed landfill and Ross et al (1990) used DC resistivity (Dipole-Dipole) methods to detect hydrocarbon chemical-waste disposal pits which show up as high resistivity areas at the Hill Air Force Base, Utah, USA.

Groundwater contaminants travel through various lateral and vertical inhomogenities present in the aquifers and the successful mapping of these contaminants depends on the locations of monitoring wells (Benson et al. 1988; Osiensky, 1995). These monitoring wells have to be strategically placed both up and down gradient from the landfill to cover an area large enough which increases the probability of finding the contaminants. Using geophysical methods would assist in accurately determining the position of the monitoring wells, which maximizes its ability to detect contaminants. There are various parameters that can be used to study the extent of contaminants in aquifers such as pH, total dissolved solids (TDS), chemical oxygen demand (COD), biological oxygen demand (BOD), water conductivity (µS), temperature (°C), turbidity (NTS) and lab tests for various cations

and anions that serve as indicators inorganic, organic, nuclear and biological waste. The indicators for detecting leachate discussed in this paper are chloride ions (Cl^-), Boron (B), and chloro-vinyl (CH_2-CHCl), however, for the case of simplicity, the concentration fluctuations of only chloride (Cl^-) ions will be studied in the groundwater modeling part of this thesis.

Two geophysical methods, DC resistivity and EM conductivity, were used to determine the extent of contamination at a closed municipal landfill site in southwestern Ontario. The landfill site contains primarily industrial, commercial and institutional (ICI) waste and leachate produced from these waste materials appear as a high conductivity or low resistivity reading that can be easily differentiated from the surrounding soil/rock. This is due to the amount of dissolved ions in leachate which makes it electrically conductive compared to the surrounding soil and rock. This is one of the reasons why geo-electrical methods have seen so much success in environmental geophysics. The results from geophysical surveys were used to develop two conceptual models of the landfill site using a 2D transient flow/transient mass transport using finite-element solution in FEFLOW. The groundwater modeling results were simulated for 1, 10, 100, 1000 and in one case up to 10,000 year(s) to predict the flow of contaminants in aquifers considering three scenarios: a) Regular precipitation - simulating average annual rainfall, b) No precipitation – simulating dry periods and c) Double precipitation - simulating wet periods. The behavior of contaminant flow under these conditions were analyzed which can assist in predicting the areal extent of contaminants in future.

2.2 Study Area

The site chosen for this study was a closed municipal solid waste landfill in southwestern Ontario. The site covers an area of 34 hectares (ha) which comprises of the decommissioned landfill and a transfer station. The site stopped accepting waste in October, 1993 (Biennial Operations Report, 2010).

The landfill sits on a beach ridge deposit of fine sand underlain by a glacial till deposit of sand and silt. The sand has been extensively mined in the area which is evident from the quarry and sand exploration pits situated south of the landfill. The glacial till is exposed on the western portion of the site and this layer thins southwards and eventually disappears forming a local groundwater divide (Annual Monitoring Report, 2011). The upper sand unit and the upper portion of the silt/sand till forms the surface water aquifer and the direction of flow observed in this aquifer is mainly easterly to south-easterly. The shallow water aquifer flow patterns are governed by the local variation in water level, sand pit construction and the presence of the leachate collection system. The average thickness

of the upper sand aquifer is about 10-15m with the waste occupying majority of the layer. Water levels within the upper aquifer fluctuate greatly during different times of the year. The water levels in the upper aquifer are low during the Summer and Fall due to lower amounts of precipitation and inversely higher during Spring. Underlying the upper sand aquifer is a glacial till deposit, comprising a mixture of primarily sand and silt. This layer has the hydrogeological properties of an aquitard and measures about 12m in thickness. This silt/sand aquitard gradually thins and eventually disappears south of the landfill (Fig.2.0a – dotted line showing the extent of the glacial till). There is a confined aquifer system associated with the lower sand unit underlying the silt/sand aquitard and the direction of flow in this aquifer is north to north-easterly with its thickness ranging from 8-10m (Annual Monitoring Report, 2011). The lower sand aquifer merges with the upper sand aquifer south of the landfill where the silt/sand aquitard disappears. Waste is located and occupies most of the upper aquifer, with a thin layer of sand between the waste and the silt/sand aquitard (Annual Monitoring Report, 2011).

A total of 3670 species of trees and shrubs were planted by the Essex County Field Naturalists in 2001 and 2002. The vegetation was constantly trimmed, pruned and weeds were treated to ensure good quality and thick vegetation growth in areas which show poor vegetation cover. The thick vegetation cover also ensured low erosion, low surface water infiltration and cell cap desiccation rates (EWSWA Biennial Operations Report, 2010).

The southern and western portion of the landfill has seen major development in the past decade. The southern periphery of the landfill is owned by the Lake Erie Sand and Gravel construction company and is used for sand extraction activities. Due to extensive extraction activities the upper sand aquifer and the underlying silt/sand aquitard were accidently removed, resulting in non-compliance issues of contaminating the groundwater with respect to drinking water standards. Elevated chloride ion concentrations were seen in well 2 in the northeast, well 6 in the northwest and well 3 in the southeast portion of the site. The wells in the northeastern portion of the site did not have high boron concentrations and they were well within their historic ranges. This suggests that the high chloride concentrations were caused by factors other than the landfill waste. The most likely cause could be roadside salting during the winter months (Annual Monitoring Report, 2011), which tends to elevate chloride concentrations annually. In general the chloride concentrations were within the Ontario Drinking Water Quality Standards (ODWQS) of 139 mg/L. However, the concentrations of all parameters (Cl^-, B, and CH_2-CHCl) have decreased since the landfill stopped accepting waste. To prevent any unacceptable off-site impacts of leachate escaping from the landfill, the landfill authorities proposed the construction of a Contaminant Attenuation Zone (CAZ) south of the landfill

(Fig. 2.0a - shown in green). The CAZ was completed in October, 2004 (Annual Monitoring Report, 2010). Three monitoring wells (40, 33 and 32) were installed south of the landfill to monitor the effectiveness of the CAZ over time. An increase in the chloro-vinyl (CH_2-CHCl) concentration was reported in monitoring wells 32 and 33, located south of the landfill. Higher concentrations were seen in the fall than any other time during the year, due to a decrease in precipitation rates. However, chloro-vinyl (CH_2-CHCl) concentration never exceeded the compliance limit set by the Ministry of Environment (MOE).

Greenhouse construction activities west of the site also resulted in the removal of the silt/sand aquitard. This caused changes in the hydraulic flow patterns on the northwestern portion of the site, which was detected in monitoring well 6. This issue was resolved by applying a thick clay barrier which not only reversed the hydraulic flow patterns back to its original state but, in the process, prevented any unacceptable off-site impacts (Annual Monitoring Report, 2011).

To prevent excess surface water runoff from entering back into the landfill, the Fleming-Wiggle Drain (SW12) was hydraulically separated from the site by a clayey soil dyke. The dyke was installed in 1998, and the surface water was monitored annually after periods of heavy rainfall (>30 mm/hour). However, since there was no hydraulic connection between the site and SW12, the drain was always dry and showed no evidence of flow even after rainfall in excess of 50 mm/hour (Annual Monitoring Report, 2011). The quantity of leachate produced varied annually and was dependent primarily on the amount of precipitation received in that year (Table 2.0). A higher amount of precipitation led to an increase in surface water infiltration which resulted in the production of higher volume (but diluted) leachate. The leachate was siphoned by the collector system and is sent to a treatment facility. In 2010, approximately 19,241.26 m^3 of leachate material was collected through the collector system for treatment and in 2011, 43,359.48 m^3 of leachate material was collected at the site (Biennial Operations Report, 2010). The leachate quality was similar to the leachate found in any closed municipal southwestern Ontario landfill. At this site, the leachate showed a higher concentration of parameters ($Cl^-$and CH_2CHCl) on the western portion compared to the eastern portion of the site. One of the reasons for this dilution of leachate in the eastern portion of the site is because of the presence of the leachate collector system in the southeastern periphery of the site which draws most of the surface water towards itself thus diluting the leachate in the process. To differentiate leachate samples between the western and eastern portion of the site, two separate monitoring wells were installed, well 8 (western portion of the site) and well 6 (eastern portion of the site). These wells provide a good representation of the change in leachate parameters over time from their respective cells (Table 2.1).

Water Budget Summary				
Year	Landfill		Kingsville Climatological Station	
	Total Precipitation (mm)	Potential Water Surplus (mm)	Total Precipitation (mm)	Potential Water Surplus (mm)
1961-1987	N/A	N/A	880.1	235.7
1988	N/A	N/A	704.7	41.2
1989	N/A	N/A	1032.2	410.3
1990	N/A	N/A	1135.7	481.8
1991	N/A	N/A	889.6	191.7
1992	N/A	N/A	1019.7	414.4
1993	N/A	N/A	810.5	179.7
1994	730.5	72.5	909.7	251.7
1995	725.7	51.8	811.6	137.7
1996	815.9	178.1	948.1	310.3
1997	828.4	337.1	915.1	423.8
1998	716	162.3	777.8	224.1
1999	864.6	312.7	794.2	242.3
2000	921.7	369.7	903.4	369.9
2001	845.8	309.9	717.1	181.2
2002	782.6	252.8	709.6	179.8
2003	884.3	384.7	990.8	490.7
2004	696.4	190.5	772.9	267
2005	593.8	60.9	641.4	108.5
2006	1134.7	512.2	854.6	344.8
2007	688	138.1	746.9	376.5
2008	888.8	368.9	758.7	238.8
2009	808	302.7	736.7	231.4
2010	730.1	142.3	710.2	122.4

Table 2.0: Table showing the average annual precipitation and water surplus at the landfill site (Modified from Annual Monitoring Report, 2011).

Leachate Quality Results for MH 6 and MH 8								
Parameter	MH 6 (East)				MH 8 (West)			
	Apr, 2010	Oct, 2010	Apr, 2011	Oct, 2011	Apr, 2010	Oct, 2010	Apr, 2011	Oct, 2011
pH	6.83	6.78	7.02	7.82	7.07	7.15	7.1	7.06
Conductivity (mS)	2688	2680	1751	783	3270	6690	1742	1367
Chloride (mg/L)	247	184	181	84	255	819	178	75
Boron (mg/L)	0.6	0.5	0.5	0.3	0.56	1.4	0.53	0.3
Vinyl Chloride (mg/L)	39.8	200	13.5	BDL	BDL	BDL	BDL	BDL

Table 2.1: Table showing the change in parameters over time for MH 6 and MH 8 (Modified from Biennial Operations Report, 2010)

*BDL = Below Detection Limit

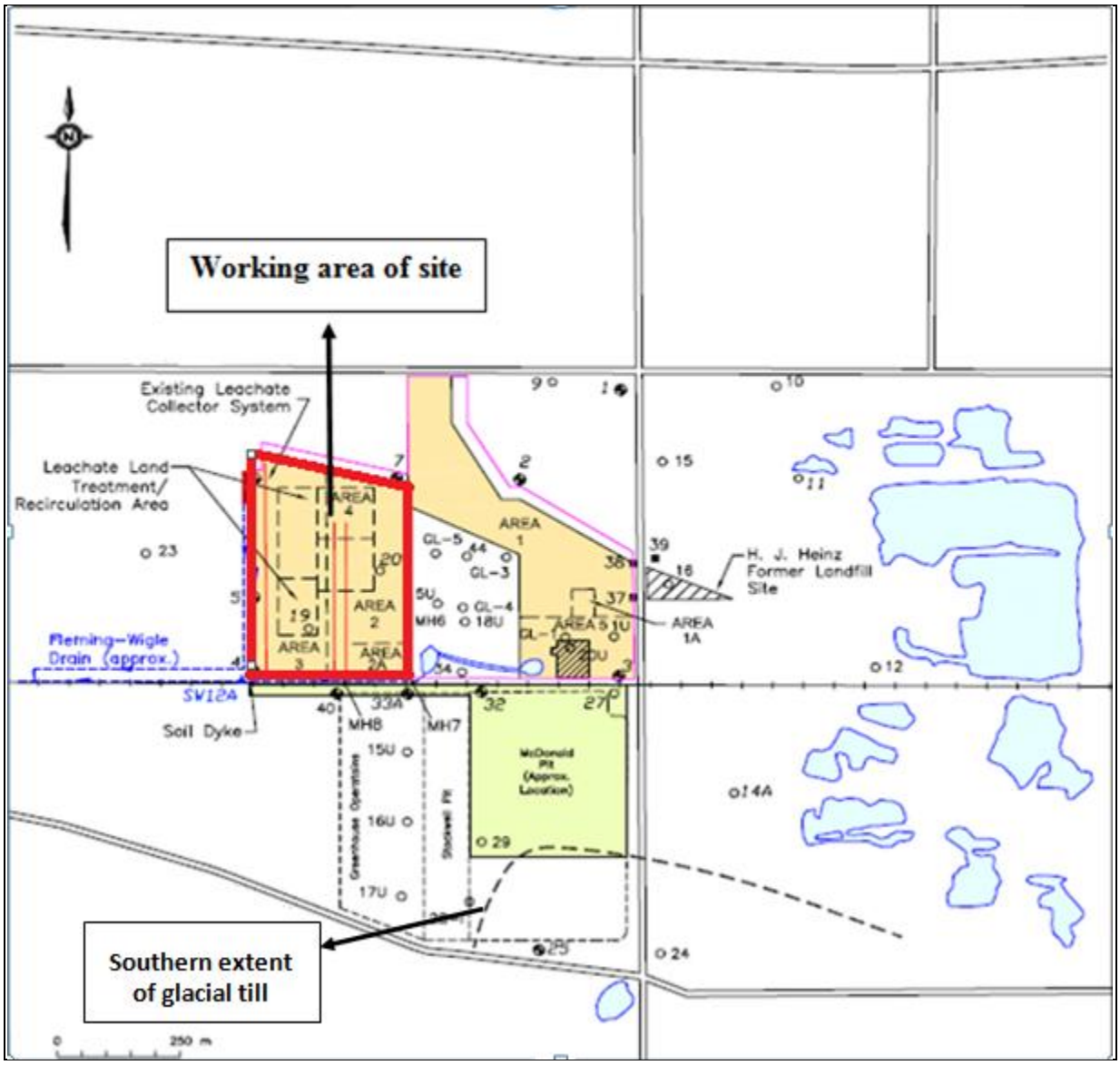

Figure 2.0a: Site plan map of the landfill site (Annual Monitoring Report, 2011)

In addition to monitoring the groundwater and surface water, combustible gas monitoring was also performed at the site to ensure the safety of nearby residences. In general, the different stages in the decomposition of waste produces two major gases; a) Carbon-dioxide (CO_2) and b) Methane (CH_4), since CO_2 is the heavier gas it sinks to the bottom and remains within the waste, however, CH_4 being lighter than air rises above the waste unless there is a trap (clay layer or frost) that prevents it from escaping. In this case, the gas travels laterally against the trap taking the direction of least resistance. This gas if increases in concentration above a certain value can pose an explosive hazard for the communities nearby. Thus, the concentration of such gases was monitored over time since the landfill was decommissioned back in 1993 at wells 36, 37 and 39 (Fig 2.0b - square black box in the

eastern portion of the site). Since 2009, methane (CH_4) has not been detected in large amounts at these wells. The concentration of CH_4 has been well below the explosive limit and as a result poses no explosion hazard to nearby communities. Thus a decision was made by the landfill authorities in 2011 to discontinue the combustible gas monitoring at the site (Biennial Operations Report, 2010).

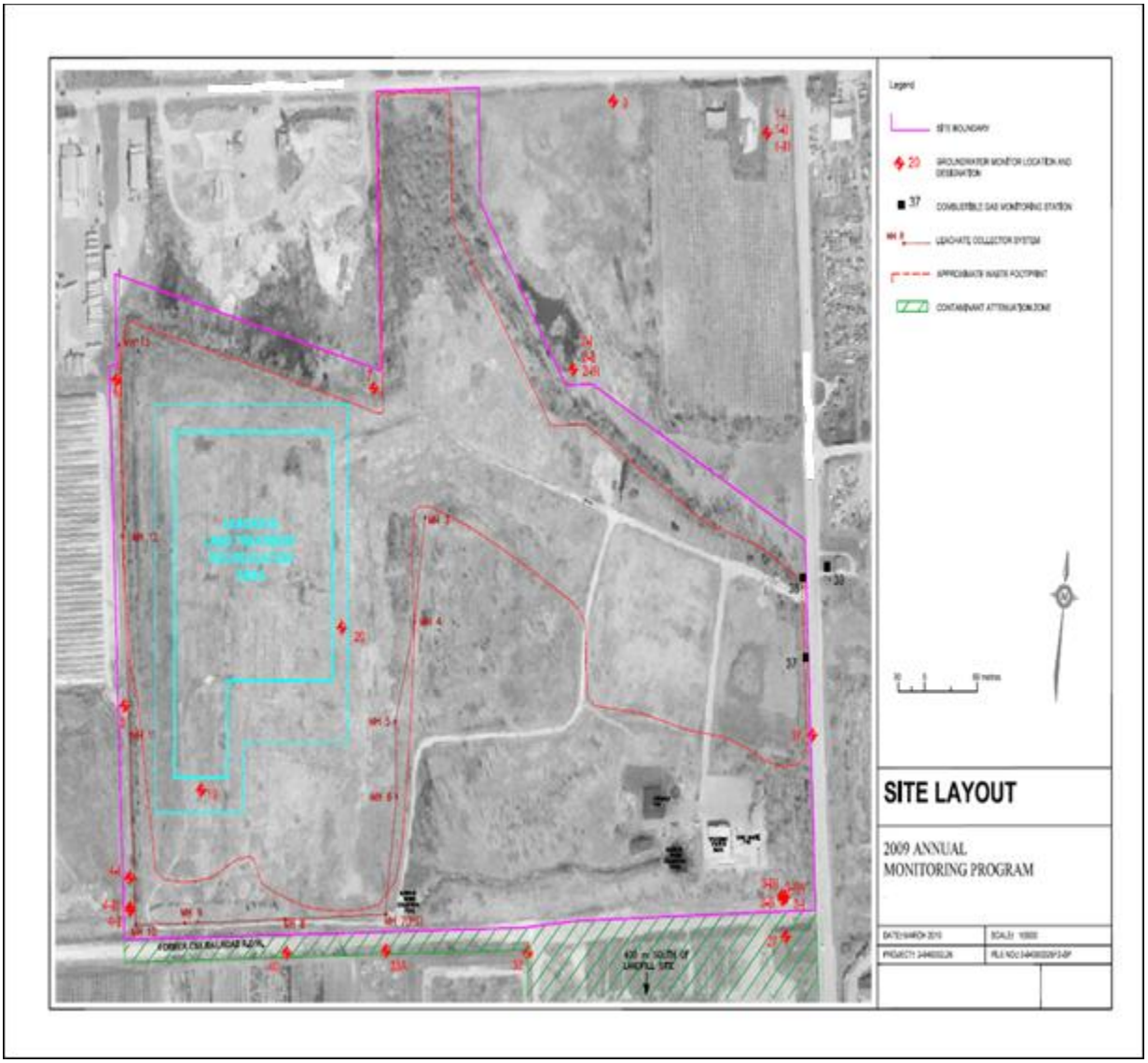

Figure 2.0b: Leachate collector system (red) linking all monitoring wells along with the leachate treatment/recirculation (blue) area (Annual Monitoring Report, 2009)

2.3 Methodology

This study examines at the application of geophysical methods and groundwater modeling to map the extent of underground leachate distribution at the site and to determine its flow pattern through the aquifers over time by groundwater modeling. As mentioned in the introduction, the landfill is mainly composed of ICI type waste, which degrades over time in the presence of water to form leachate. The anions and cations present in this leachate make it a highly conductive or low resistive material compared to the surrounding rock/soil thus making the EM conductivity and DC resistivity methods ideal for mapping the extent of leachate plumes.

2.3.1 Geophysical Methods

The EM conductivity method was first utilized to determine the apparent conductivity measured in milliSeimens/meter (mS/m) of the decommissioned landfill using two coil separations. A Frequency-Domain (FD) terrain conductivity instrument measures the apparent conductivity of the ground using an audio frequency to energize the transmitter (T_x) coil with a receiver coil (R_x) located at a small distance (s). As the distance between the transmitter and receiver coil increases the depth of signal penetration also increases. The transmitter coil (T_x) sends out a primary EM field (H_p) into the ground. If the ground consists of a conducting body, then the primary field induces a potential difference in the conducting body which produces a secondary EM field (H_s) that is sensed by the receiver coil (Fig.2.1a). The receiver coil compares the signal strength and phase angle between the H_p and H_s fields to determine the apparent conductivity of the ground and it is usually expressed as a ration of H_s/H_p as evident from the equation below:

$$\sigma_a = (4/\omega\mu_0 s^2) * (H_s/H_p) \quad (1)$$

where σ_a is the apparent conductivity (mS/m), ω is the angular frequency (Hz), μ_0 is the permeability of free space and s is the intercoil spacing between the transmitter and receiver coils (m) (Wait, 1962; Keller and Frischknecht, 1966; McNeill, 1980; Tezkan, 1999). The instrument used for measuring the conductivity is the DualEM 2S/4S which consists of dual coil geometries for the receiver namely the Horizontal Co-Planar (HCP) and the Perpendicular Planar (PRP). The distance between the transmitter and receiver coils can be adjusted to either 2m or 4m depending on the desired depth of investigation (DOI). The DOI for the HCP coil with a 2m separation can be calculated as 1.5 * (Distance between T_x-R_x coils) = 3m and the DOI for the PRP coil with a 2m separation is 0.6 * (Distance between T_x-R_x coils) = 1.2m. For the 4m coil separation, the DOI for HCP coil is 6m and the PRP coil is 2.4m (DualEM User manual, 2002). The actual depth of investigation is dependent on the height above the ground the instrument is carried. For example, if the instrument is carried at

0.3m above the ground, then the actual DOI for the 4m HCP coil would be 6m-0.3m = 5.7m and for the 4m PRP coil would be 2.4m-0.3m = 2.1m. The terrain conductivity meter is relatively easier to use and requires little setup time and labor. The instrument requires no physical contact with the ground, thus it can measure the apparent conductivity as fast as the surveyor can walk. However, in order to improve the accuracy of results and reduce noise, it is advisable for the surveyor to walk at a constant slow pace.

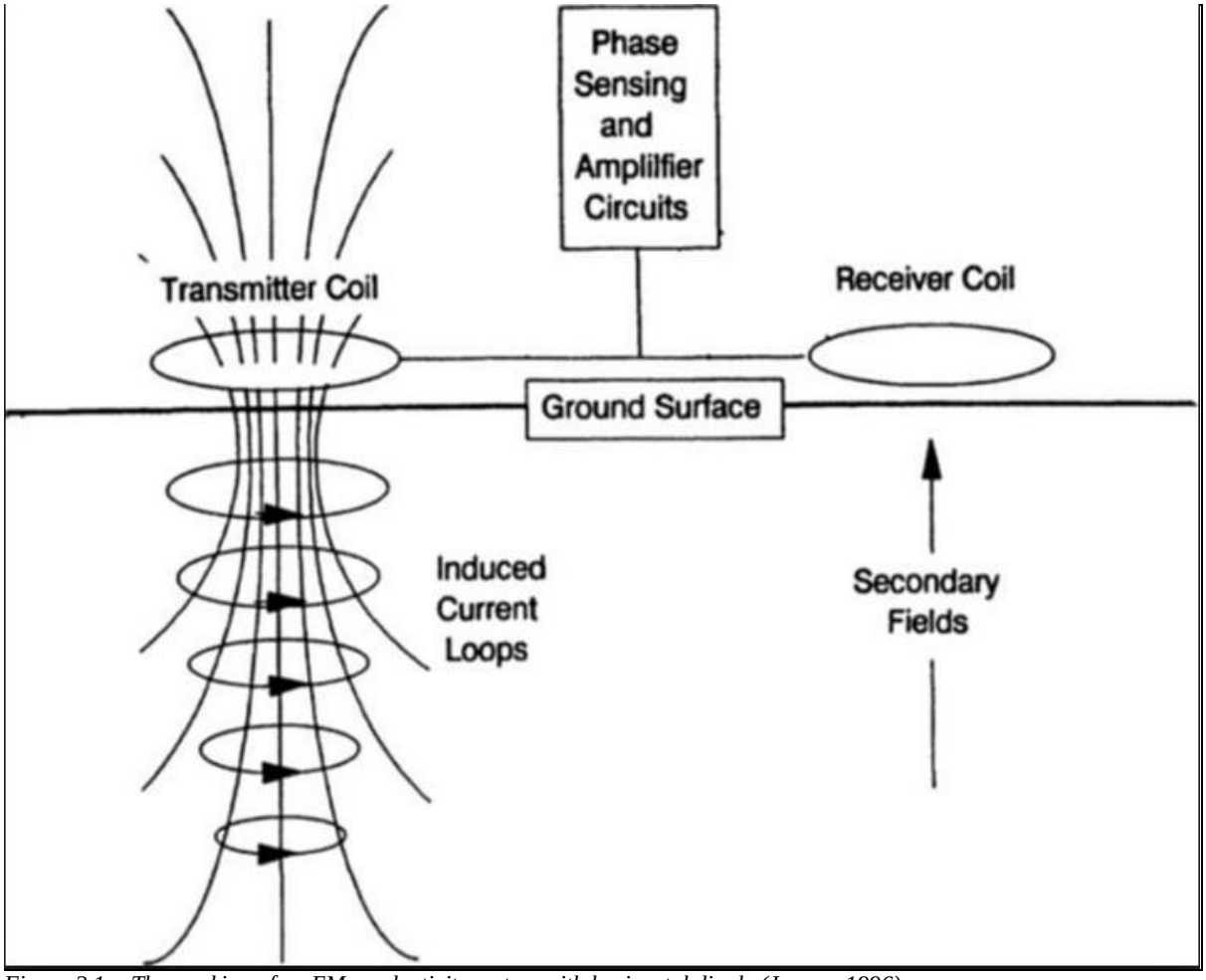

Figure 2.1a: The working of an EM conductivity system with horizontal dipole (Jaynes, 1996)

The terrain conductivity was measured first using a 2m T_x-R_x separation boom with the instrument setup to measure every second with a 'Flip' line option which allows the user to flip the coordinates of the profile when moving from one profile to another. This option is really useful in large scale surveys and the surveyor save precious time by not having to go back to start of the next profile (DualEM User manual, 2002). The profile lines were setup using wooden stakes measuring about 1.2m in length as stations and their GPS position were marked using a Garmin GPS 60 device.

The conductivity profiles were oriented in the north-south direction and the profiles were 5m apart (west-east) covering the entire site with 55 profiles. Once the 2m conductivity measurements were complete, the terrain conductivity of the landfill was re-measured using the 4m T_x-R_x separation boom. Due to time constraints, the conductivity profiles were setup 10m apart measuring to 27 profiles in total. The conductivity readings were matched with their respective GPS locations in Excel and later transferred to ArcMap 10.1 for plotting using inverse distance weighting method. The HCP-2m, PRP-2m, HCP-4m and PRP-4m were used for interpreting conductive anomalies.

After completing the conductivity surveys and plotting the results, the resistivity survey was designed to assess the underground leachate distribution at the site. The instrument used to measure the apparent resistivity (ρ_a) was the ABEM Terrameter SAS 4000 which is capable of performing resistivity profiling, sounding, SP and IP surveys. The resistivity method utilizes two current electrodes which inject current into the ground and the resulting potential difference is measured between the two potential electrodes and by applying Ohm's law (V=IR) the resistance can be calculated. The apparent resistivity is calculated from the resistance by applying a geometric factor which is dependent on the array. A Gradient array would show a different apparent resistivity model when compared to a Schlumberger array at the same location. Thus, the apparent resistivity can be represented by the following equation:

$$\rho_a = 2\Pi (\Delta V/I) * (1/G) \quad (2)$$

where ρ_a is the apparent resistivity measured in (Ω*m), $\Delta V/I$ is the change in potential difference over current (Ω) and G is the geometric factor which varies from array to array and is defined as the spacing between the current and potential electrodes (m) (Sharma, 1997). This study will utilize the Continuous Vertical Electric Sounding (CVES) method to measure the sub-surface resistivity and as a result outlining the underground extent of leachate and the subsurface geology. The CVES method is a combination of profiling and sounding methods, where the electrodes are strategically placed on the ground depending on the type of array. The electrode selector automatically selects two pairs of electrodes (2 current and 2 potential) at each time and measures the apparent resistivity between them. The spacing between the electrodes is constantly increased as specified to the instrument before the start of the measurement. By this method, the instrument plots a depth profile at the midpoint of the electrodes based on the a-spacing and n-factors (Fig. 2.1b) which is the same for a Wenner array (ABEM Instruction manual, 2006).

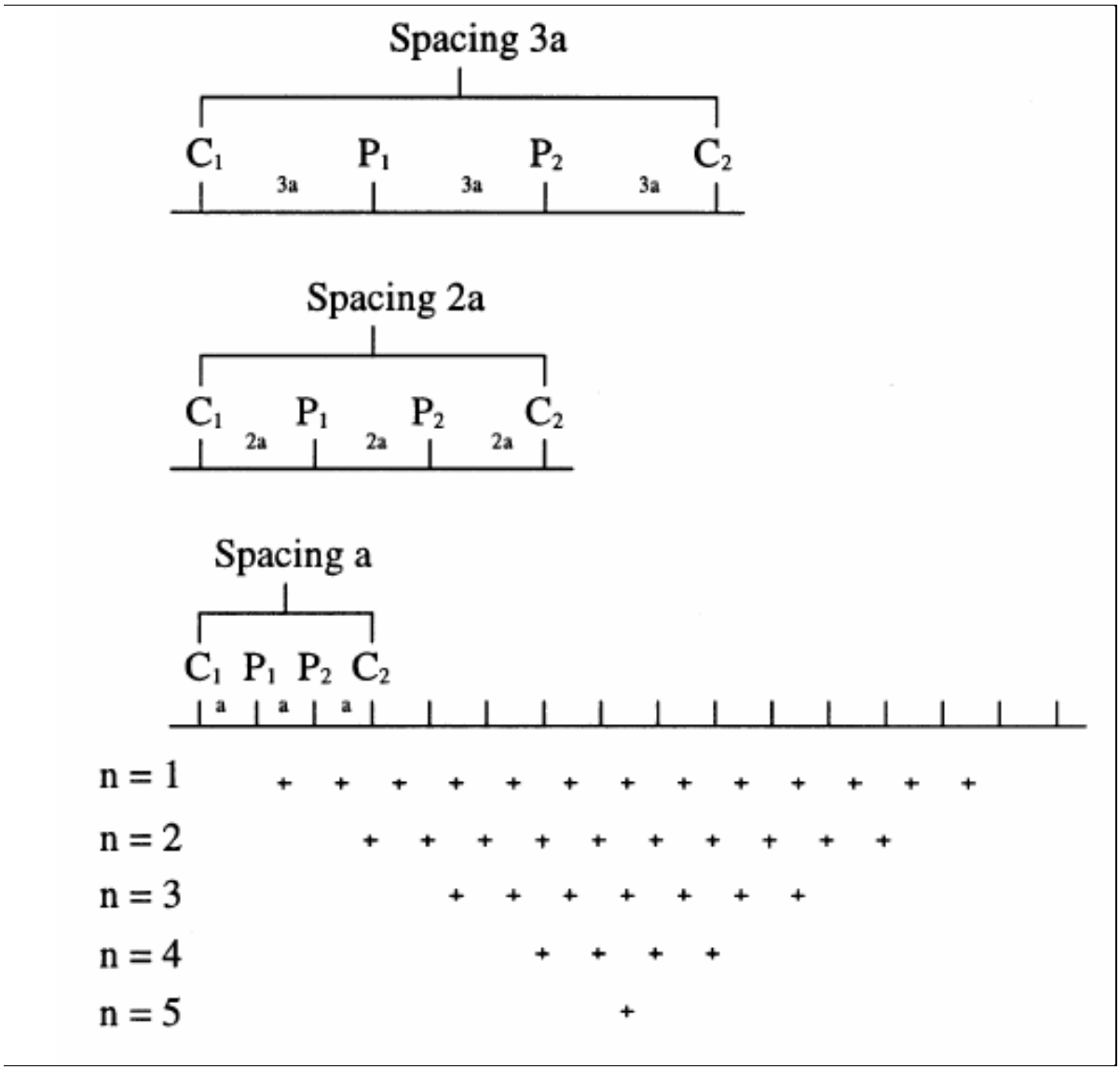

Figure 2.1b: Plotting the resistivity pseudo-section for a Wenner array (ABEM Instruction manual, 2006)

The resistivity profiles were setup using wooden stakes (1.2m in length) which covered the area highlighted by the conductivity anomaly maps shown in the conductivity results section (Fig.2.3). The area highlighted covered an area of 200m (S-N) by 80m (W-E) situated in the western half of the site. Even though the highlighted area measured 80m (W-E), the survey was done for 200m to try and detect changes in apparent resistivity from west to east. The profile lines were setup using two electrode cables measuring 100m in length with an electrode takeout every 5m covering a total length of 200m both in the (S-N) and (W-E). The two electrode cables were connected to an electrode selector (ES-10-64) which then connects to the main display unit. The main unit is powered by an external car battery (14V, 900Ah) which allows for extensive measurement requirements. Stainless

steel electrodes were used to setup the profile lines which are beneficial in reducing noise around the electrodes. To ensure limited probability of noise generated from electrodes separated by a greater a-spacing, the electrodes should be buried about 0.2-0.3m into the ground especially when the ground is dry. Watering the area next to the electrodes will ensure proper contact between the electrodes and the ground (ABEM Instruction manual, 2006). The electrodes were connected to the cable takeout using crocodile clippers. To ensure that the instrument works well for an extended period of time the connectors of the instrument and clippers should be regularly checked for dirt and oxide as this might affect measurement quality later on. The protocol file used to the measure the apparent resistivity is the WEN32X which allows using the roll-along survey with two electrode cables. The protocol files and changes to an already existing protocol file can be added to the instrument using the ABEM Terrameter Utilities software. Other array protocol files (e.g. Schlumberger, Gradient, Pole-Dipole and Dipole-Dipole) can be added to the main unit of the instrument as well. Procedure on changing parameters on the protocol files and adding different protocol files can be reviewed in ABEM Terrameter Instruction manual (2006). The DC resistivity readings taken in the field were in the .xyz format and since the inversion software would not recognize this format, software named Erigraph was used to convert the .xyz into .dat format which could be easily handled by the RES2DINV software. There was not much topography in the south-north lines, however topographic correction was added in the west-east lines using the Schwarz-Christoffel S-C transformation which allows limited use of the damping tool and the iterations for each inversion was maintained on an average of 7 to ensure accurate results (RES2DINV manual, 2006).

2.4 Results and Discussion

The EM conductivity maps are shown first followed by the DC resistivity inversion models (Erigraph and RES2DINV)

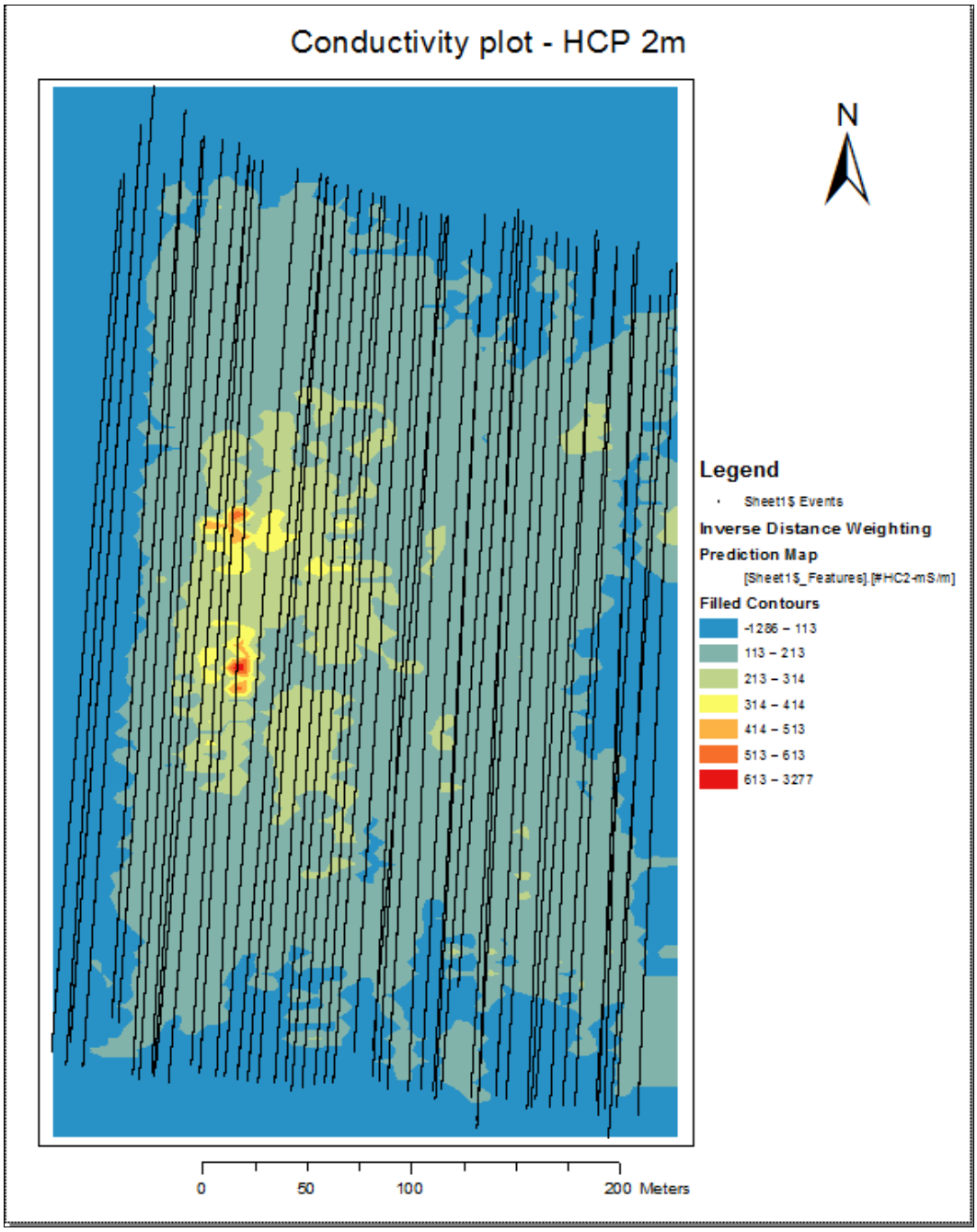

Figure 2.2a: The HCP-2m conductivity map underlain by the survey lines (55 lines)

2.4.1 EM Conductivity Results

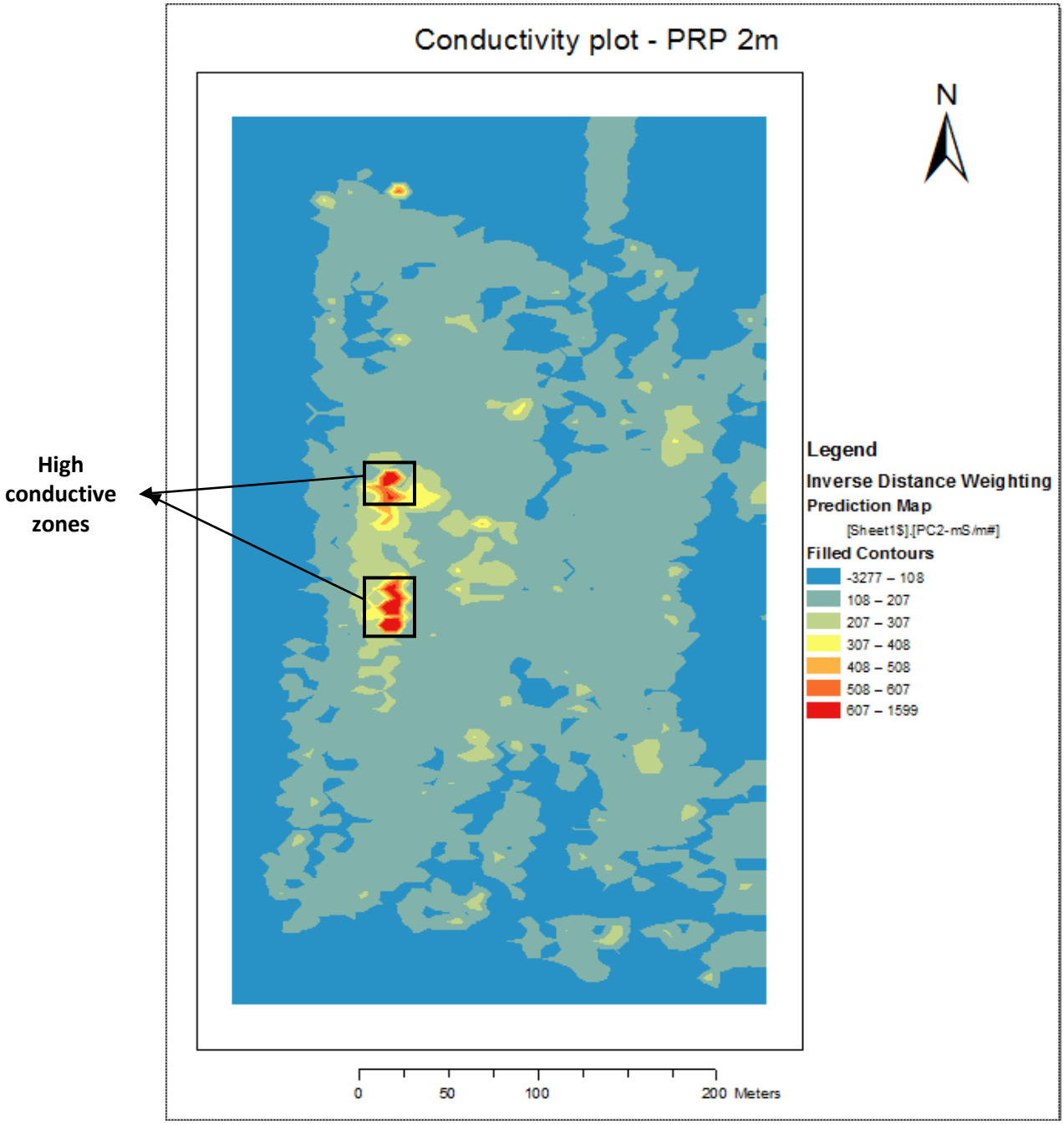

Figure 2.2b: Conductivity map showing an anomalous zone for PRP-2m configuration (mS/m)

The PRP-2m coil separation (Figure 2.2a) shows two areas of high conductivity anomalies at the western portion of the site. The conductivity values range between 607-1600 mS/m. The PRP coil configuration can accurately measure terrain conductivity with high sensitivity to values up to 1600

mS/m. However, with increasing conductivity the DOI and resolution suffers. Thus to improve the interpretation from these conductivity maps both the in-phase and quadrature measurements of HCP and PRP should be considered. The PRP-2m coil separation offers an estimated Depth of Investigation (DOI) of 1.2m.

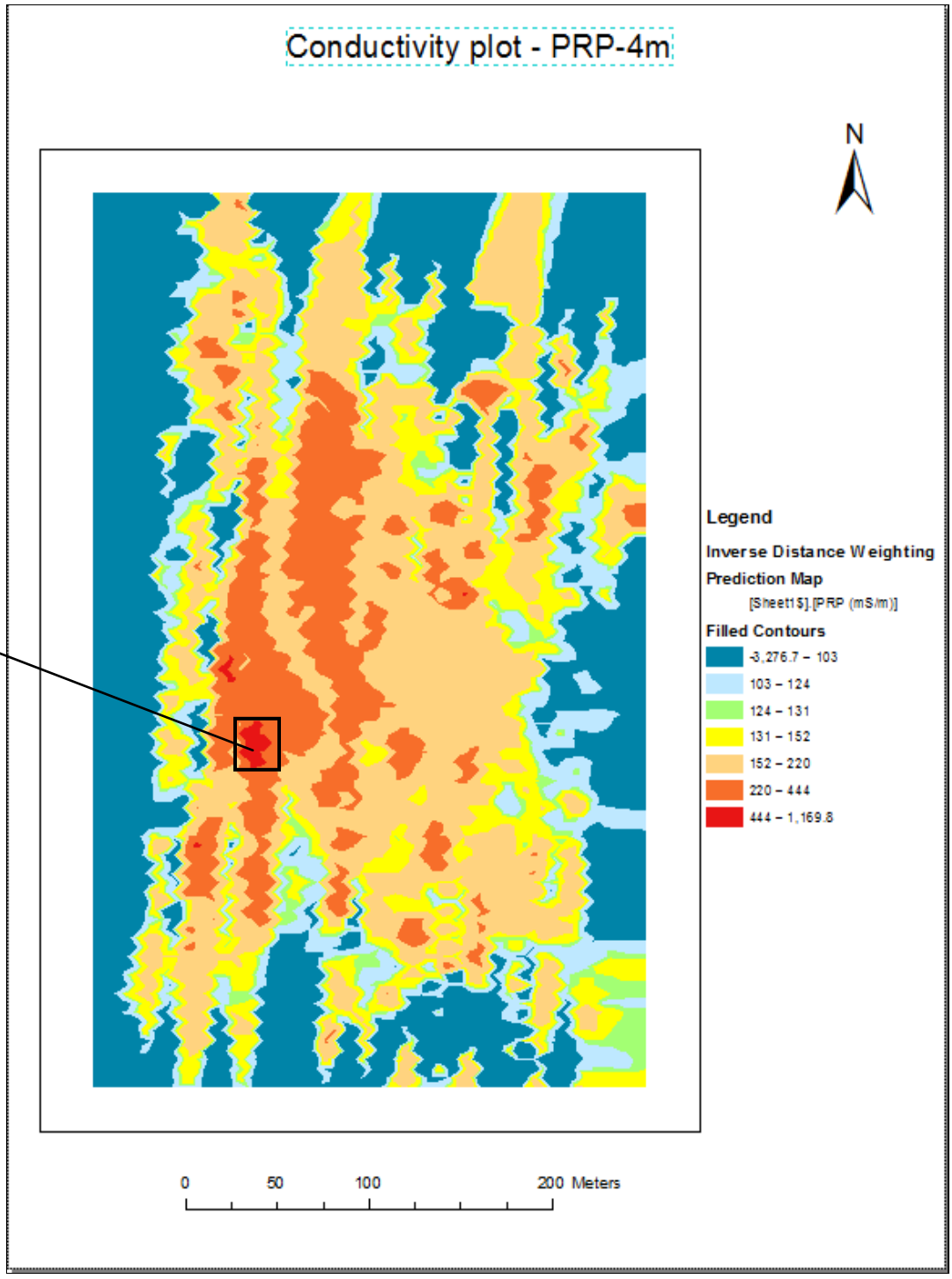

Figure 2.2c: Conductivity map showing an anomalous zone for PRP-4m configuration (mS/m)

The PRP-4m coil configuration (Figure 2.2b) highlights the same area of high conductivity anomaly as seen in the PRP-2m plot with conductivity values measuring between 444-1170 mS/m in the western portion of the landfill site. The general trend of decreasing conductivity from the west to the east is also seen in the PRP-4m conductivity map. This same spot was seen in the PRP 2m coil configuration which confirms the fact that the PRP coil configuration is more suited to detect really high conductive zones. Another reason why the western portion of the landfill appears to be more conductive is because the western cell is older than the eastern cell, which means that the waste in the western cell has been given more time to decay which results in more inorganic ions leaching into the fluid hence increasing its conductivity over time. The estimated DOI for the PRP-4m coil configuration is 2.5m.

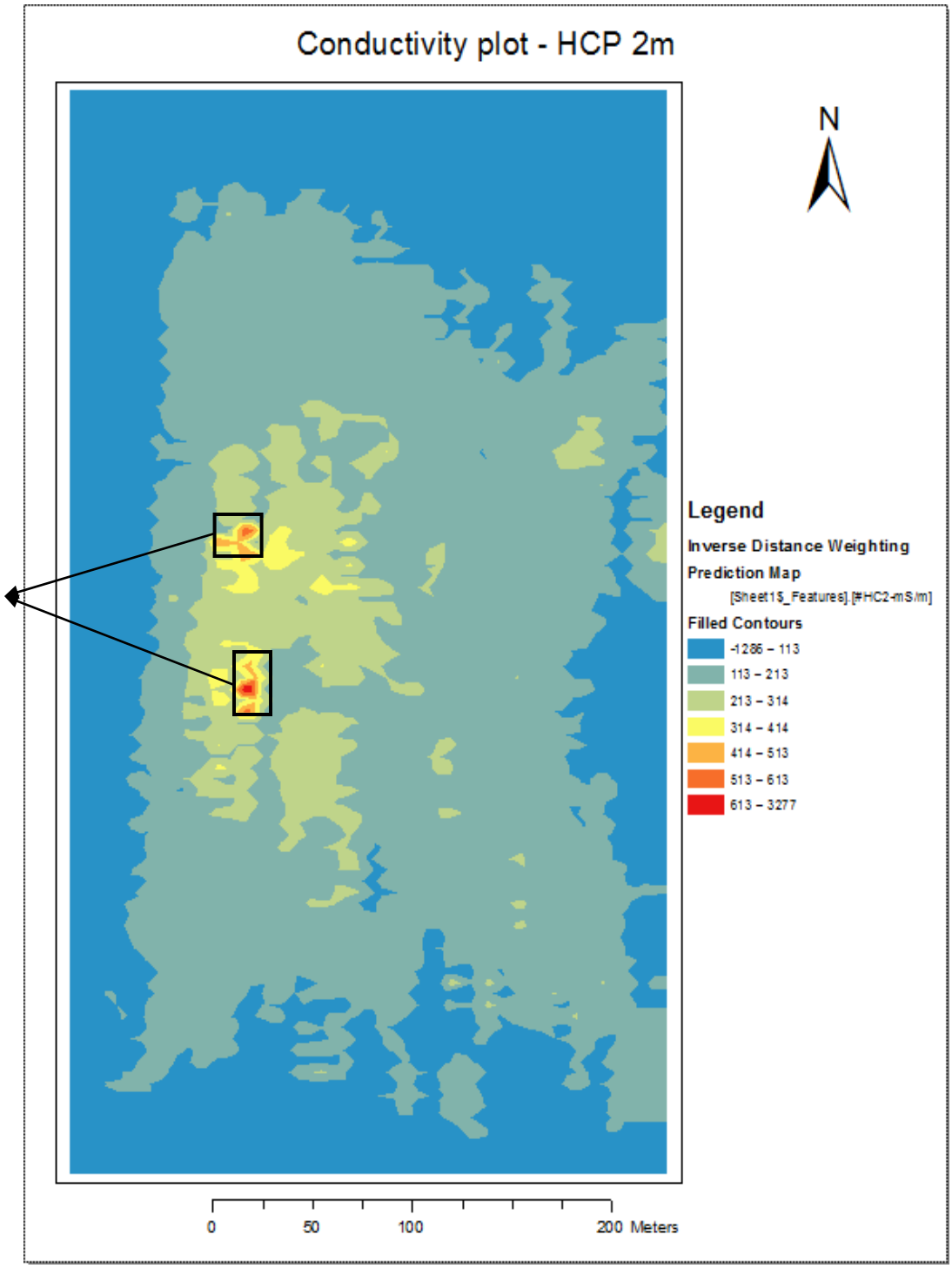

Figure 2.2d: Conductivity map showing an anomalous zone for HCP-2m configuration (mS/m)

As seen from figure 2.2c, the western portion of the landfill has a conductive anomalous zone covering an area of roughly 200m (S-N) by 80m (W-E) with majority of the conductivity values ranging between 213-314 mS/m. Two spots on the northern and southern portion of the anomalous zone show conductivity values ranging between 513-613 mS/m. The waste buried at the landfill site is primarily ICI waste, with the eastern portion of the site being diluted as it draws most of the water to the east due to the presence of the leachate collector system on the southeast. As a result the terrain conductivity values tend to decrease as measurements are taken from west to east. Evidence from monitoring well 6 (eastern portion) and well 8 (western portion) agrees with the conductivity maps. The HCP-2m coil separation gives an estimated DOI of 3m.

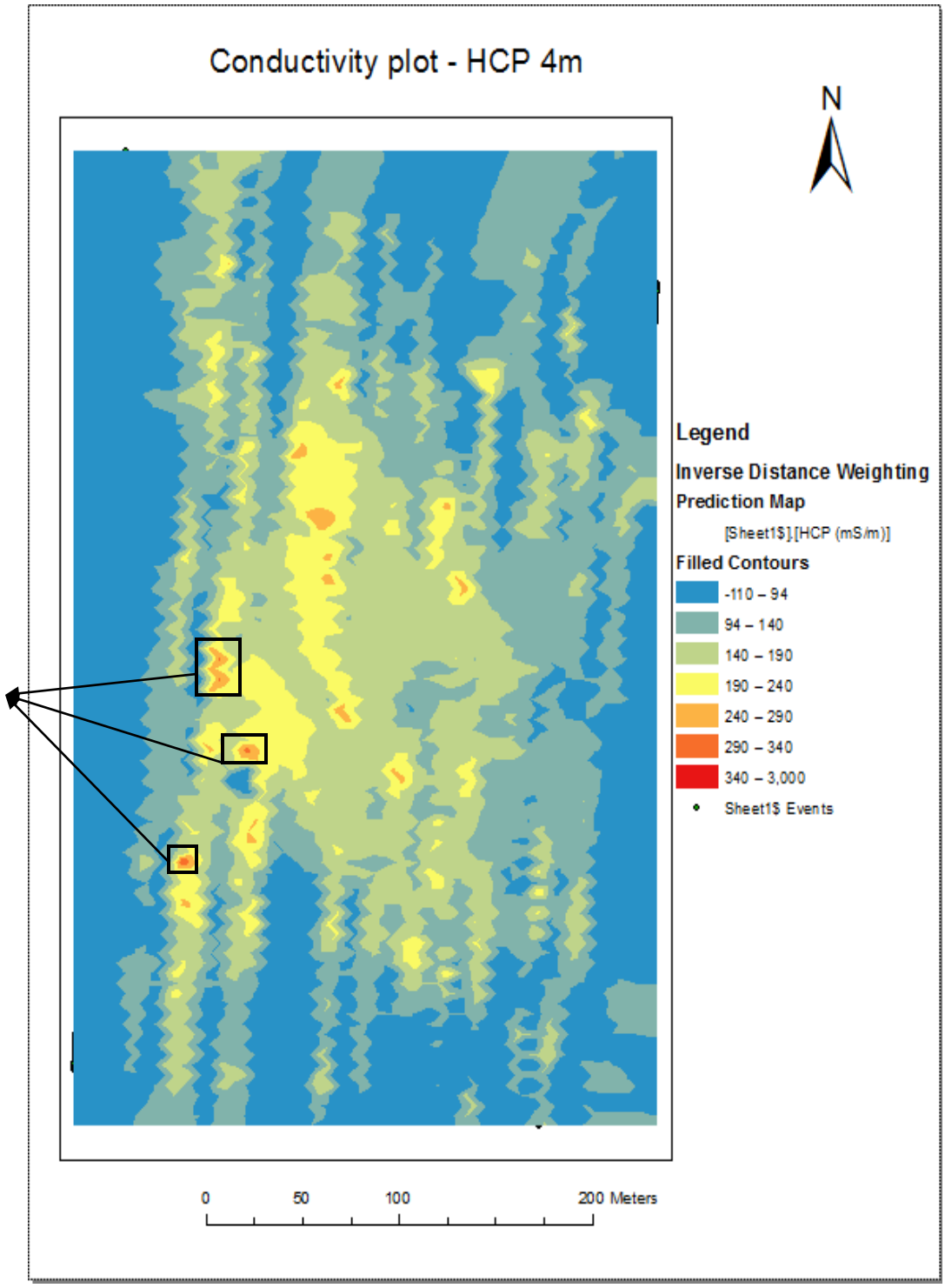

Figure 2.2e: Conductivity map showing an anomalous zone for HCP-4m configuration (mS/m)

The HCP-4m coil configuration (Figure 2.2d) does show the change in terrain conductivity as the measurements proceed from west to east at the landfill site but the two high anomalous zones seen in the HCP-2m and PRP-2m conductivity maps do not show up in the HCP-4m map. One possible reason for this is that while measuring the HCP-4m and PRP-4m coil configuration, the profile spacing was set at 10m instead of the 5m spacing which was used to measure the HCP-2m and PRP-2m coil configuration. This change in surveying procedure could have resulted in the instrument missing the anomalous zone completely and as a result the two high conductivity zones did not show up on the HCP-4m conductivity plots. Another reason could be that the HCP-4m coil configuration is not as sensitive to terrain conductivities higher than 40 mS/m. This means that areas having conductivity measurements greater than 40 mS/m, would not be accurately mapped and the PRP coil configuration would be required to assess the accuracy of the conductivity mapped by the HCP coil configuration. The estimated DOI for the HCP-4m coil configuration is 6m.

2.4.2 DC Resistivity Results

Figure 2.3 shows the profile lines (both S-N and W-E) for the DC resistivity survey on the PRP-4m conductivity map. This figure shows the reasoning behind the selection of the area used to measure the resistivity. Since the western portion of the site shows a higher conductivity variation, the DC resistivity was measured in this area to understand the extent of the underground leachate distribution and to delineate whether or not the contaminants have escaped the upper aquifer region.

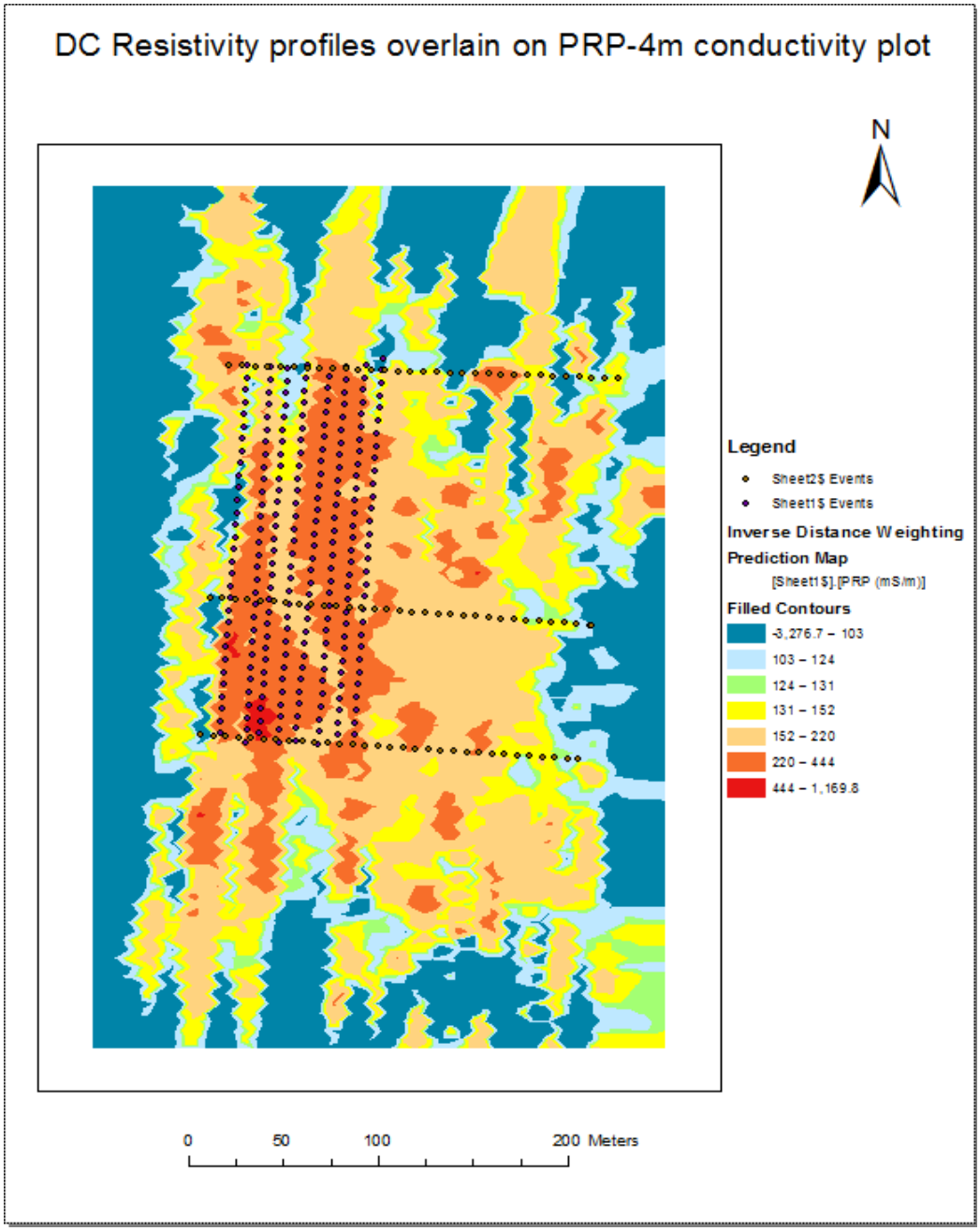

Figure 2.3: DC resistivity survey lines shown on the PRP-4m conductivity map

In Figure 2.3, the dotted lines are the (S-N) resistivity profiles with profile 1 located at the west end and profile 8 located at the east end. The three continuous black lines show the (W-E) profiles with profile 1 located at the south end, profile 4 located in the center and profile 6 located at the north end.

2.4.2.1 South-North Resistivity Profiles

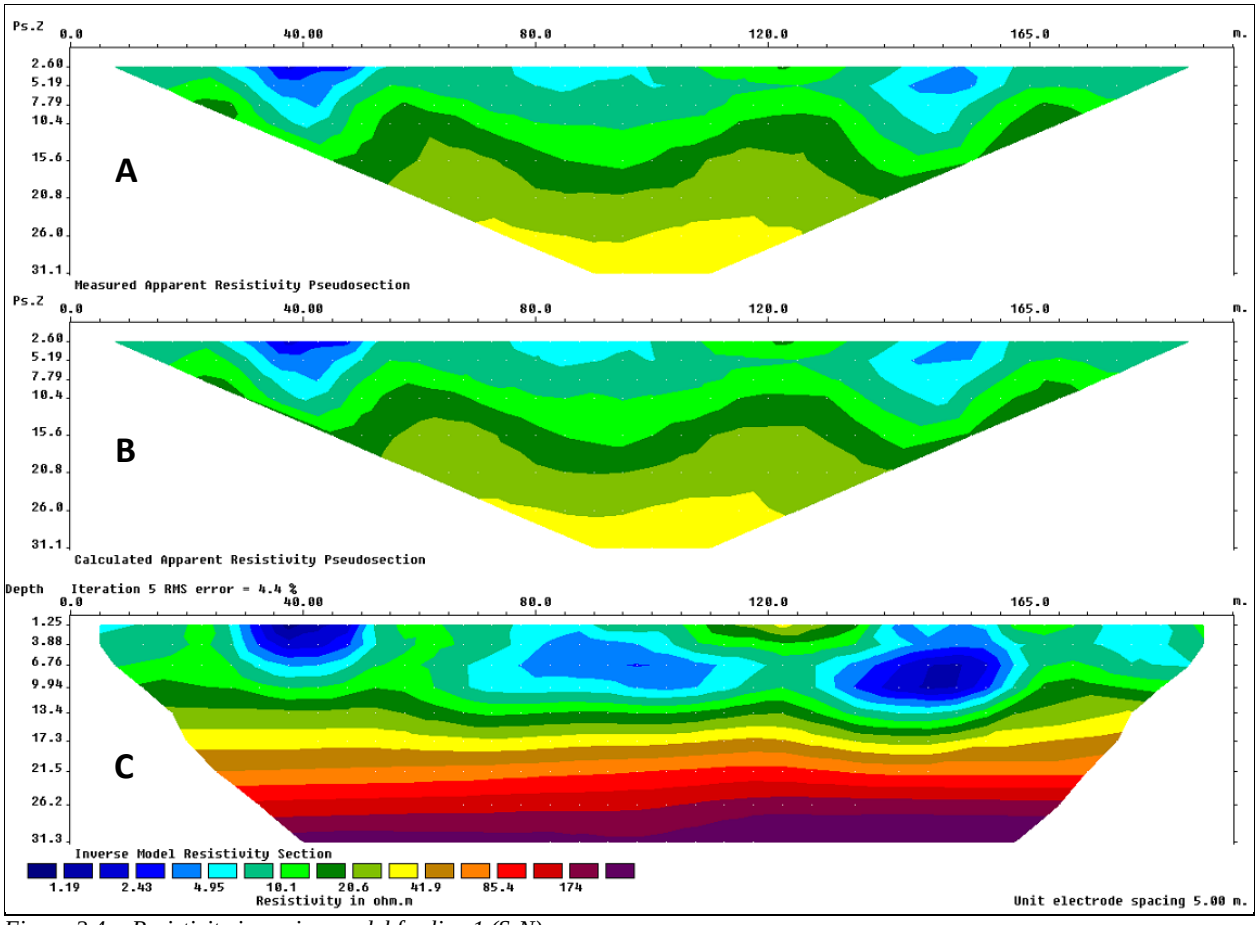

Figure 2.4a: Resistivity inversion model for line 1 (S-N)

The resistivity of the conductive anomalous zone highlighted in Figure 2.3 was tested using the DC resistivity method. Eight profiles were measured in the south-north direction each measuring 200m in length (Figure 2.3). The Wenner-α array with a unit electrode spacing of 5m was used with a DOI of 30m. Figure 2.4a shows the observed resistivity (A), calculated resistivity (B) and the resistivity inversion model (C) of the first (S-N) profile. The interpretations were made using the final inversion model (C). Three low resistivity zones measuring 1.19 – 4.95 Ω*m were measured in the upper 10m of the resistivity subsurface model. The upper 10-12m consists of the upper sand aquifer which is predominantly occupied by waste. The first low resistivity zone is seen between 30-50 m horizontal distance along the profile and extends to just under 7m depth from the surface. This first

low resistivity anomaly extends all the way to the top of the surface which shows a decrease in the functionality of the clay cap. The second low resistivity anomaly is found between 75-110 m horizontal distances along the profile and occurs slightly deeper at 10m below the surface. The resistivity reading at this anomaly is higher (4.95 Ω*m) than the previous anomaly found between 30-50m, the second resistivity anomaly has a greater horizontal spread. The third low resistivity anomaly is found between 135-160 m along the profile, and has the resistivity values between 1.19-4.95 Ω*m. This low resistivity anomaly extends deepest to approximately 13m below the surface, thus likely entering the upper weathered portion of the silt/sand aquitard. The clay cap, which assists in preventing leachate springs at the surface of the landfill berm, is not consistent in thickness along this profile. At around 120m horizontal distance along the profile, the clay cap is thicker than 2.5m however, other areas have either a really thin layer or none at all. This could be due to the extensive erosion or destruction of clay cap due to the washing away of the upper top soil and gravel.

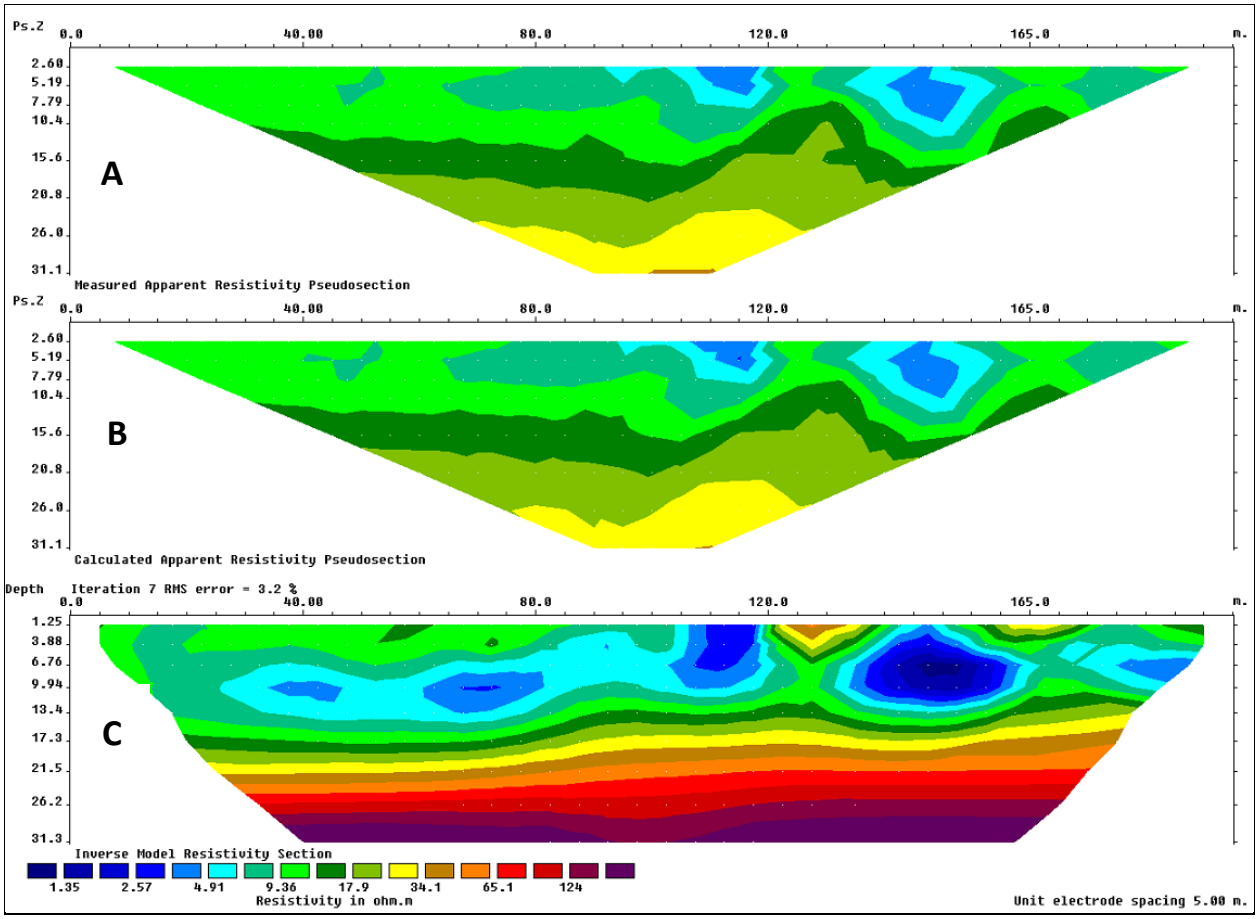

Figure 2.4b: Resistivity inversion model for line 2 (S-N)

Figure 2.4b shows the observed resistivity (A), calculated resistivity (B) and the resistivity inversion model (C) of the first (S-N) profile. The interpretations were made using the final inversion model (C).The second resistivity profile was measured 10m east of the first profile (Figure 2.4b). This resistivity model shows two low resistivity anomalies, one at horizontal distances of 110-120m and the other between 135-165m with both areas measuring apparent resistivity between 1.35-4.91 Ω*m. The first low resistivity anomaly zone shows a horizontal plume migration southwards which agrees well with the direction of flow of water in the upper aquifer. The plume extends 95 m southwards from its origin and due to the process of dispersion the resistivity of the plume increases to just under 5Ω*m. However, there is some evidence of another low resistivity zone found between 60-80m within the plume. This could be the reason why the plume extends that far horizontally. The clay cap found above the waste found at 60-80m is thicker than any other area along the profile; this could be the reason why the waste in this area appears deeper than usual. The second low resistivity anomaly zone at distances between 135-165m extends from the surface to about 13m deep into the upper weathered surface of the silt/sand aquitard. The resistivity measurement in this area measures between 1.35-4.91 Ω*m and there is no evidence of horizontal plume migration in this area of the profile. The area between 120-135 m horizontal distances seems to have a high resistivity anomaly close to the surface. The apparent resistivity in this area measures between 34-65 Ω*m, which means that the clay cap in this area has been laid down with a mixture of sand and gravel which tend to have higher apparent resistivity values compared to clay. Similar to the previous profile, there is no evidence that suggests the plume is migrating into the lower sand aquifer.

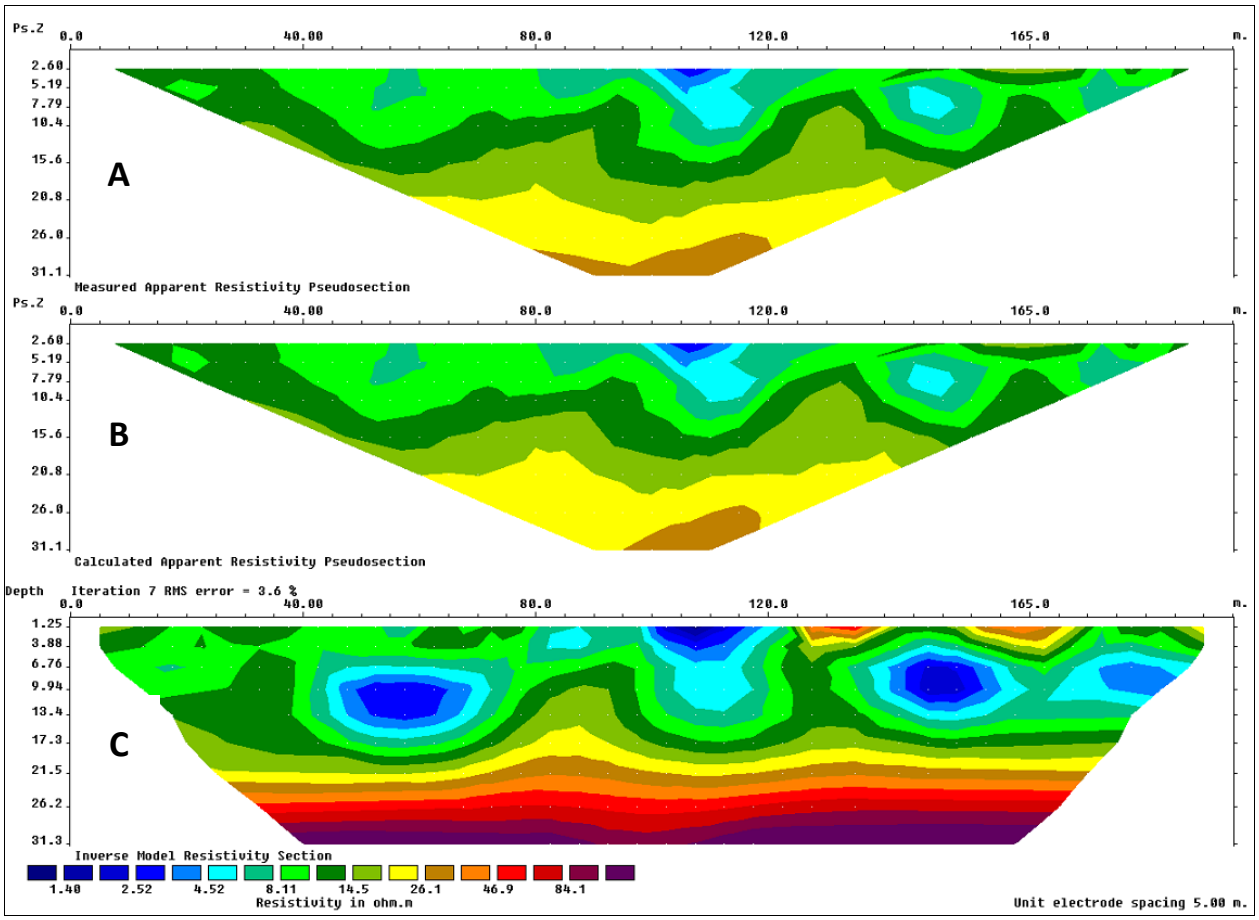

Figure 2.4c: Resistivity inversion model for line 3 (S-N)

Figure 2.4c shows the observed resistivity (A), calculated resistivity (B) and the resistivity inversion model (C) of the first (S-N) profile. The interpretations were made using the final inversion model (C).The third resistivity profile (Figure 2.4c – profile 3) showed three low resistivity anomaly zones, with the first one at 55-65 m with the resistivity measuring between 2.52-4.52 Ω*m. There is not sufficient evidence to prove horizontal plume migration from this low resistivity anomaly however, this anomaly occurs deeper than usual at around 17m below the surface which extends into the silt/sand aquitard. However due to the low hydraulic conductivity of the silt/sand aquitard, the plume does not escape this layer. The second low resistivity anomaly occurs between horizontal distances of 100-120m and along the surface which suggests a lack of cover material in this area. This anomaly shows minor evidence of vertical plume migration into the silt/sand aquitard which extends to a depth of approximately 17m below the surface. There is no evidence to suggest that the plume would be entering the lower sand aquifer due to the lower hydraulic conductivity of the aquitard layer. The third low resistivity anomaly occurs between horizontal distances of 140-155 m and at a depth of 10m below the surface. The apparent resistivity reading at this anomaly is between 2.52-4.52 Ω*m with no strong evidence of horizontal or vertical plume migration. The area between horizontal

profile distance of 125-145m and 155-170m shows a high resistivity anomaly close to the surface measuring between 26.1-46.9 Ω*m which was the area similar to the previous profile and suggests the presence of sand and gravel mixed with the clay cap.

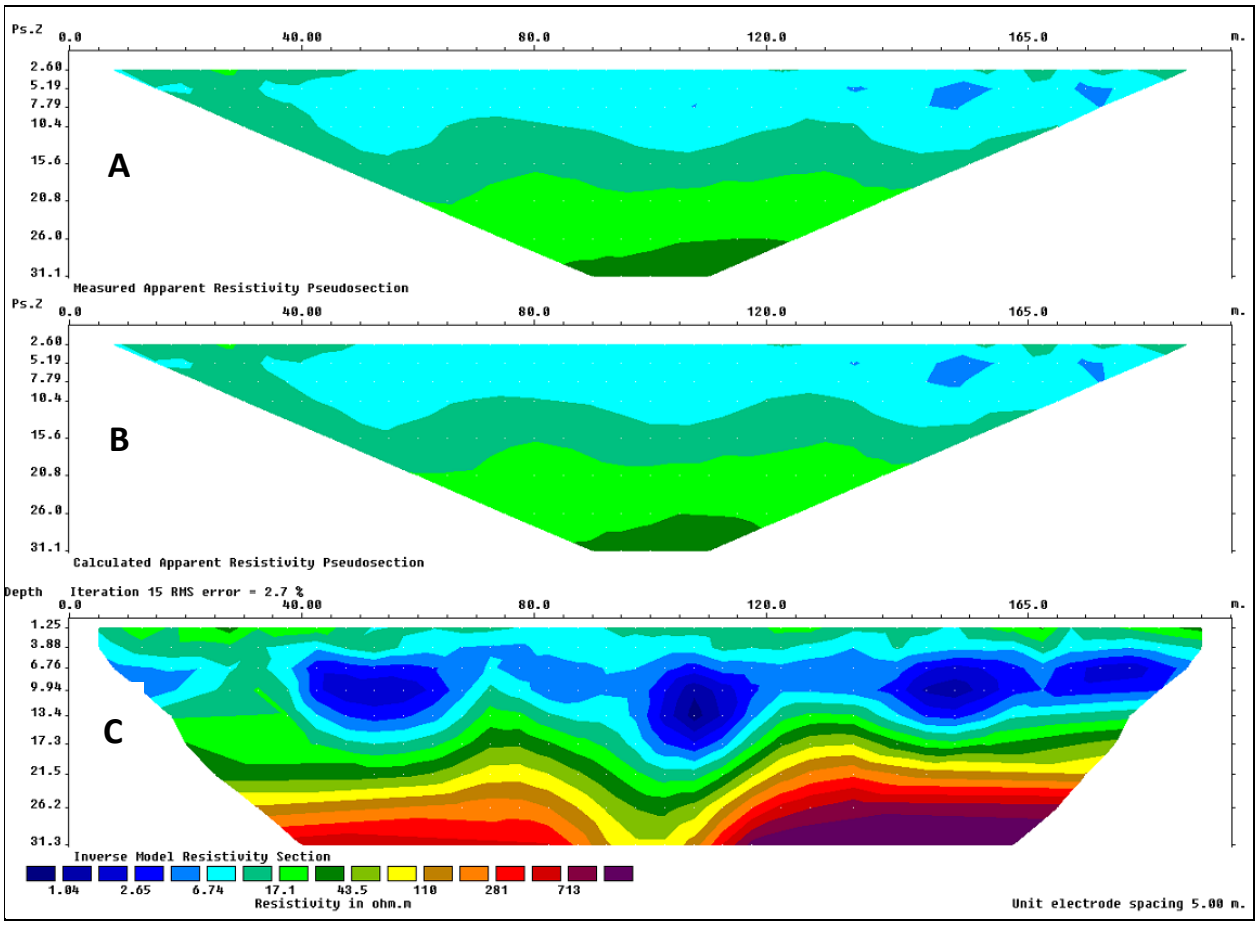

Figure 2.4d: Resistivity inversion model for line 4 (S-N)

Figure 2.4d shows the observed resistivity (A), calculated resistivity (B) and the resistivity inversion model (C) of the first (S-N) profile. The interpretations were made using the final inversion model (C).The fourth resistivity profile (Figure 2.4d) was measured 10m east of the third profile and consists of three low resistivity anomalies. The first one occurs between horizontal distances of 40-70m with its apparent resistivity measuring between 2.94-5.73 Ω*m occurring at a depth of approximately 13.5m below the surface. There is good evidence to suggest plume migration occurring horizontally (southwards) away from the low resistivity anomaly. The second low resistivity anomaly occurs around 85-120 m horizontal distance and at the same depth as the first low resistivity anomaly with strong evidence suggesting horizontal plume migration. The third low resistivity anomaly zone occurs between the horizontal distances of 145-200m at the same depth as the other two anomalies with the apparent resistivity measuring between 1.15-5.73 Ω*m. This low resistivity anomaly also

shows good evidence of horizontal plume migration towards the south. Another important feature to notice here is that none of the low resistivity anomalies occur close to the surface and there is a consistent thickness in the clay cap with little or no evidence of sand and gravel mixing. The silt/sand aquitard appears to thicken around thee 100m horizontal distance mark. This variation in thickness could affect the migration pattern of contaminants from the waste.

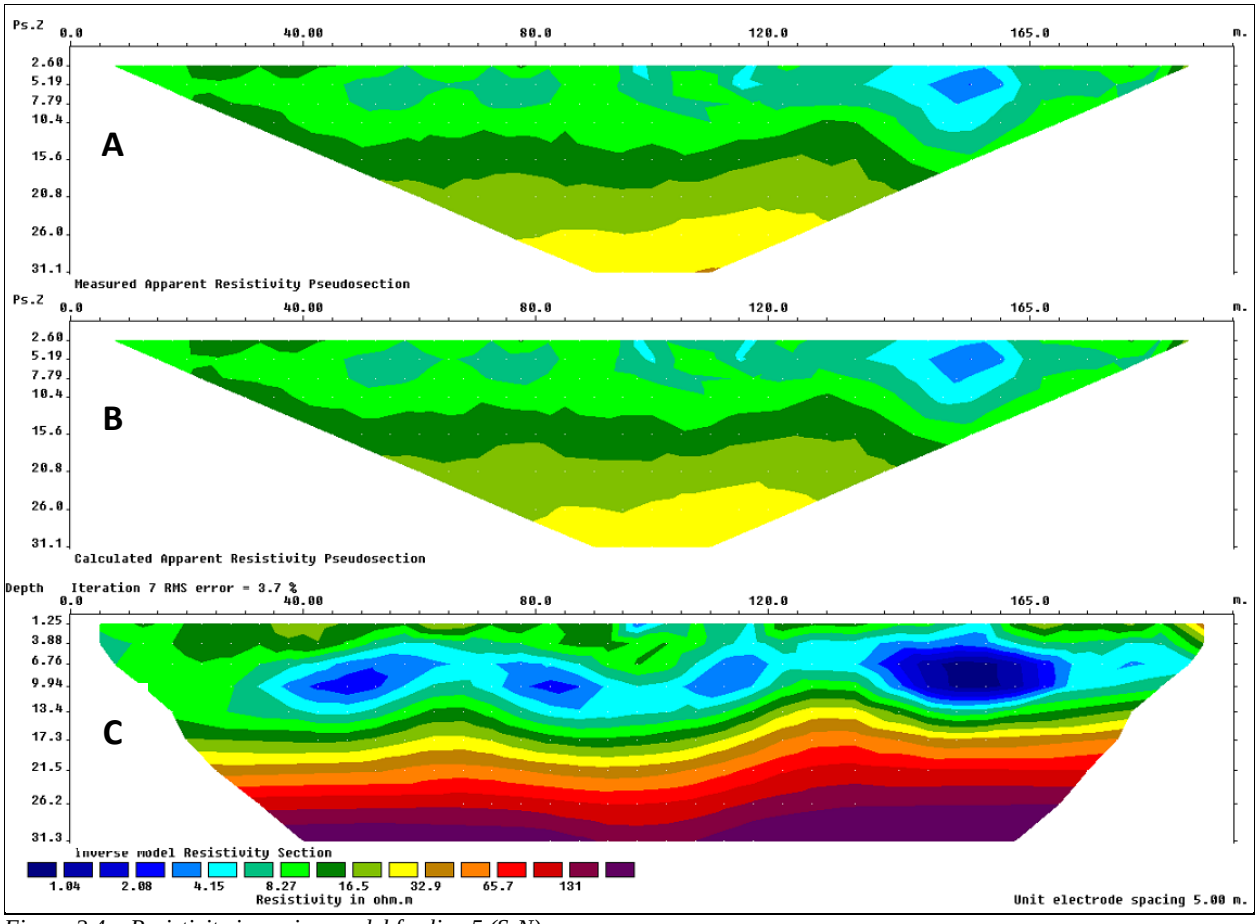

Figure 2.4e: Resistivity inversion model for line 5 (S-N)

Figure 2.4e shows the observed resistivity (A), calculated resistivity (B) and the resistivity inversion model (C) of the first (S-N) profile. The interpretations were made using the final inversion model (C). The fifth profile was measured 10m east of the fourth. This profile has one major low resistivity anomaly and three minor ones. The major anomaly is situated towards the end of the profile between the horizontal distances of 140-170 m at a depth of approximately 12m with the apparent resistivity measurement between 1.84-4.15 Ω*m. This anomaly shows a strong evidence of a contaminant plume emerging and moving south with minor resistivity anomalies occurring between 105-120m, 75-90m and 35-65m horizontal distances respectively. These minor anomalies occupy a smaller area and their apparent resistivity measures in the range of 2.08-4.15 Ω*m. The clay cap

thickness is consistent for majority of the profile except at 95-105m, 110-120m and 150-160m. Similar to the other profiles, there is no evidence in this one that suggests that the contaminant plume is entering the lower sand aquifer.

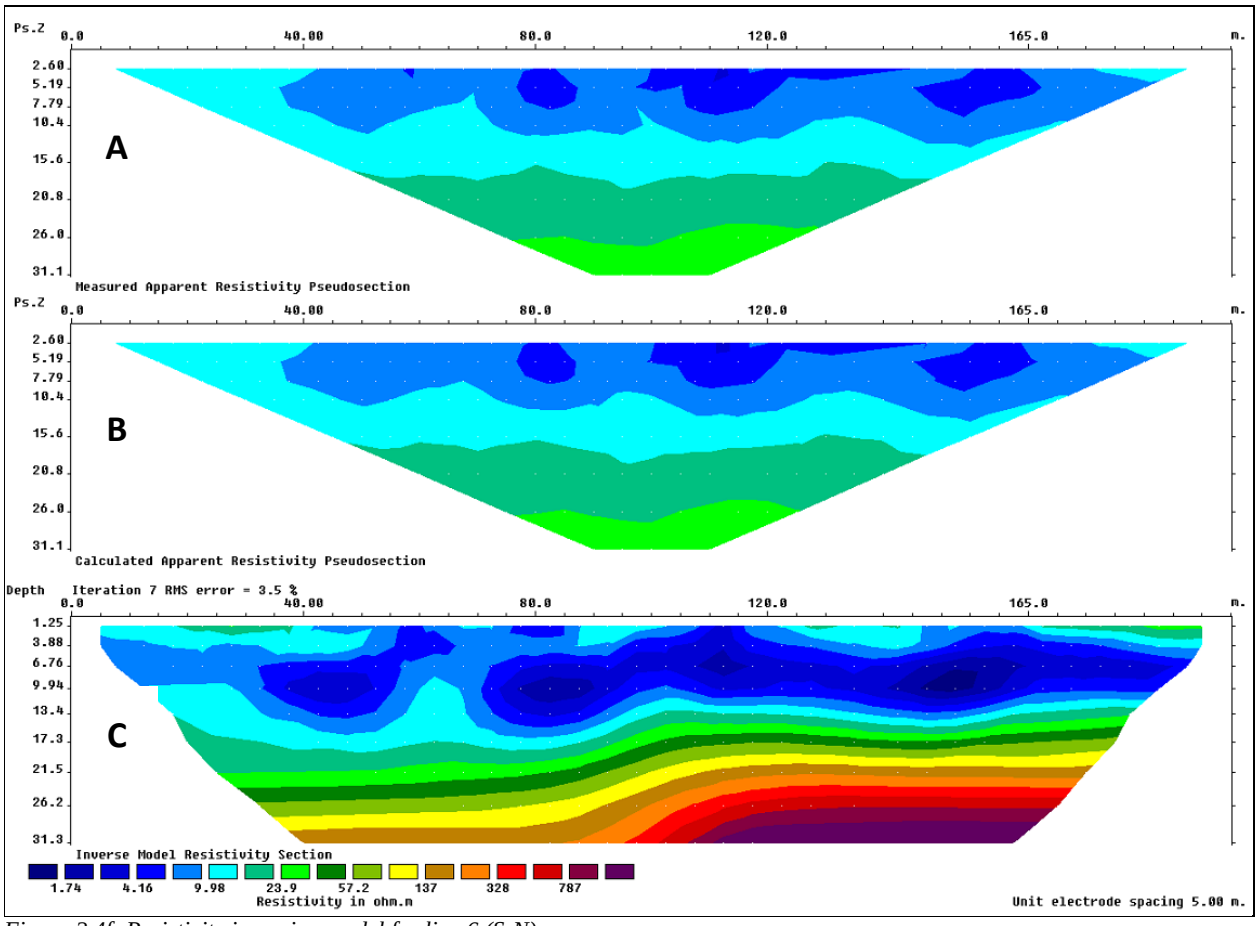

Figure 2.4f: Resistivity inversion model for line 6 (S-N)

Figure 2.4f shows the observed resistivity (A), calculated resistivity (B) and the resistivity inversion model (C) of the first (S-N) profile. The interpretations were made using the final inversion model (C).The sixth profile was measured 10m east of the fifth (Figure 2.4f) and consists of low resistivity anomalies throughout the upper aquifer and the upper weathered portion of the silt/sand aquitard. There are two major low resistivity anomalies seen in this profile, one occurring between horizontal distances of 30-65m and the other being more extensive, covering a larger area between 70-200m. The apparent resistivity measurements for both anomalies range between 1.74-9.98 Ω*m, extending to a depth of 17 m entering the silt/sand aquitard. This is evident by the contaminant plume propagating primarily in the vertical direction due to the low hydraulic conductivity associated with this layer. However, no evidence is seen that suggests that the contaminant plume enters the lower sand aquifer, since the resistivity increases gradually with depth. The clay cap layer across this profile

is virtually non-existent with remnants of the contaminant plume coming up to the surface. However, no evidence of leachate springs was seen while measuring the apparent resistivity of these profiles. Another important feature to note is the reduction in the thickness of the lower sand aquifer which is not visible in the first half of the profile. This could be a local variation in thickness of the lower aquifer, however this cannot be confirmed until the other resistivity profiles are looked at.

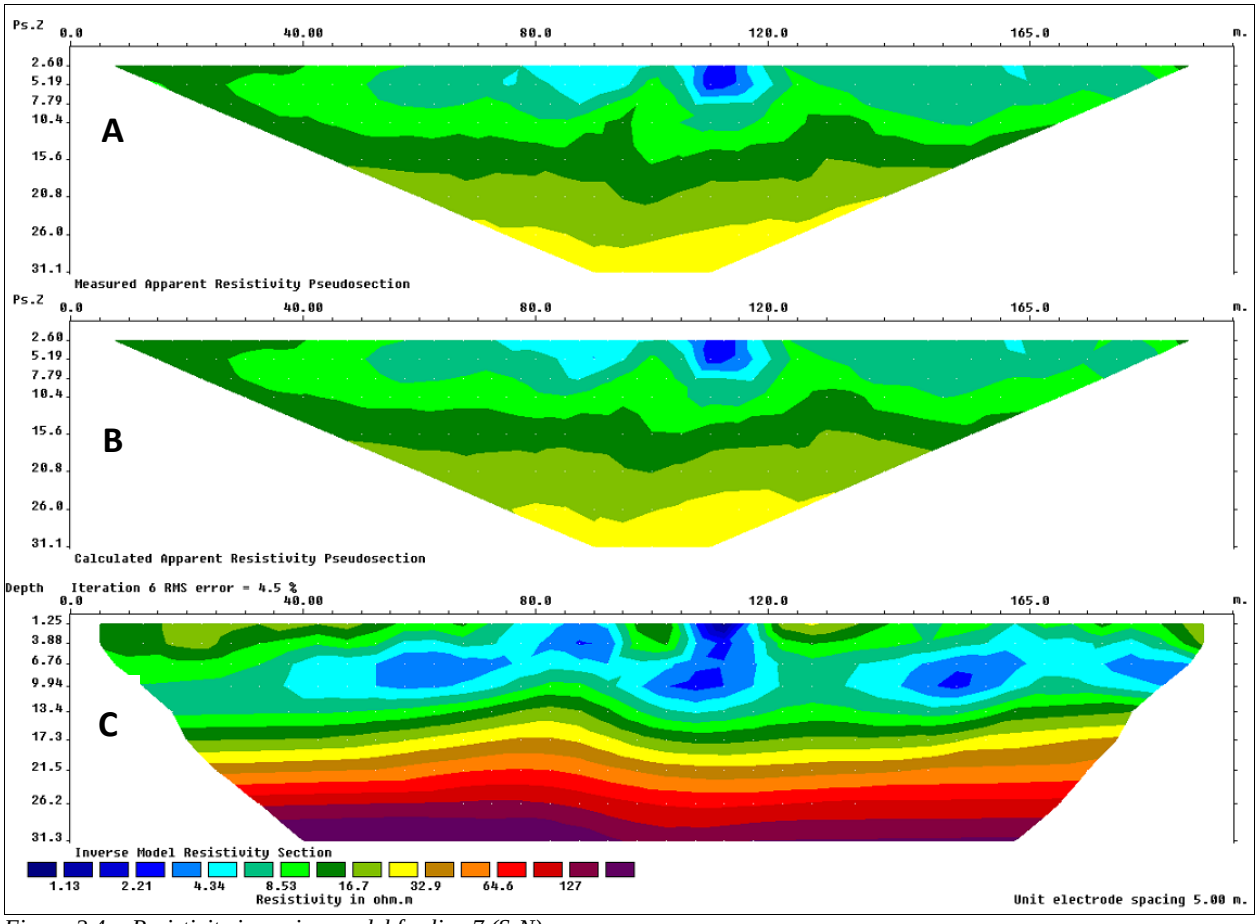

Figure 2.4g: Resistivity inversion model for line 7 (S-N)

Figure 2.4g shows the observed resistivity (A), calculated resistivity (B) and the resistivity inversion model (C) of the first (S-N) profile. The interpretations were made using the final inversion model (C).The seventh profile was measured 10m east of the sixth (Figure 2.4g) and consists of two low resistivity anomalies occupying a large area, the first anomaly occurring at horizontal distances between 105-120m and the other anomaly extending between 135-200m across the profile at a depth of 13m below the surface. The apparent resistivity measurements for both these anomalies measure between 1.13-4.34 Ω*m with the first resistivity anomaly showing strong evidence of a horizontal plume emanating and moving southwards and a small component moving vertically downwards into

the upper weathered portion of the silt/sand aquitard. The second low resistivity anomaly also shows evidence of horizontal plume migration but the spread of contaminants is not as extensive as the first anomaly. The clay cap thickness is consistent for most of the profile except at regions around 80-95m and 105-115m where the plume from the waste reaches the surface, no evidence of leachate ponds or springs were seen in the area. The thickening of the lower sand aquifer in this profile suggests that the variation in thickness shown in the previous profile was a minor local change.

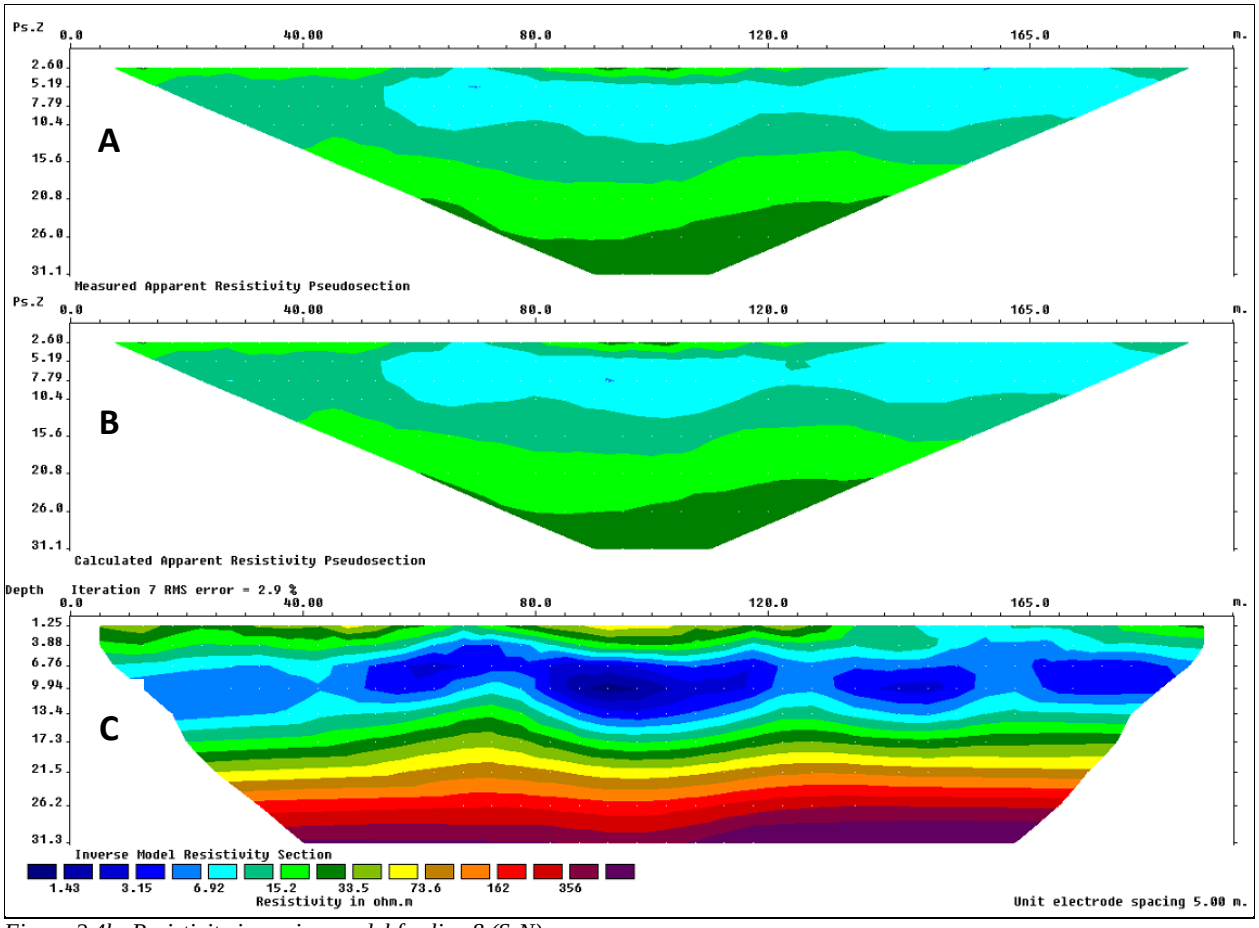

Figure 2.4h: Resistivity inversion model for line 8 (S-N)

Figure 2.4h shows the observed resistivity (A), calculated resistivity (B) and the resistivity inversion model (C) of the first (S-N) profile. The interpretations were made using the final inversion model (C).The final and eight resistivity profile (Figure 2.4h) was measured 10m east of the seventh profile and shows a continuous spread of waste and the emanating horizontal and a small vertical contaminant plume associated with the low resistivity reading. The low resistivity anomaly occurs a depth of approximately 17m extending into the upper weathered surface of the silt/sand aquitard measuring in the range of 1.43-6.92 Ω*m. There is no clear evidence that the contaminant plume is

leaking into the lower sand aquifer. The clay cap thickness in consistent throughout the profile except at 65-70m and 145-160m horizontal distance across the profile where the plume from the waste reaches the surface.

2.4.2.2 West-East Resistivity Profiles

The examination of all the (S-N) resistivity profiles suggests that the presence of waste primarily in the upper sand aquifer with the resulting plume showing a predominantly horizontal direction of propagation. Besides the location and the extent of waste, there is a lack of consistency in the thickness of the clay cap in most resistivity profiles. A few resistivity profiles show good or adequate covering material on top which reduces the possibility of leachate ponding and springs in warmer months. This being said, none of the profiles show any evidence of leachate stains or springs at the landfill. Almost all profiles show primarily a horizontal plume migration southwards which agrees well with the natural groundwater flow in the upper aquifer. The contaminant plume did manage to enter the silt/sand aquitard but due to its low hydraulic conductivity, the plume was contained and did not enter the lower sand aquifer. Three resistivity profiles measuring 200m in length in the (W-E) direction (Figure 2.3) were measured and are discussed below.

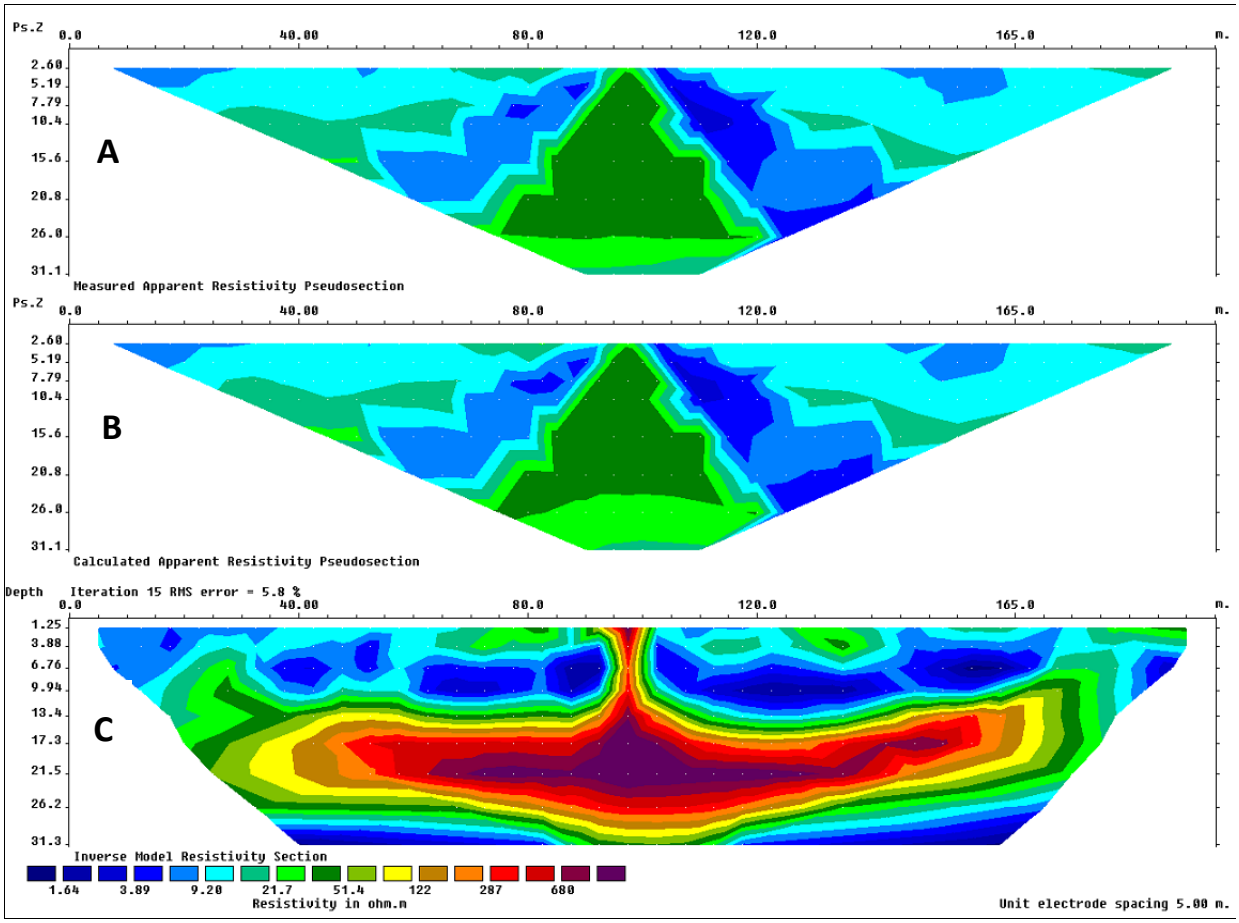

Figure 2.5a: Resistivity inversion model for line 1 (W-E)

Figure 2.5a shows the observed resistivity (A), calculated resistivity (B) and the resistivity inversion model (C) of the first (S-N) profile. The interpretations were made using the final inversion model (C).The first (W-E) resistivity profile was measured on the southern edge of the high conductivity anomaly as seen in Figure 2.3. This purpose of conducting resistivity profiles from the west to east was to measure the change in apparent resistivity from the western to the eastern portion of the site and help compliment the EM conductivity results. The profile measures the resistivity 200m towards the east and by examining the inversion model (Figure 2.5a), the feature that stands out is the high resistivity zone in the middle of the profile which extends as a thin layer from the surface to a depth of about 13m and then spreads out into a disc shaped structure extending down to about 30m which is the upper portion of the lower sand aquifer. This high resistivity zone could be the barrier between the western and eastern portion of the waste cell at the landfill, however this feature was only observed in one profile. If this was indeed the barrier between the east and west waste cell then it should be seen in all the other (W-E) resistivity profiles. The interpretation of this profile was difficult as additional profiles were not obtained. Besides the high resistivity anomaly feature, the profile shows a continuous spread of low resistivity waste material throughout the length of the profile extending to a depth of 12m below the surface. There is no evidence of the apparent resistivity increasing gradually eastwards in this profile as seen in the conductivity maps.

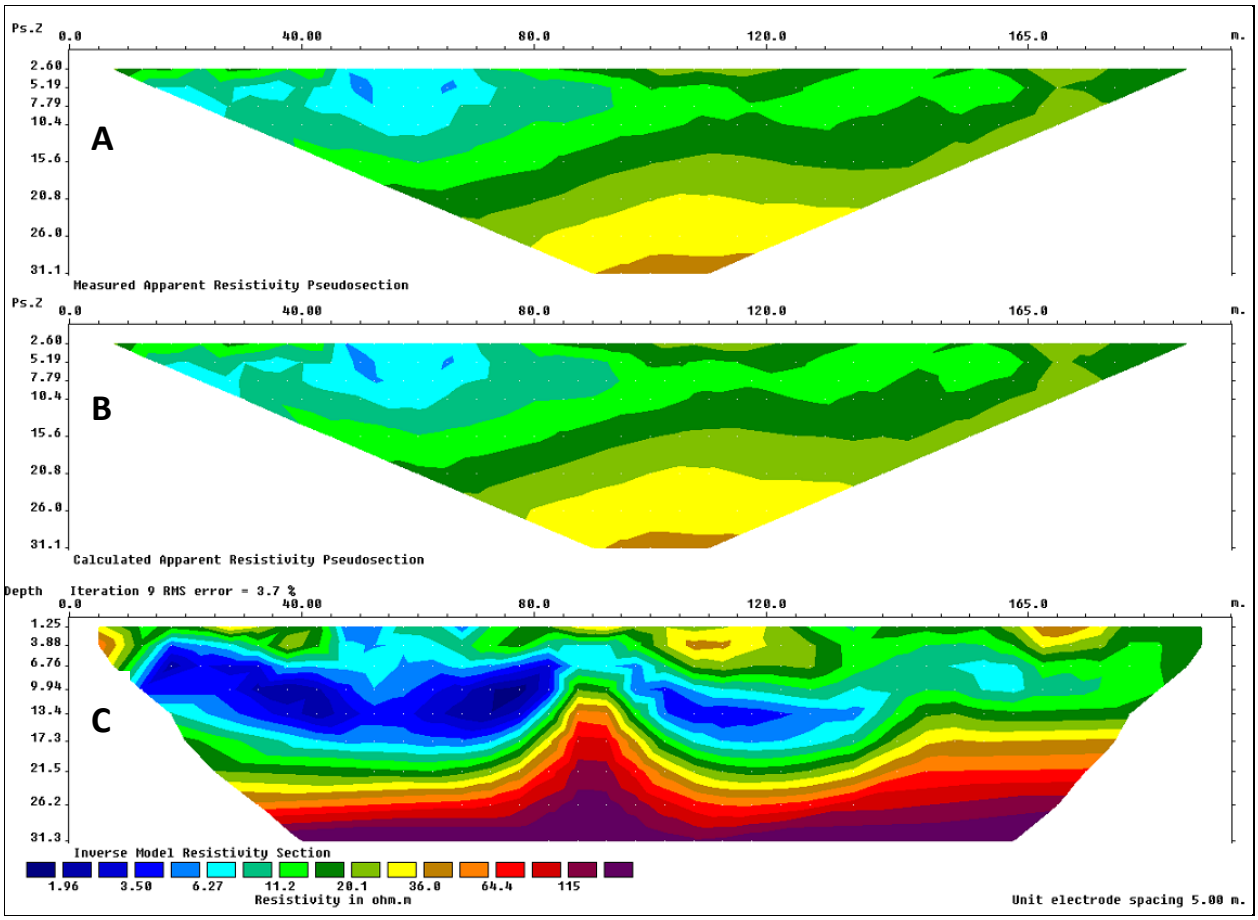

Figure 2.5b: Resistivity inversion model for line 4 (W-E)

Figure 2.5b shows the observed resistivity (A), calculated resistivity (B) and the resistivity inversion model (C) of the first (S-N) profile. The interpretations were made using the final inversion model (C).The second (W-E) profile was measured 105m north of the first profile (Figure 2.5b). This profile shows a low resistivity anomaly covering a relatively large area of 95m from the start of the profile. This low resistivity anomaly extends to a depth greater than 17m below the surface extending into the silt/sand aquitard. There is a contaminant plume associated with this low resistivity anomaly and it has a predominantly horizontal direction in the upper sand aquifer and a slight vertical direction within the silt/sand aquitard, however there is no evidence of the contaminant plume reaching the lower sand aquifer as the resistivity gradually increases with depth. The area occupied by the contaminant plume decreases due to dispersion and diffusion mechanisms and the resulting apparent resistivity increases eastwards. This variation in resistivity agrees well with the conductivity maps plotted for both HCP and PRP 2m and 4m coil configurations. The consistency of clay cap thickness is good for most of the profile except at horizontal distances between 45-70m, where the plume from the waste appears to reach the surface. There is a high resistivity anomaly associated with the upper

clay cap at horizontal distances between 165-180m along the profile measuring at 46.1 Ω*m which suggests a mixture of sand and gravel along with the clay cap material.

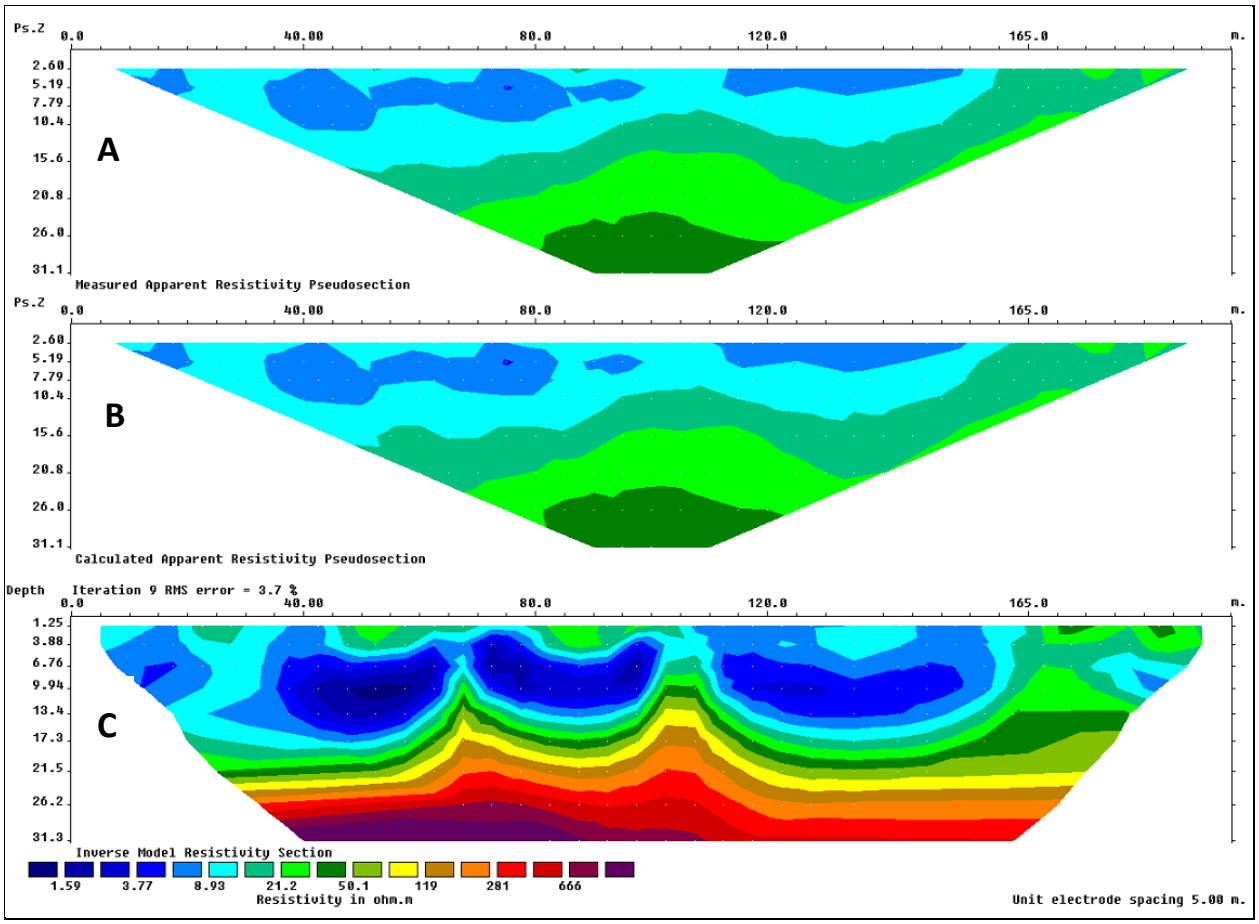

Figure 2.5c: Resistivity inversion model for line 6 (W-E)

Figure 2.5c shows the observed resistivity (A), calculated resistivity (B) and the resistivity inversion model (C) of the first (S-N) profile. The interpretations were made using the final inversion model (C).The third and final (W-E) resistivity profile was measured 70m north of the second profile (Figure 2.5c). This profile shows two low resistivity anomalies (waste) and the associated plume generated at horizontal distances between 30-100m and 115-150m respectively. The waste show up as a low resistivity anomaly measuring between 1.79-8.60 Ω*m and extending to a depth of approximately 17m into the silt/sand aquitard, however no evidence of the contaminant plume entering the lower sand aquifer was observed. The resistivity increased gradually with depth and due to the dispersion and diffusion mechanisms; the apparent resistivity of the contaminant plume increased eastwards which agrees well with the previous profile and with the conductivity maps (Figures 2.2a - 2.2d). The thickness of the clay cap was inconsistent at the following horizontal

locations: 0-20m, 35-45m and 110-150m where the plume from the waste was seen coming up to the surface, however, there was no evidence of leachate stains or springs in the area.

2.5 Conclusions

The main conclusions of this study are as follows:

a) The western portion of the landfill site shows higher terrain conductivity readings as can be seen from figures 1.9 to 2.2. This is due to the fact that the leachate collector system is located on the southeastern portion of the site which results in the most of the water in the upper sand aquifer being drained in the southeastern direction and in the process diluting the waste in the eastern portion of the site.
b) The south-north DC resistivity profiles show the waste occupies most of the upper aquifer with a thin layer of sand in between the waste and the upper weathered portion of the silt/sand aquitard. The plume originating from the waste flows primarily to the south which agrees well with the natural groundwater flow regime in the upper sand aquifer. In some cases, the plume originating from the waste is known to have a vertical component which enters the upper weathered portion of the silt/sand aquitard.
c) There is no evidence of the contaminant plume entering the lower sand aquifer from the DC resistivity surveys in any of the (S-N) profiles. The apparent resistivity of the lower sand aquifer in all the eight (S-N) profiles were high (>100 Ω*m) and since this layer is saturated it can only mean that the water in the lower sand aquifer is low in total dissolved solids (TDS).
d) As discussed in part a of this section, two out of the three (west-east) DC resistivity profiles show clear evidence of the resistivity increasing eastwards due to the presence of the leachate collector system. The plume from the waste has a net horizontal flow and moves eastwards with a small vertical component entering the upper weathered portion of the silt/sand aquitard. However, no evidence of the contaminant plume was found entering the lower sand aquifer.

Bibliography

ABEM (2006). ABEM Terrameter SAS 1000/4000 Instructions Manual.

Allen, A. (2001). Containment Landfills: the myth of sustainability. *Engineering Geology*, 60(1-4), 3-19.

Atekwana, E.A., Sauck, W.A. and Werkema, D.D. (2000). Investigations of geoelectrical signatures at a hydrocarbon contaminated site. *Journal of Applied Geophysics*, 44, 167-180.

Baski, H.A. (1979). Ground-water computer models-intellectual toys, *Ground Water*, 17(2), 177-179.

Beede, D.N. and Bloom, D.E. (1995). Economics of the Generation and Management of Municipal Solid Waste. *National Bureau of Economic Research*, Working Paper Series No. 5116.

Cossu, R. (1994). Engineering of landfill barrier systems; in: Christensen, T.H., Cossu, R. and Stegmann, R. (Eds.), Landfilling of Waste: Barriers, E & FN Sponsors, London (1994), 11-23.

Cossu, R. (1995). The multi-barrier landfills and related engineering problems; in: Christensen, T.H., Cossu, R. and Stegmann, R. (Eds.), Proceedings Sardinia 95, *Fifth International Landfill Symposium*, 2, 3-26.

Derham, J. (1995). The Engineering of (a sustainable) landfill. The Role of Groundwater in Sustainable Development, Proceedings of the *15th Annual Groundwater Seminar, Portlaoise, International Association of Hydrogeologists*, 9.

Driessen, J.H.A., Moura, M.L., Korzilius, E.P.A. and van der Sloot, H.A. (1995). The Sustainable Landfill. In: Christensen, T.H., Cossu, R. and Stegmann, R. (Eds.), Proceedings Sardinia 95, *Fifth International Landfill Symposium*, 1CISA, 15-24.

DualEM Reference Manual (2002). DualEM Inc., 1-50.

Annual Monitoring Report, (2010), 1-22.

Annual Monitoring Report, (2011), 1-22.

Biennial Operations Report (2010), 1-16.

Fullerton, D. and Kinnaman, T. (2002). The Economics of Household Garbage and Recycling Behavior. *New Horizons in Environmental Economies*, Northampton, MA, USA.

Gray, D.A., Mather, J.D. and Harrison, I.B. (1974). Review of groundwater pollution from waste disposal sites in England and Wales, with provisional guidelines for future site selection. *Quarterly Journal of Engineering Geology and Hydrogeology*, 7(2), 181-196.

Jaynes, D.B. (1996). Improved Soil Mapping using Electromagnetic Induction Surveys. *Precision Agriculture*, ACSESS, USA.

Keller, G.V. and Frischknecht, F.C. (1966). Electrical methods in geophysical prospecting. Pergamon Press, New York, USA.

Lanz, E., Jemmi, L., Müller, R., Green, A., Pugin, A. and Huggenburger, P. (1994). Integrated studies of Swiss waste disposal sites: results from georadar and other geophysical surveys. Proceedings of the *Fifth International Conference on Ground Penetration Radar* (GPR '94), Kitchener, Ontario, 1261-1274.

Loke, M.H. (1999). A practical guide to 2D and 3D surveys. *Electrical imaging surveys for environmental and engineering studies*, 8-10.

McNeill, J.D. (1980). Electromagnetic Terrain Conductivity Measurements at Low Induction Numbers, Geonics.

Orlando, L. and Marchesi, E. (2001). Georadar as a tool to identify and characterize solid waste dump deposits. *Journal of Applied Geophysics*, 48, 163-174.

Osiensky, J.L. (1995). Time series electrical potential field measurements for early detection of groundwater contamination. *Journal of Environmental Health*, 30(7), 1601-1626.

Porter, R. (2002). The Economics of Waste, Resources of the Future, Washington, D.C., USA.

Quadrio-Curzio, A., Prosperitti, L. and Zoboli, R. (1994). The management of municipal solid waste in Europe. *Economic, Technological and Environmental Perspectives*, 5.

RES2DINV manual (2006). Geoelectrical Imaging 2D and 3D, Geotomo Software, 1-50.

Reynolds, J.M. (1998). An Introduction to Applied and Environmental Geophysics, Wiley, Chichester.

Rogers, P.P. (1983). Book review of: Analyzing natural systems: analysis for regional residuals-environmental quality management, EOS, 64(25), 419.

Sharma, P.V. (1997). Environmental and Engineering Geophysics, Cambridge University Press, New York, USA, 207-237.

Tchobanoglous, G., Thiesen, H. and Vigil, S.A. (1993). Integrated Solid Waste Management: engineering principles and management issues. McGraw Hill, New York, 978.

Telford, W.M., Geldart, L.P. and Sherrif, R.P. (1990). Applied Geophysics, Cambridge University Press

Tezkan, B. (1999). A review of environmental applications of quasi-stationary electromagnetic techniques. *Surveys in Geophysics*, 20, 279-308.

Thomas, H.E. and Leopold, L.B. (1964). Groundwater in North America. *Science*, 143, 1001-1006.

Ulrych, T.J., Lima, O.A.L. and Sampaio, E.E.S. (1994). In search of plumes: A GPR odyssey in Brazil. *64th Annual International Meet, Society of Exploration Geophysicist*, Los Angeles, USA, 569-572.

Wait, J.R. (1962). A note on the electromagnetic response of a stratified earth. *Geophysics*, 27, 382-385.

Chapter III

Groundwater Modeling

3.1 Introduction

Modeling can be defined as an approximation to real world field situations. It's a simplistic approach to explain real-world complicated problems. Although modeling helps scientists to arrive at a conclusion with a respectable degree of accuracy, it cannot be used as a stand-alone tool for research. Thus, field work is required to assess the accuracy of the results and, if these results satisfy the prediction of the model for an extended period of time, the model is accepted for that particular location (Anderson and Woessner, 1992). Before a model can be accepted for a particular site, the model needs to be calibrated to simulate conditions observed in the aquifer. This step can be performed by comparing the model results to the groundwater elevation available for the region under investigation. The next step would be to verify the model with the natural conditions of the aquifer to ensure that the predictions are accurate. To ensure proper model verification, a transient model is simulated to match the historical changes in the aquifer due to external stresses such as pumping. To guarantee accurate results from groundwater modeling, and to ensure proper calibration and verification, the model parameters have to be constantly altered. In case of physical models, this would require constantly rebuilding the model whenever there is a change in either flow or material properties. Thus numerical models have been developed which allow changing these conditions with relative ease and with minimal investment of time and money (Fetter, 1994). The steps involved in developing and simulating the model are shown in figure 3.0 (Modified from Pinder, 1984).

Studies related to groundwater modeling to predict the extent of contaminants at landfill sites have not been attempted in the Windsor and Essex County region for over a decade (Personal comment - Dr. Bolisetti, 2011). Due to the uncertain behavior of contaminants in such closed settings, it becomes critical to simulate the flow of contaminants through aquifers over time. The model requires the input of a wide array of information from regional geology to groundwater flow patterns. The closer the model approaches to real-world situations, the more complicated its simulation becomes, thus it is imperative to find a common ground between accuracy of simulation and computation time. The simulation of contamination in aquifers was studied for 1, 10, 100, and 1000 year(s).

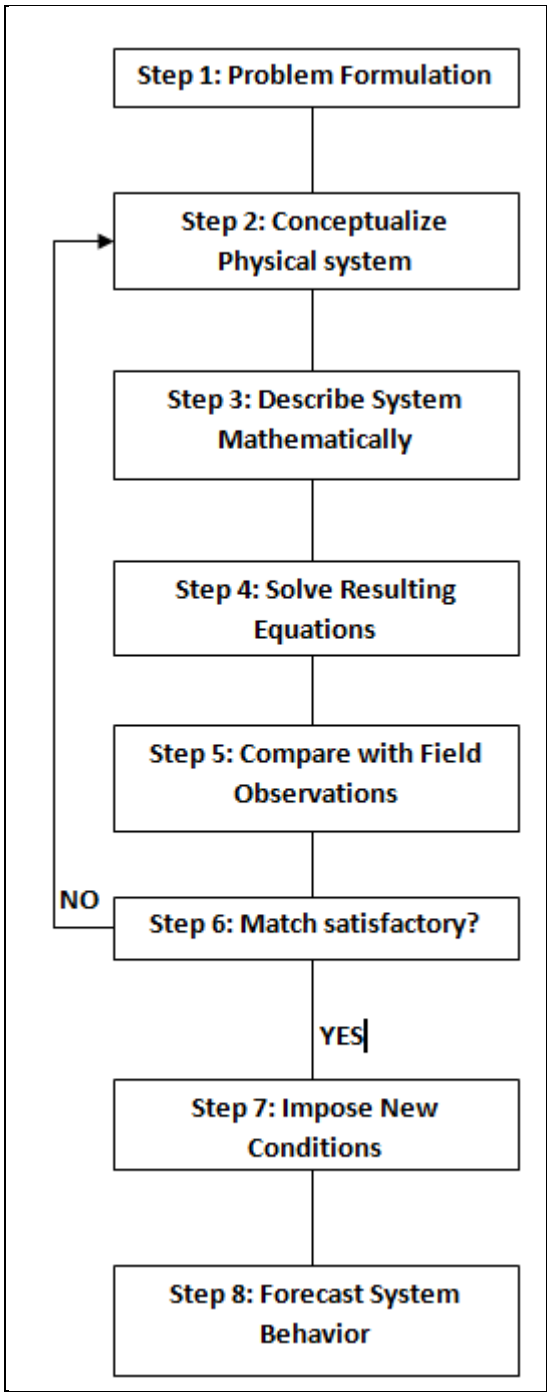

Figure 3.0: Flow chart showing the steps involved in the development and simulation of model (Modified from Pinder, 1984)

There are many authors who refute the use of modeling, regarding it as a cumbersome, inaccurate, highly dependent ordeal (Chargaff, 1978; Baski, 1979; Rogers, 1983). On the other hand, numerous authors have called the use of models a boon to groundwater modeling studies by assisting scientists in efficient and accurate calculations along with outlining proper management strategies (Thomas and Leopold, 1964; Darr, 1979; Hamilton, 1982; Friedman et al. 1984). Applications of groundwater modeling studies vary from assessing groundwater flow patterns, solute transport and heat transport in porous or fractured media (Prickett and Lonquist, 1971; Trescott, Pinder and Larson, 1976; Pinder and Gray, 1977; Konikow and Bredehoeft, 1978; Mercer and Faust, 1980; Wang and Anderson, 1982; McDonald and Harbaugh, 1984).

Analytical models require minimum amount of information and can be solved easily with the help of a computer. Analytical models cannot take into account the effect of moving boundary conditions and complexities in geology. They can simulate homogenous/isotropic media with exact solution from the governing equations. Numerical models, on the other hand are to be used in complex situations (boundary conditions, changing aquifer thickness, solute concentration changes etc.) and require more time and powerful software and computers for simulation (Fetter, 1994). Numerical models can be defined by either the a) Finite-Difference method or by b) Finite-Element method. The finite-difference method uses a rectangular network of nodes to form a grid that covers the model area. The finite-difference method is further subdivided into two different grid formations: a) Block-centered and b) Mesh-centered grids as can be seen in figure 3.1a.

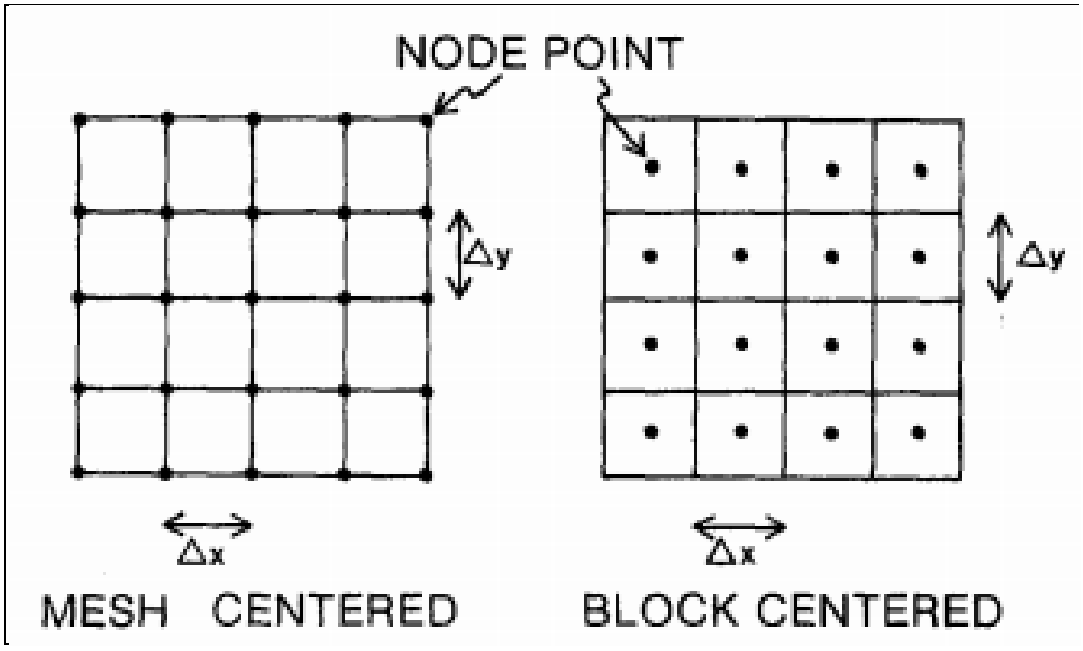

Figure 3.1a: Finite-Difference grid showing mesh-centered and block-centered mesh (Faust and Mercer, 1980)

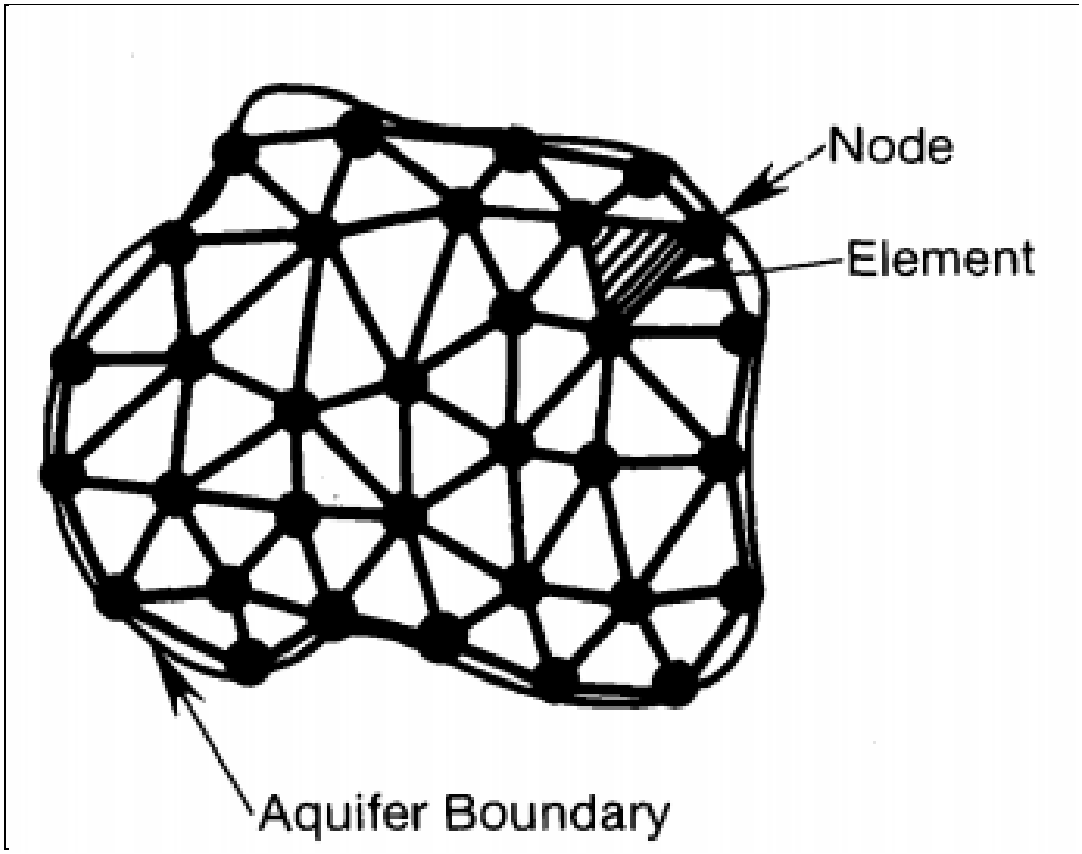

Figure 3.1b: Finite-Element grid showing nodes and elements in triangular mesh (Faust and Mercer, 1980)

The node points in Figure 3.1a show values of unknown parameters such as hydraulic heads, storativity, transmissivity and many others which are calculated based on the governing equations. A mesh-centered grid is used when a head is specified (Dirichlet condition) at the edges of the model and a block-centered model is used when a flux is specified (Neumann condition) across a boundary (Fetter, 1994). However, this study uses the finite-element grid which has polygonal cells (usually triangular) covering the model area as can be seen in figure 3.1b. The nodes are areas of unknown head values which can be calculated by interpolation. The mathematics behind the finite-element method can be found in Wang and Anderson, (1982) and will not be discussed here. Finite-element mesh grids are used to model complex moving boundary conditions and contaminant transport models (Wang and Anderson, 1982) as discussed in this study.

3.2 Conceptual Model

There were two conceptual models described in this study and they were developed and constrained by the results obtained from the geophysical surveys at the site. The models were designed in a finite-element software programmed using C language called Finite-Element Flow (FEFLOW) to conduct a 2D transient flow + transient mass simulation. The conceptual models were designed in the graphic user interface (GUI) using the polygon and line function keeping the scale of the models in mind. Figure 3.2a and 3.2b show the (S-N) and (W-E) conceptual models respectively along with description on the location of the upper sand aquifer, lower sand aquifer, silt/sand aquitard and the clay cap.

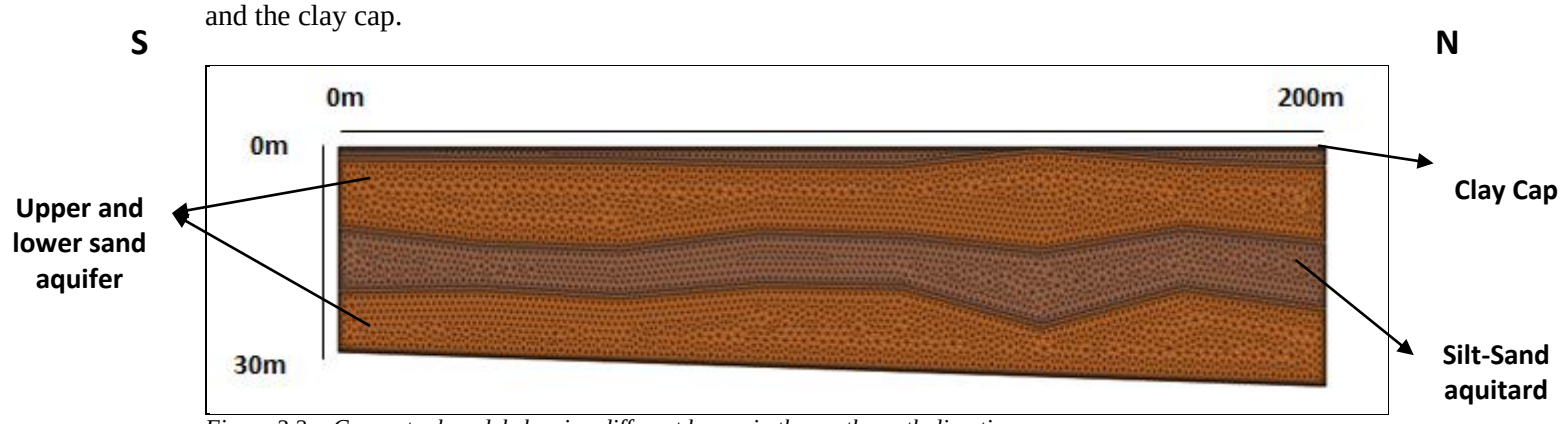

Figure 3.2a: Conceptual model showing different layers in the south-north direction

The above conceptual model (Figure 3.2a) was created to predict contaminant flow within the layers in the south-north direction. As can be seen from the figure, the two light brown layers are the upper and lower sand aquifers respectively. The middle (dark brown) layer is the silt/sand aquitard and the uppermost thin layer on top is the clay cap. The length and depth of the model as constrained from the DC resistivity surveys were kept at 200m and 30m respectively.

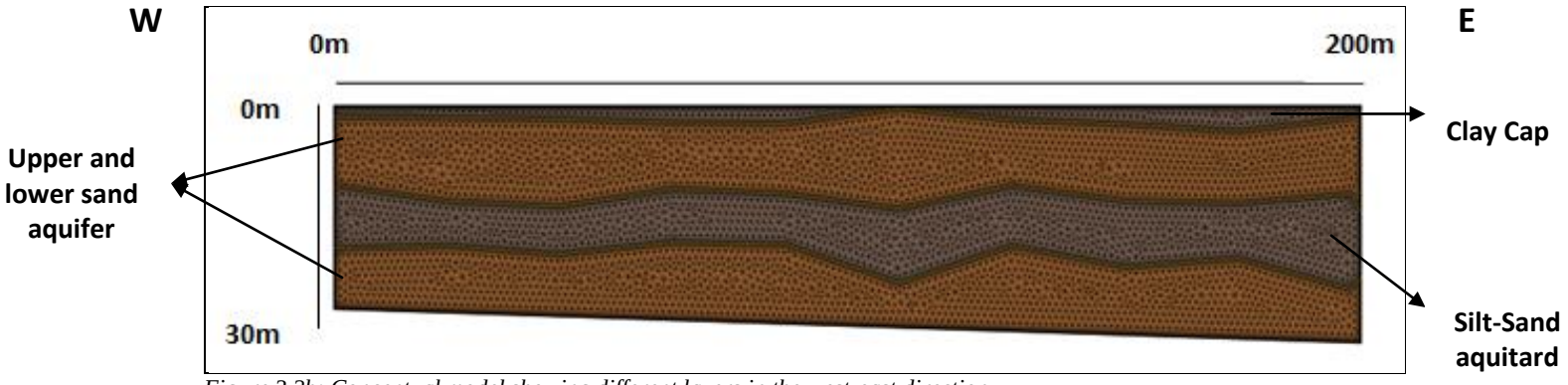

Figure 3.2b: Conceptual model showing different layers in the west-east direction

The conceptual model for the (W-E) direction is similar in comparison with the (S-N) model with slight differences in thickness seen in the silt/sand aquitard. The material properties of the aquifers and aquitard remain the same.

Dirichlet (first-type) boundary conditions were assigned to the southern and northern boundary (S-N models) and western and eastern boundary (W-E models). Neumann (second-type) boundary conditions were assigned to the bottom (no fluid-flux) and top (fluid-flux to resemble precipitation) boundaries. Initial conditions for flow in both the upper sand aquifer and the lower sand aquifer were determined based on the data from the monitoring wells. A preliminary fluid-flow model was run to verify the results of the simulation with the natural groundwater flow pattern in the layers at the landfill. The boundary and initial conditions for mass were set at three different locations on the (S-N) models (Figure 3.3a) of the upper aquifer and in one location on the (W-E) models (Figure 3.3b) of the same layer measuring at 200mg/L. Material properties for flow including transmissivity, conductivity, anisotropy of conductivity, specific storage and density ratio were assigned to different hydrostartigraphic units and material properties for mass transport including aquifer thickness, porosity, molecular diffusion, longitudinal dispersivity and transverse dispersivity were assigned to each unit as well. The values of each of these parameters are shown in Table 3.0. The area considered for simulating groundwater and contaminant flow in the three hydrostartigraphic units was at the western portion of the site covering an area of 200m (South-North) by 200m (West-East). As mentioned earlier, simulations were run for 1, 10, 100, 1000 and in one (W-E) model for 10,000 years to predict the movement of contaminants in layers.

Flow and Material Properties								
	Southern Boundary	Northern Boundary	Top boundary	Bottom boundary	Upper aquifer	Silt/Sand aquitard	Lower aquifer	Clay Cap
Hydraulic Head BC (m)	210	210	N/A	N/A	N/A	N/A	N/A	N/A
Fluid-Flux BC - Regular precipitation (m/s)	N/A	N/A	-1.186E-08	0	N/A	N/A	N/A	N/A
Fluid-Flux BC - No precipitation (m/s)	N/A	N/A	0	0	N/A	N/A	N/A	N/A
Fluid-Flux BC - Double precipitation (m/s)	N/A	N/A	0	0	N/A	N/A	N/A	N/A
Conductivity (m/s)	N/A	N/A	N/A	N/A	2.50E-05	1.00E-07	2.50E-05	1.00E-09
Anisotropy of conductivity	N/A	N/A	N/A	N/A	0.036	1.00E-05	0.036	0.01
Density Ratio	N/A	N/A	N/A	N/A	-0.991	N/A	N/A	N/A
Specific Storage (m^{-1})	N/A	N/A	N/A	N/A	4.960E-04	2.70E-03	4.960E-04	4.95E-03
Aquifer thickness (m)	N/A	N/A	N/A	N/A	11.4	9	9.5	2
Porosity	N/A	N/A	N/A	N/A	0.3	0.05	0.3	0.01
Molecular Diffusion (m^2/s)	N/A	N/A	N/A	N/A	2.03E-09	N/A	N/A	N/A
Longitudnal Dispersivity (m)	N/A	N/A	N/A	N/A	1	N/A	N/A	N/A
Transverse Dispersivity (m)	N/A	N/A	N/A	N/A	0.1	N/A	N/A	N/A

Table 3.0: Flow and material properties parameters assigned to model boundaries and hydrostartigraphic units

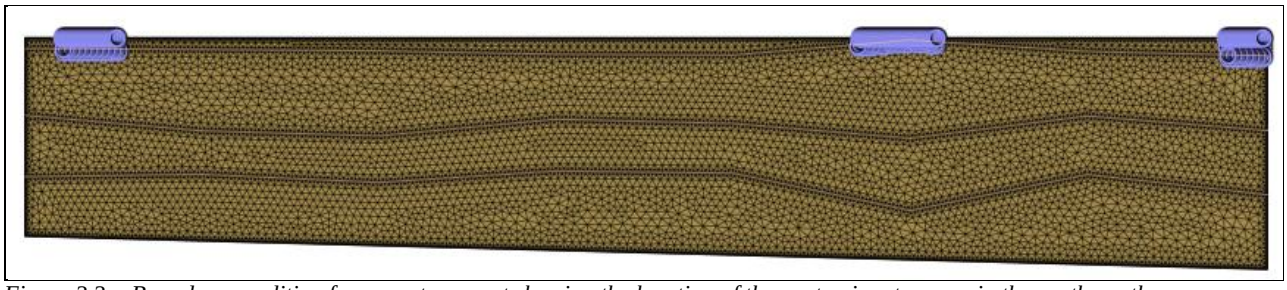

Figure 3.3a: Boundary condition for mass-transport showing the location of the contaminant source in the south-north model

Figure 3.3b: Boundary conditions for mass-transport showing the location of the contaminant source in the west-east model

3.3 Governing Equations

Every model requires a set of governing equations dependent on the type and dimension of the simulation - steady-state or transient – flow only, flow + mass and flow + mass + heat and1D, 2D or 3D models respectively. The model used for this study was a 2D transient flow and transient mass transport with a triangular finite-element mesh and the list of important governing equations associated with this study are as follows:

$$q_x = -K_x\left(\frac{dh}{dx}\right);\ q_z = -K_z\left(\frac{dh}{dz}\right) - (K\rho_r) \quad (3)$$

$$\frac{d}{dx}\left[K\frac{dh}{dx}\right] + \frac{d}{dz}\left[K\frac{dh}{dz} + (K\rho_r)\right] = S_s\frac{dh}{dt} \quad (4)$$

$$\frac{d}{dx}\left(\theta D_x\frac{dC}{dx}\right) + \frac{d}{dz}\left(\theta D_z\frac{dC}{dz}\right) - \frac{d}{dx}(q_xC) - \frac{d}{dz}(q_zC) = \frac{d}{dt}(\theta RC) \quad (5)$$

Equation (3) explains the basic Darcy's Law which relates hydraulic conductivity (K_x) to a change in hydraulic gradient ($\frac{dh}{dx}$) where h is the change in hydraulic head measurements and x represents the horizontal distance over which the heads change. This parameter is a dimensionless quantity. Another variation of Darcy's Law in the measured in the vertical direction with (K_z) being the hydraulic conductivity in the vertical direction and ($\frac{dh}{dz}$) is the change in hydraulic head measured in the vertical direction. The value ($K\rho_r$) is the product of the hydraulic conductivity and the fresh water density Equation (4) describes the flow mass balance equation which relates the hydraulic conductivity (K_x, K_z) and the change in hydraulic head (h) in x and z directions to volume storage (S_s - Specific Storage) of aquifer per unit hydraulic head (h) per unit time (t) and equation (5) describes the solute mass balance equation where the mass inflow rate – mass outflow rate = change in concentration and sink/source term over time. The parameters D_x and D_z are hydrodynamic dispersion coefficients in x and z directions. C is concentration (mg/L), R is source/sink term, q_x and q_z are Darcy flux values in x and z directions and θ is the moisture content.

3.3 Results and Discussion

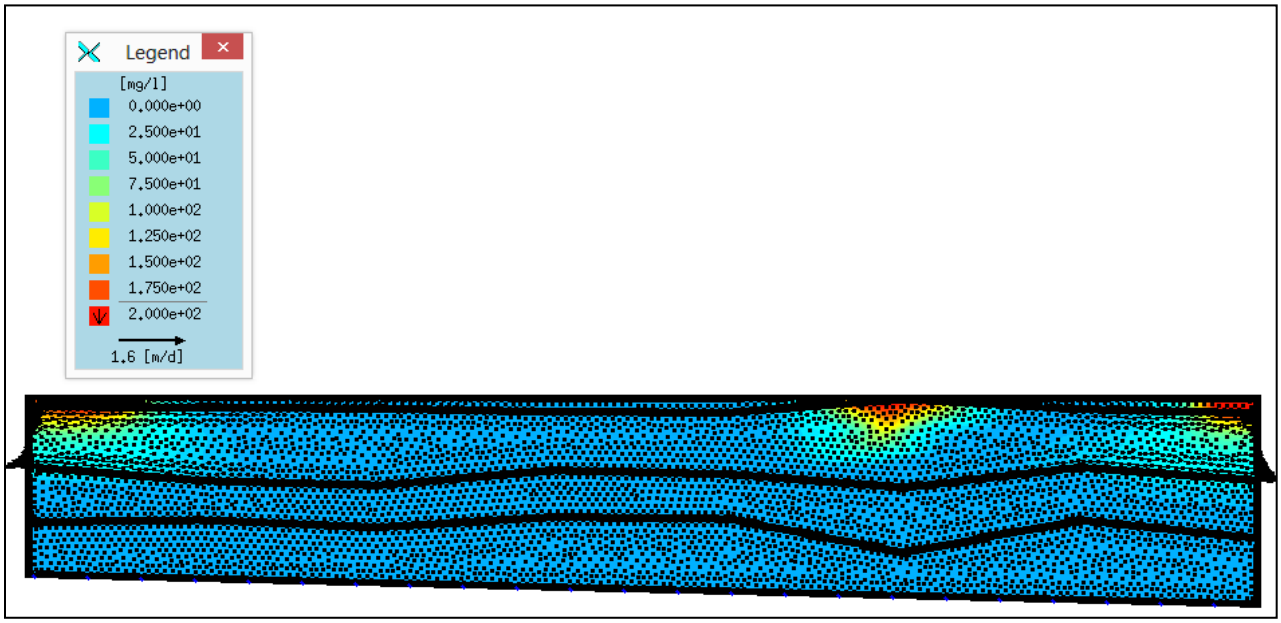

Figure 3.4a: Contaminant transport model showing the extent of plume migration with regular precipitation (1.864E-08 m/s) from top boundary after 1 year

Figure 3.4a shows a simulation of the (S-N) profile which had no fluid flux from south, north and bottom boundary. The only source of fluid entering the model was the average annual precipitation from the top boundary calculated from the Kingsville Climatological Data Center to be -1.864E-08 m/s (588 mm/year). The model has three contaminant sources which are placed at their respective locations based on evidence from the resistivity inversion models. The contaminant source modeled in this study was mainly chloride ions (Cl^-) due to its prevalence in leachate contaminated groundwater. The initial concentration of these contaminant zones were set at 200 mg/L and their change in concentration was simulated over 1 year. The area in close proximity to the contaminant zone shows early signs of diffusion of contaminants as the water from precipitation infiltrates through the top layer and tends to dilute the contaminant sources changing the concentration from 200 mg/L to 100 mg/L and as the distance increases radially away from the contaminant source, the concentrations in those areas are as low as 25mg/L. After one year of simulation, the contaminants have just dispersed slightly with good indication that the plume emanating in both lateral and vertical directions. There is no evidence that the contaminants have entered the silt/sand aquitard or the lower sand aquifer after a year.

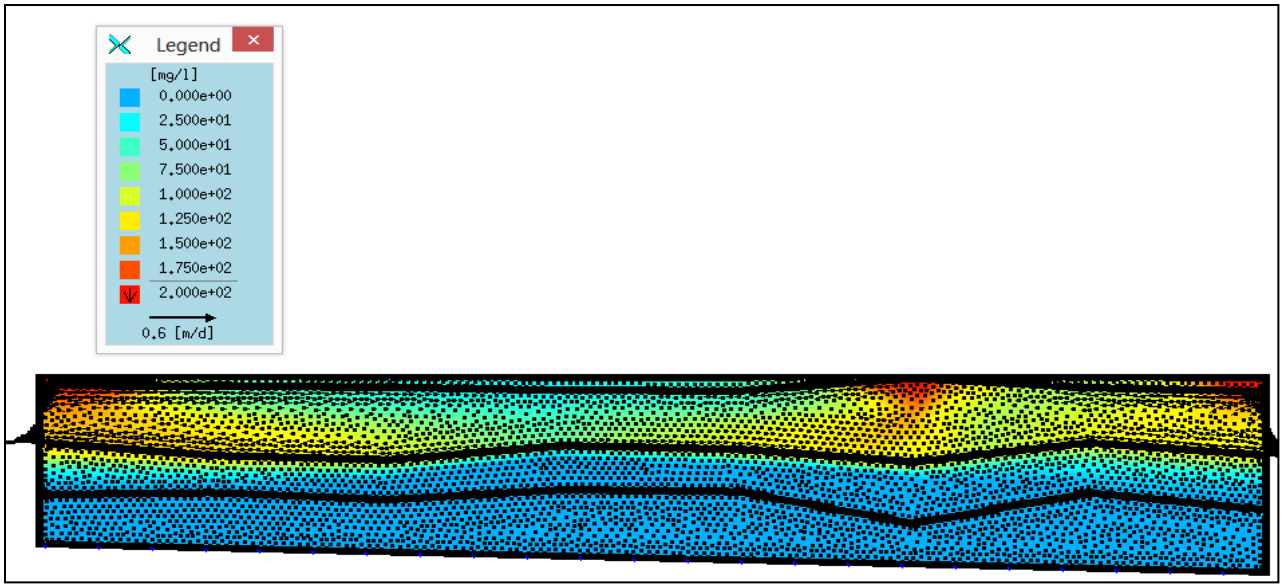

Figure 3.4b: Contaminant transport model showing the extent of plume migration with regular precipitation (1.864E-08 m/s) from top boundary after 10 years

Figure 3.4b shows the same initial concentration but predicted after a simulation for 10 years. The contaminants had time to spread even further in both the vertical and horizontal direction with a greater vertical component spread mainly due to the density differences between the waste and the upper aquifer water. The extent of the plume have reached the base of the upper sand aquifer with concentrations ranging between 75-100 mg/L with slight indication that the plume has reached the upper weathered portion of the silt/sand aquitard. However, most of the aquitard and the lower sand aquifer remain free from contamination after 10 years.

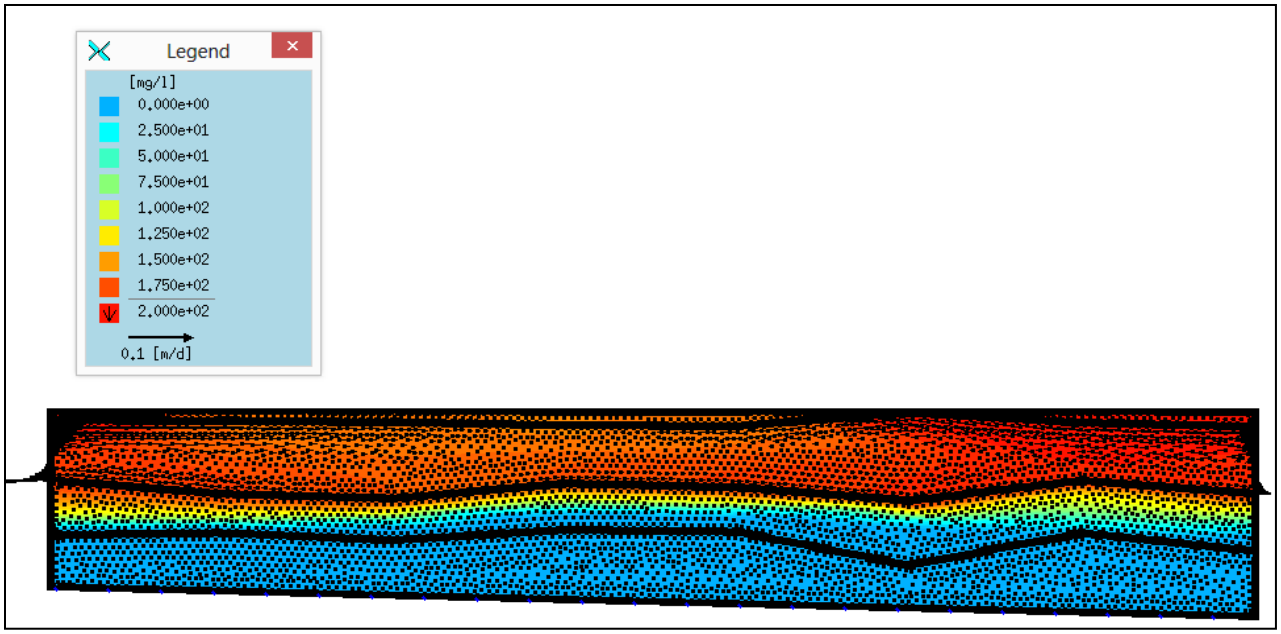

Figure 3.4c: Contaminant transport model showing the extent of plume migration with regular precipitation (1.864E-08 m/s) from top boundary after 100 years

Figure 3.4c shows the simulation of contaminants through the aquifers after a period of 100 years. The extent of the contaminant plume has completely covered the upper sand aquifer with concentrations ranging between 150-200mg/L. The contaminant plume has also reached the upper weathered portion of the silt/sand aquitard with concentrations ranging around 100mg/L. The influx of contaminants into the silt/sand aquitard is higher at the edges of the model where the contaminant source is located. Movement of contaminants in the aquitard seems to be mainly vertical; however this needs to be confirmed with models simulating contaminant transport at a later time interval.

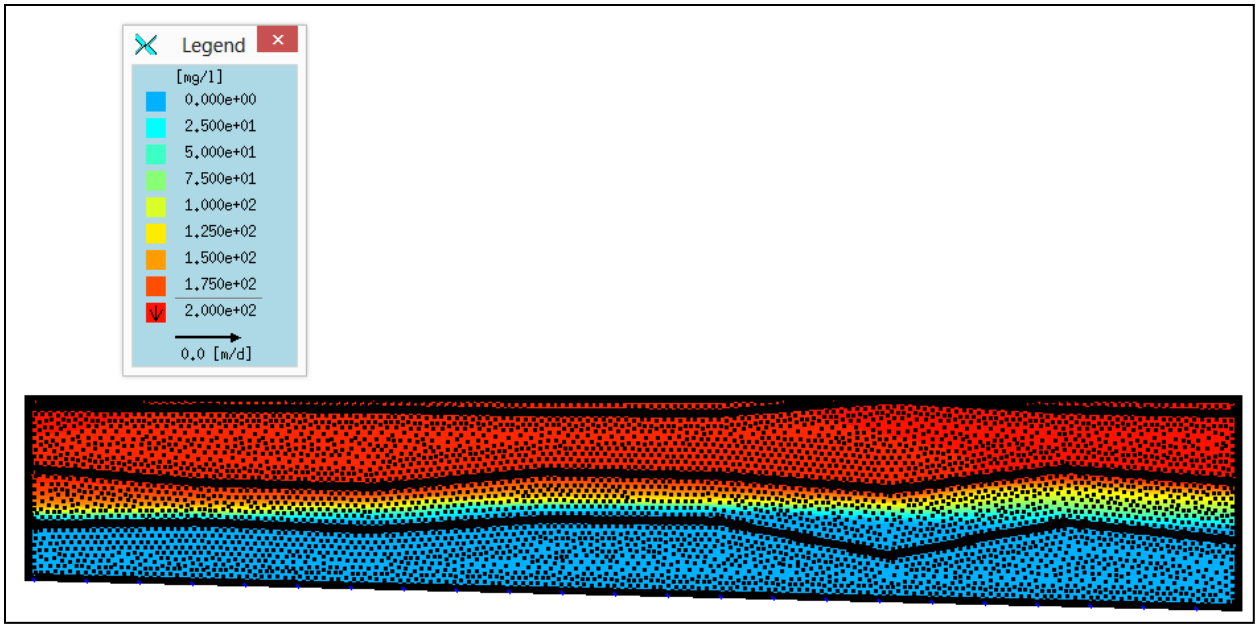

Figure 3.4d: Contaminant transport model showing the extent of plume migration with regular precipitation (1.864E-08 m/s) from top boundary after 1000 years

The final case showing the path taken by contaminants simulated with regular precipitation from top boundary for 1000 years is shown in Figure 3.4d. In this simulation, the concentration of the contaminated water in the upper aquifer and the upper weathered portion of the silt/sand aquitard is homogeneous at 200mg/L. Propagation of contaminants in the silt/sand aquitard is much slower and predominantly vertical mainly due to the extremely low permeability of the materials that constitute the aquitard. The low permeability retards the movement of contaminants in the aquitard which can be easily determined by examining the models for both 100 and 1000 years (Figures 3.4c and 3.4d). The movement of contaminants in the silt/sand aquitard for these two time frames has been modest.

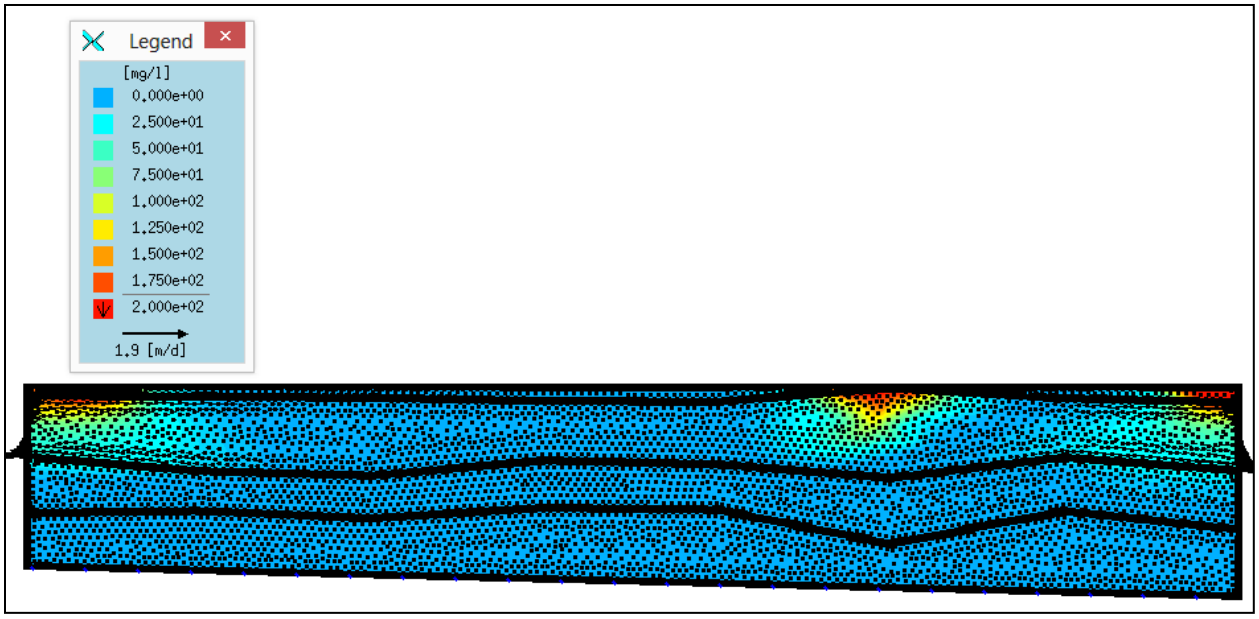

Figure 3.5a: Contaminant transport model showing the extent of plume migration with no precipitation (0 m/s) from top boundary after 1 year

The next set of models (Figures 3.5a - 3.5d) show the movement of contaminants through layers with no precipitation from the top boundary simulated for 1, 10, 100 and 1000 year(s). The idea behind this simulation was to compare the extent of contaminants from the source with and without the influence of precipitation. Figure 3.5a show three sources of contaminants placed at the top of the upper sand aquifer with initial concentrations measured at 200mg/L. After simulating the state of contaminant flow after 1 year, there is not much difference in the extent of the plume generated from the contaminant source for models with or without the influence of precipitation. The movement of contaminants seems to be predominantly in the vertical direction which will become clearer during later time frames.

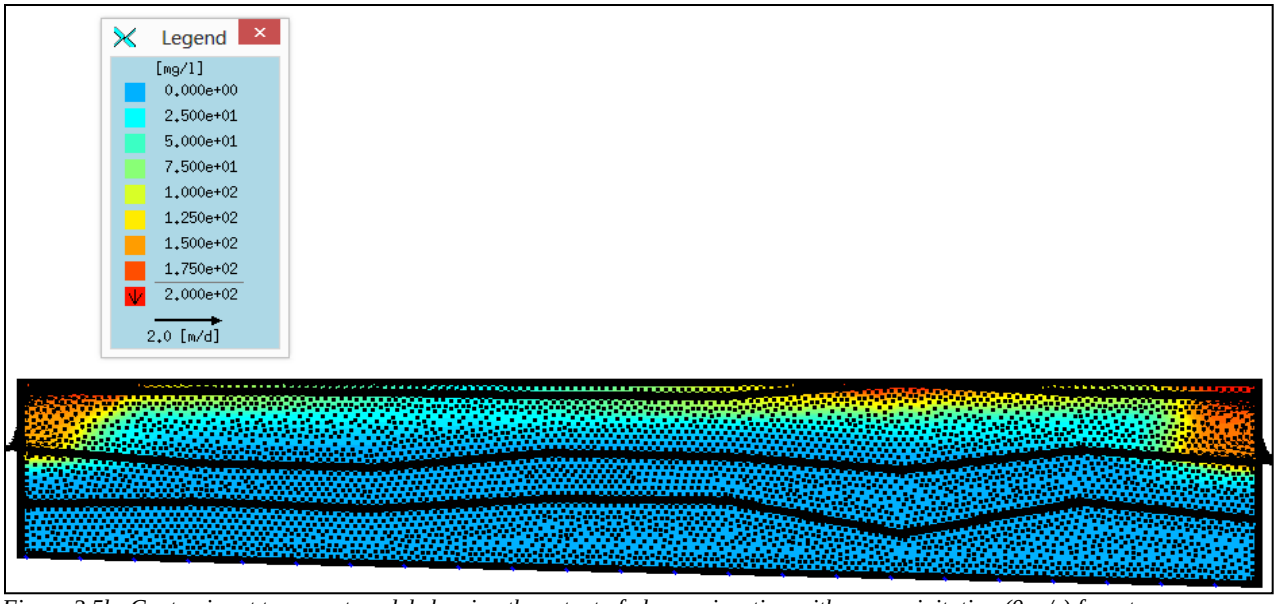

Figure 3.5b: Contaminant transport model showing the extent of plume migration with no precipitation (0 m/s) from top boundary after 10 years

The next case shows the same initial conditions simulated for a period of 10 years. It becomes clear that, with negligible influx of water, the contaminant plume is confined to a smaller area and the movement is primarily vertical as can be seen in figure 3.5b. Two high concentration zones are seen to be forming at the edges of the model and the movement of contaminants in the top part of the upper aquifer is taking place due to diffusion and hydrodynamic dispersion. The upper aquifer still has not been completely contaminated by the waste and there is no evidence as yet that the plume is migrating vertically downwards into the silt/sand aquitard.

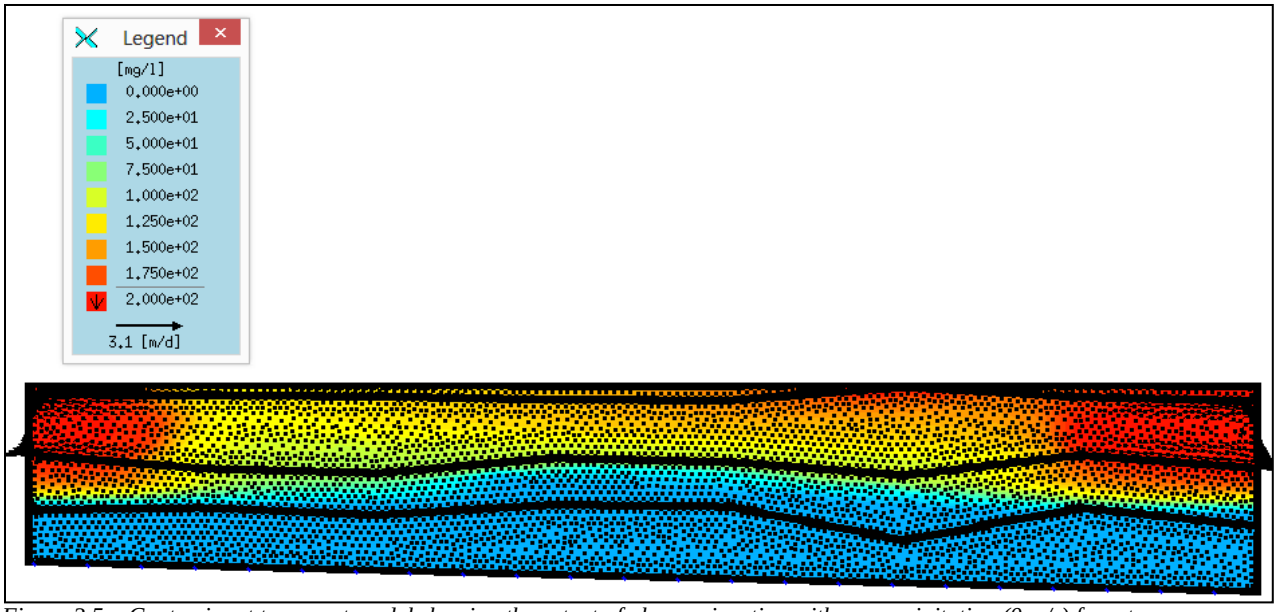

Figure 3.5c: Contaminant transport model showing the extent of plume migration with no precipitation (0 m/s) from top boundary after 100 years

For the next simulation, the movement of contaminants was simulated through the layer after a time period of 100 years. As explained in the previous model, the confinement of the contaminant zone to the edges is clearer in this simulation, with two high concentration zones (200mg/L) at the edges and a vast region of lower concentration (100mg/L) covering most of the upper aquifer. However, due to the primarily vertical propagation of plume from waste and no net fluid flux, there is little opportunity for the dilution of contaminants in the plume which results in the plume reaching the silt/sand aquitard in a more concentrated form as can be seen in figure 3.5c. Besides the edges, most of the silt/sand aquitard remains essentially free of contaminants after 100 years of simulation.

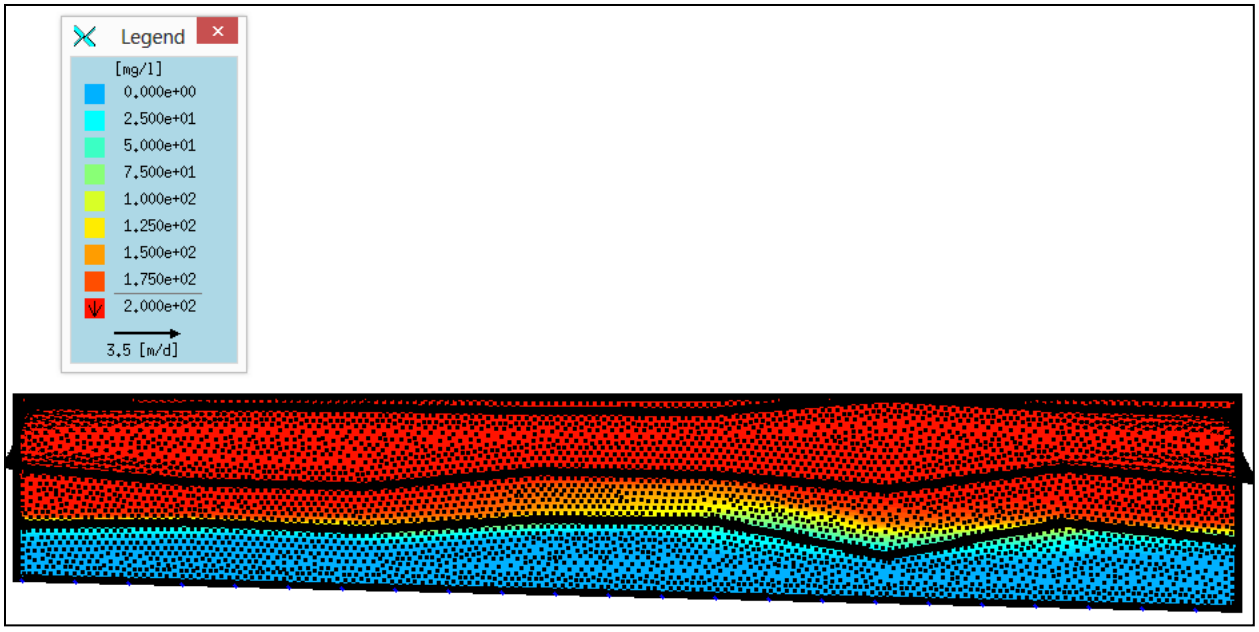

Figure 3.5d: Contaminant transport model showing the extent of plume migration with no precipitation (0 m/s) from top boundary after 1000 years

Simulating the same initial conditions for the model over 1000 years shows the contaminant plume covering the entire upper sand aquifer and the silt/sand aquitard (Figure 3.5d). While comparing the results for this model to the extent of contaminants seen in the model with the influence of precipitation (Figure 3.4d) after the same time frame, one notices that without the influence of precipitation, the contaminants can occupy the entire silt/sand aquitard whereas for the model with precipitation, the contaminants only partly occupy the silt/sand aquitard. One reason for this phenomenon is the difference in concentration of the contaminants in both models when they reach the aquitard. Due to the influence of precipitation, the contaminants are diluted which result in a small concentration difference thus delaying the diffusion and dispersion process. However, if the contaminants are not diluted by fluid influx from precipitation there is a vast difference in the concentration which speeds up the diffusion and dispersion process thus covering the area with contaminants faster.

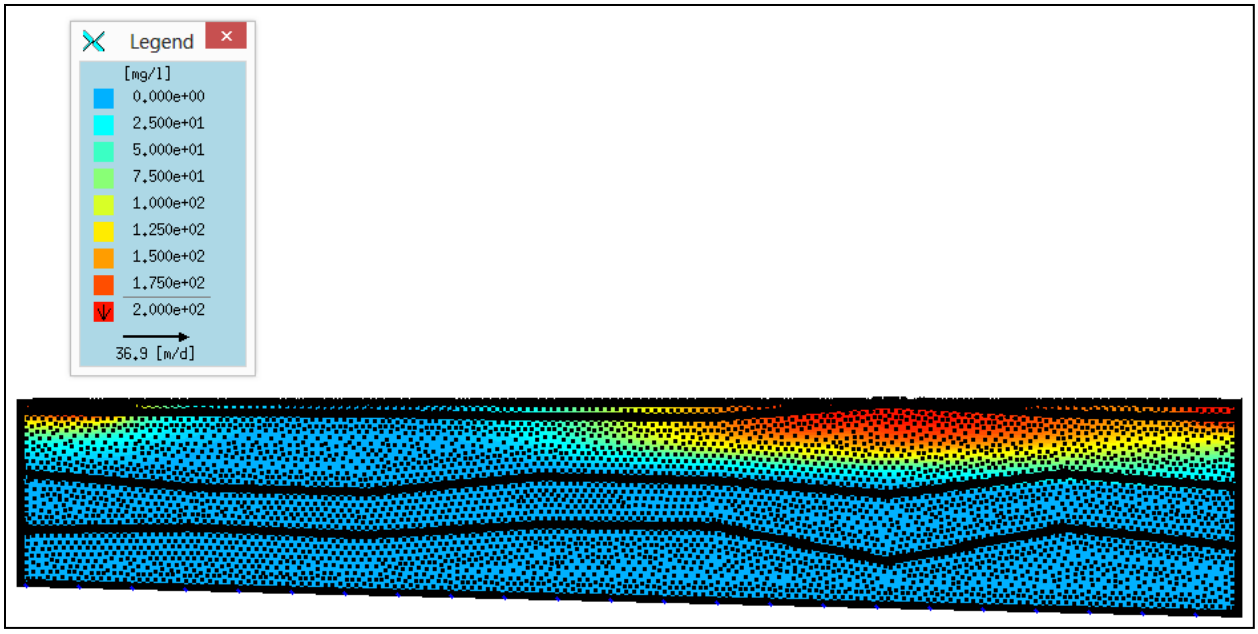

Figure 3.6a: Contaminant transport model showing the extent of plume migration with double the precipitation (3.728E-08 m/s) value from top boundary after 1 year

The following models (Figures 3.6a - 3.6d) predict the movement and extent of contaminants in various layers with double the fluid-flux (precipitation) from top boundary simulated for 1, 10, 100 and 1000 year(s). The idea behind this simulation was to compare the vertical and horizontal extent of contaminants in various layers with previous models using regular and negligible fluid-flux. Scientific research suggests that increased precipitation will result in the production of excess leachate. The leachate produced will be less viscous, highly diluted and mobile, thus the risk that the leachate will contaminate the subsurface layers rapidly is prevalent. Hence it becomes important to model this scenario and determine the consequences of increased precipitation. The first case shows the extent of contamination originating from three sources in the upper aquifer, the initial concentration of these sources was fixed at 200 mg/L and the simulation was observed after 1 year. As can be seen from figure 3.6a, the plume from the contaminants has a predominantly horizontal spread with a small vertical movement in the upper aquifer. The concentration in the plume tends to disperse quickly within the upper parts of the aquifer with concentration ranging from 200-100mg/L. This sudden decrease in concentration of the contaminants was caused by the increase in fluid influx from the top boundary.

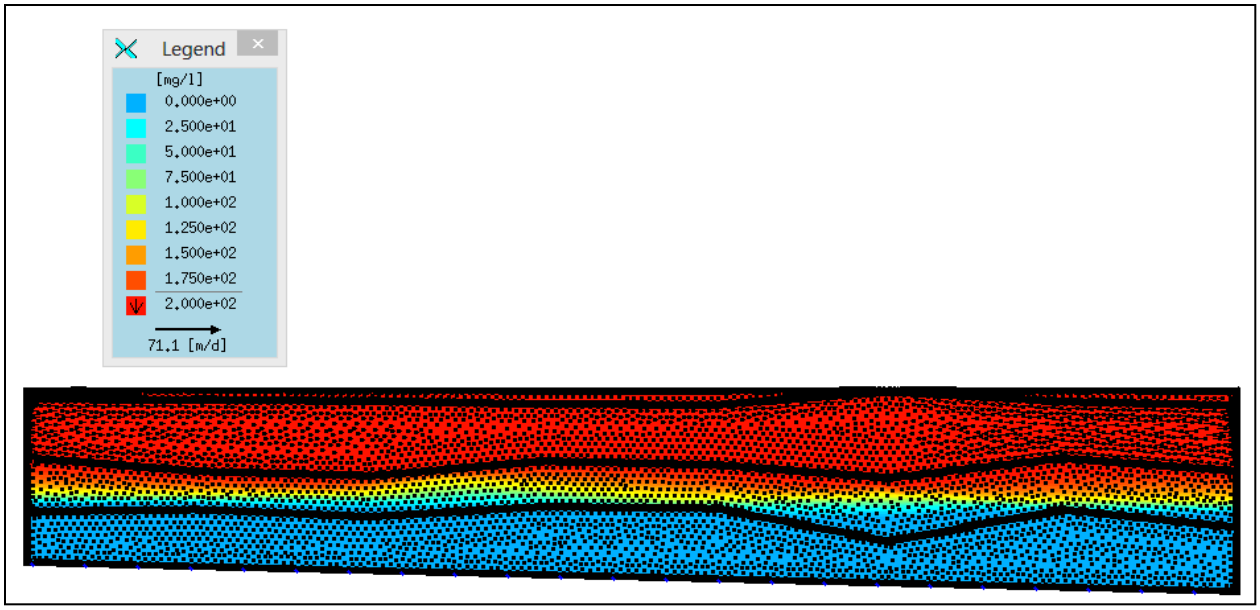

Figure 3.6b: Contaminant transport model showing the extent of plume migration with double the precipitation (3.728E-08 m/s) value from top boundary after 10 years

The next case simulates the same initial conditions for mass and fluid-flux but for a longer period of time (10 years) (Figure 3.6b). The simulation after 10 years shows that the entire upper aquifer and most of the silt/sand aquitard has been contaminated. By comparing this result with the simulations for the models with no precipitation and regular precipitation for the same time frame, it is clear that the effect of increased precipitation has resulted in the contaminants occupying a larger area in a shorter span of time.

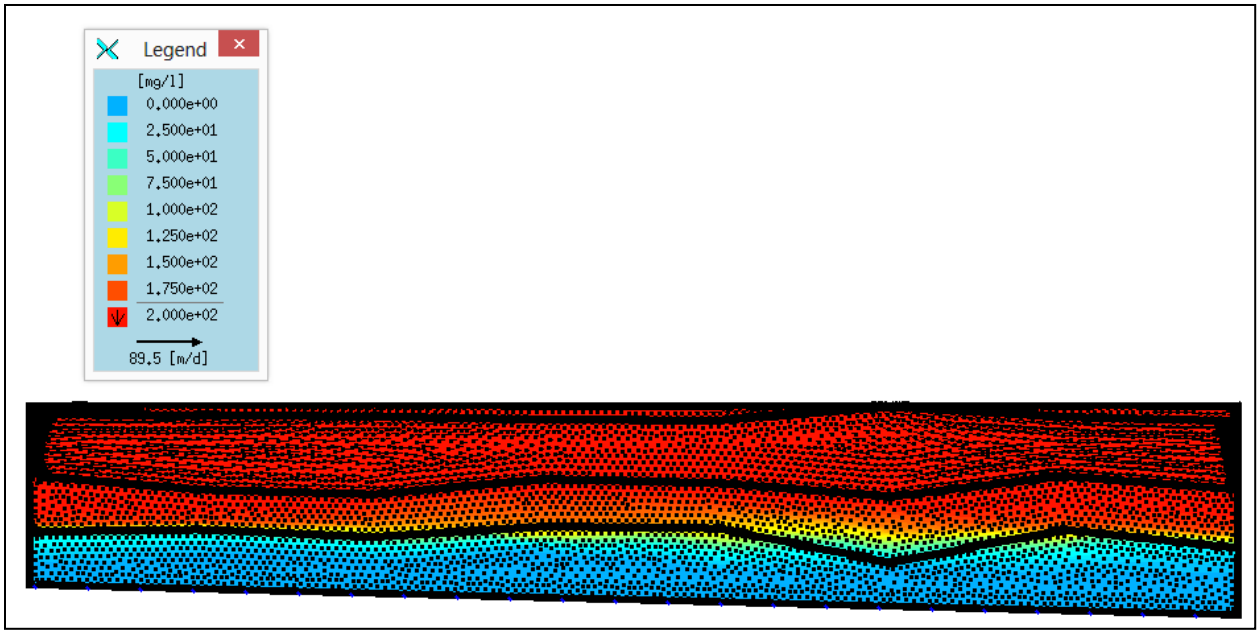

Figure 3.6c: Contaminant transport model showing the extent of plume migration with double the precipitation (3.728E-08 m/s) value from top boundary after 100 years

The simulation for the same initial conditions after 100 years (Figure 3.6c) shows that the contaminants have occupied the entire upper aquifer and the silt/sand aquitard. Due to the low hydraulic conductivity of the silt/sand aquitard, it took the contaminants an extra 90 years to cover the aquitard. However, at the end of the 100 year simulation there is still no clear evidence of the contaminants escaping into the lower sand aquifer.

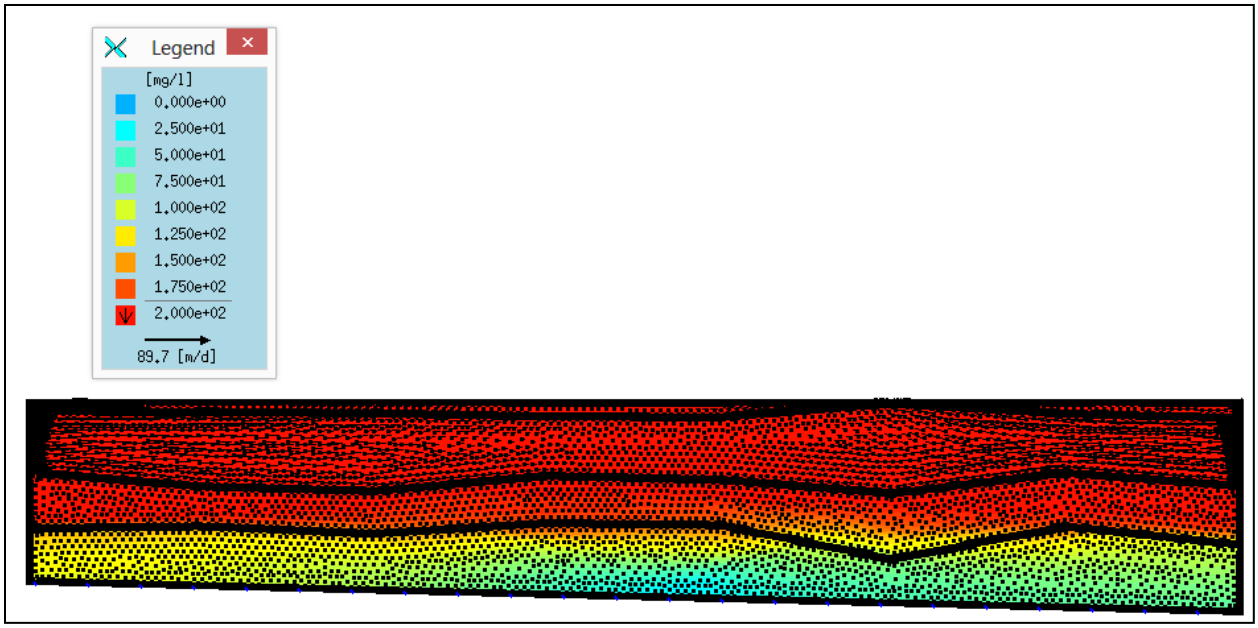

Figure 3.6d: Contaminant transport model showing the extent of plume migration with double the precipitation (3.728E-08 m/s) value from top boundary after 1000 years

After 1000 years of simulation with the same initial conditions for mass and fluid-flux, the contaminants have spread into the lower sand aquifer as can be seen from figure 3.6d. The concentration of the contaminants in the lower sand aquifer range between 110-130mg/L and can be seen spreading from the south towards the north which is the direction of fluid flow in the lower aquifer. The northern part of the lower aquifer still shows traces of contamination measuring at 18.5mg/L however, with time the concentration of contaminants within the lower aquifer will normalize by the diffusion and dispersion process.

The numerical results of mass and fluid-flux explained above were based on the results from south-north resistivity profiles. Since three resistivity profiles were performed in the west-east direction which had different fluid flow patterns with most of the waste concentrated in the western portion of the site, it was decided to conduct groundwater modeling to simulate the flow of contaminants with a different fluid-flow pattern and waste location in the west-east direction. The contaminant transport and extent was simulated with one contaminant source on the western edge of the upper aquifer with the difference in the regional boundary condition set to zero. Initial hydraulic heads were specified in both upper and lower sand aquifers with the mass concentration in the upper western portion of the upper sand aquifer set to 200mg/L. Three scenarios were conducted to predict the influence of 1) Regular precipitation (-1.186E-08 m/s), 2) No precipitation (0 m/s) and 3) Double precipitation (-3.728E-08 m/s) on contaminant transport in the layers.

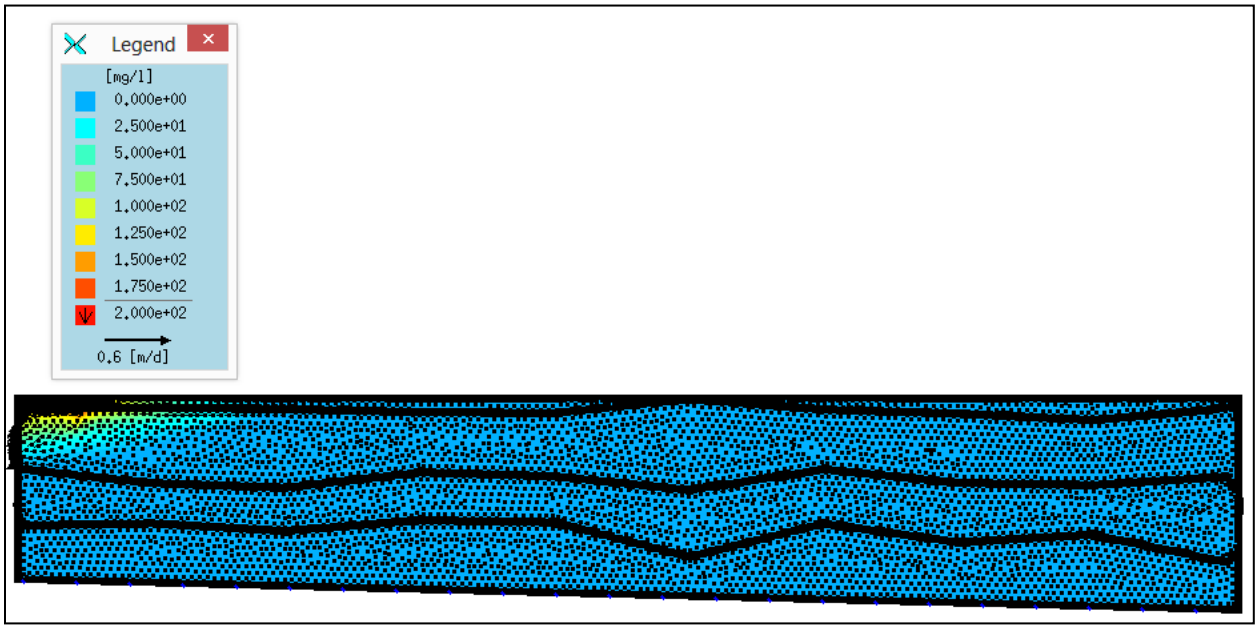

Figure 3.7a: Contaminant transport model showing the extent of plume migration with regular precipitation (1.864E-08 m/s) from top boundary simulated after 1 year for west-east model

The first (W-E) scenario predicted the extent of the contaminant plume from the source simulated after 1 year. The plume originating from the waste has both a horizontal and vertical direction of propagation with the horizontal plume component diffusing faster than the vertical component (Figure 3.7a) with concentrations ranging between 200mg/L to 20mg/L in the horizontal direction and between 200mg/L-125mg/L in the vertical direction. A small portion (first 40m) of the upper aquifer has been influenced by the contaminant plume, the rest of the aquifer and the other two layers are free of contamination after 1 year of simulation.

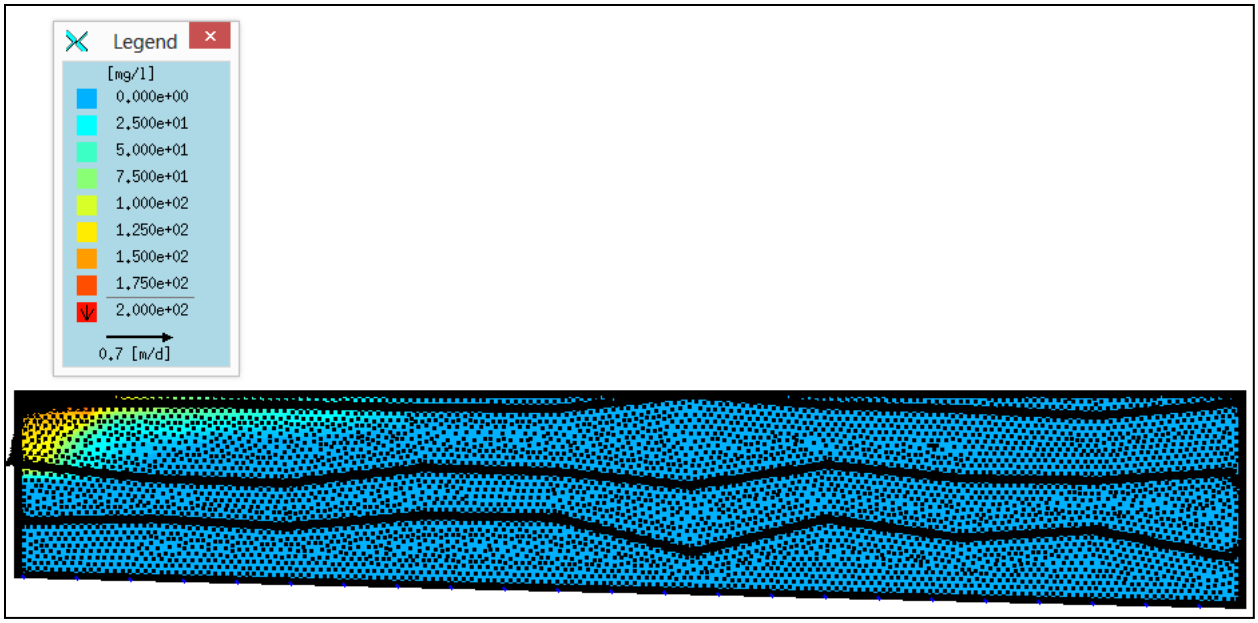

Figure 3.7b: Contaminant transport model showing the extent of plume migration with regular precipitation (1.864E-08 m/s) from top boundary simulated after 10 years for west-east model

The next case shows the movement of contaminants in the layers with the same initial conditions for fluid-flow and mass simulated after 10 years. In this model (Figure 3.7b), the contaminant plume occupies a larger area of the upper sand aquifer in both the horizontal (close to 80-90m from the western portion) and vertical direction (base of upper aquifer) with the concentrations ranging between 200mg/L-98mg/L in the vertical direction and between 200mg/L-22mg/L in the horizontal direction. The silt/sand aquitard and the lower sand aquifer still remain free of any contamination after 10 years of simulation.

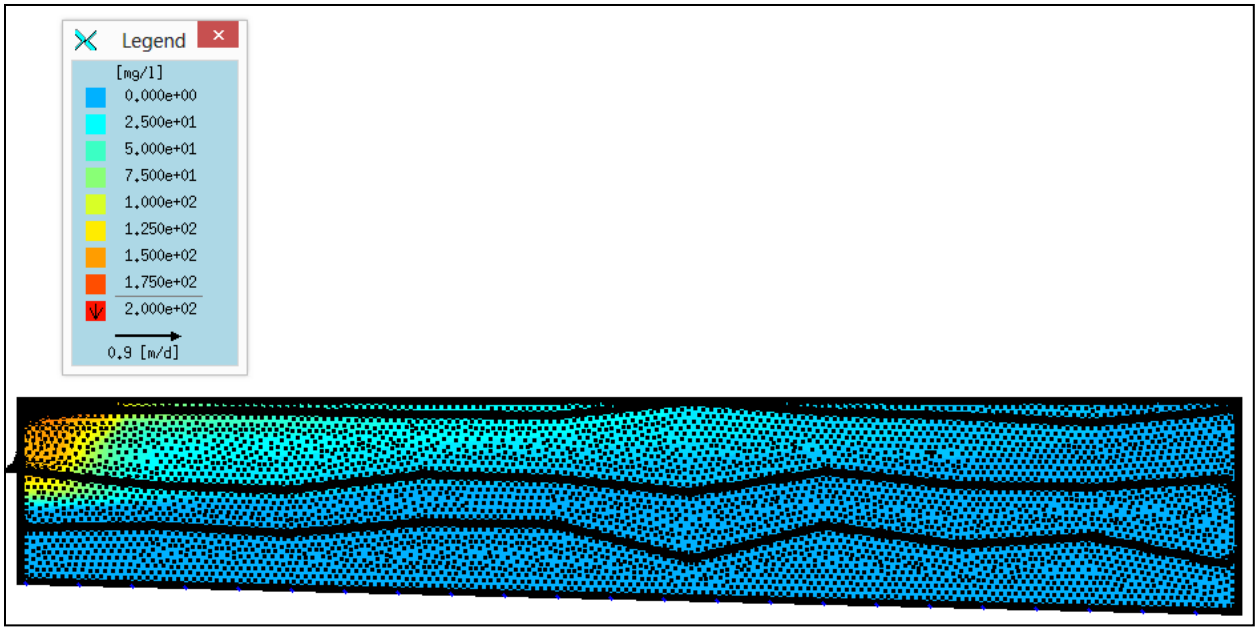

Figure 3.7c: Contaminant transport model showing the extent of plume migration with regular precipitation (1.864E-08 m/s) from top boundary simulated after 100 years for west-east model

Simulation after 100 years shows that the contaminant plume has influenced half of the upper sand aquifer and has reached the upper weathered portion of the silt/sand aquitard (Figure 3.7c). Concentration gradient in the vertical direction range between 200mg/L-123mg/L and range between 200mg/L-46mg/L in the horizontal direction. The contaminants have escaped the confinement of the upper sand aquifer and entered into the western portion (0-10m) of the silt/sand aquitard, however the rest of the aquitard and the lower sand aquifer remains free of any contamination towards the end of 100 years.

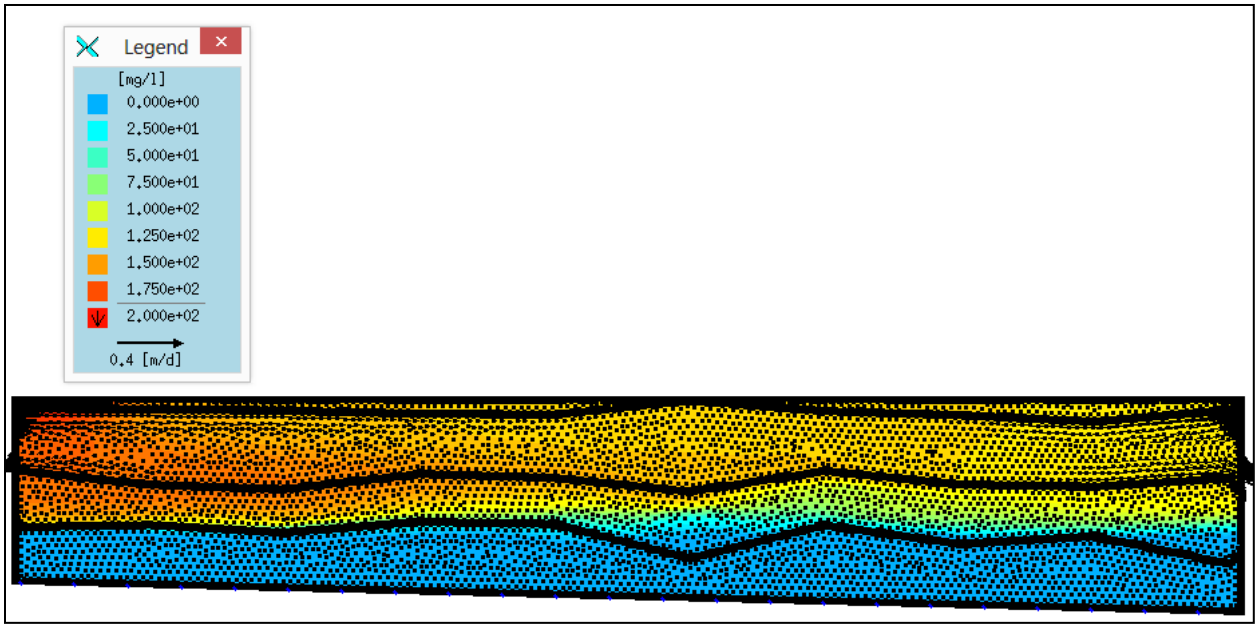

Figure 3.7d: Contaminant transport model showing the extent of plume migration with regular precipitation (1.864E-08 m/s) from top boundary simulated after 1000 years for west-east model

After 1000 years of simulation, the plume from the waste has occupied the entire upper sand aquifer and most of the silt/sand aquitard (Figure 3.7d). Concentration gradients in both layers range between 200mg/L-96mg/L horizontally and between 200mg/L-148mg/L vertically just beneath the western portion with the lower sand aquifer still free of any contamination after 1000 years of simulation.

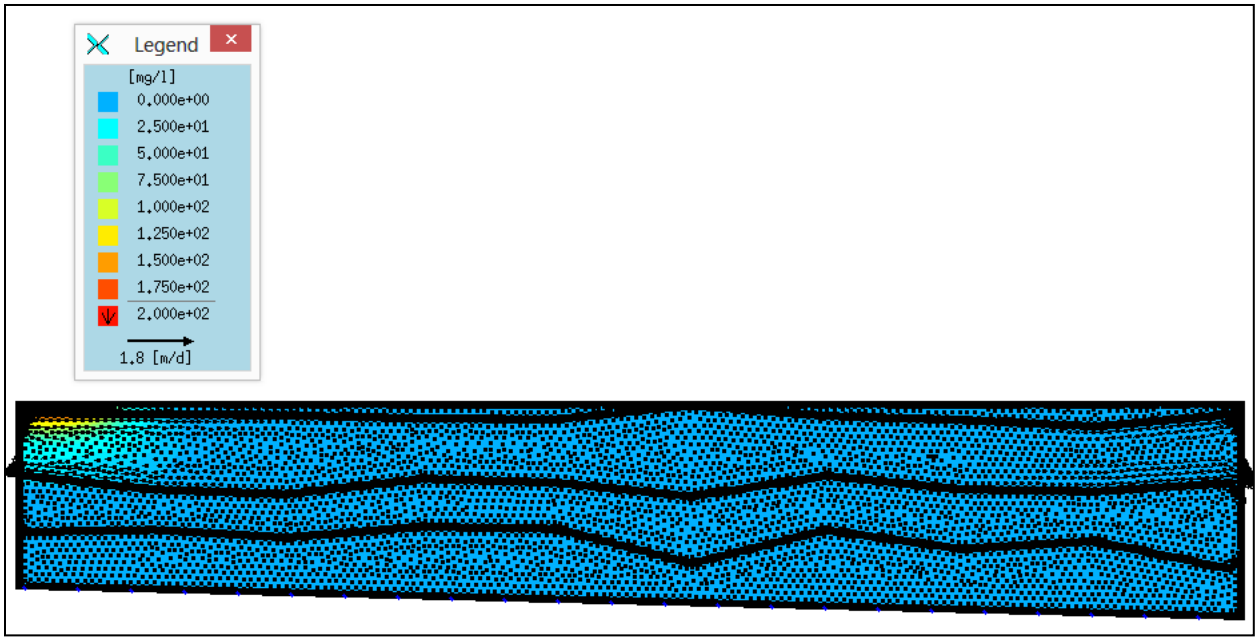

Figure 3.8a: Contaminant transport model showing the extent of plume migration with no precipitation (0 m/s) from top boundary simulated after 1 year for west-east model

The next set of models (Figures 3.8a - 3.8d) show the pathway taken by the contaminant plume within the layers with the same initial condition for mass concentration and without the influence of fluid-flux from top boundary (dry period) being simulated for 1, 10, 100 and 1000 years. The idea behind this simulation was to compare the extent and concentration gradient of the contaminant plume in the layers with and without the influence of excess precipitation. The first case (Figure 3.8a) shows the horizontal and vertical migration of the plume originating from the contaminant source occupying the western portion of the upper sand aquifer with the concentration gradient in both directions ranging between 200mg/L to 25mg/L. Majority of the upper sand aquifer, and the entire silt/sand aquitard and lower sand aquifer remain free of contamination at the end of 1 year.

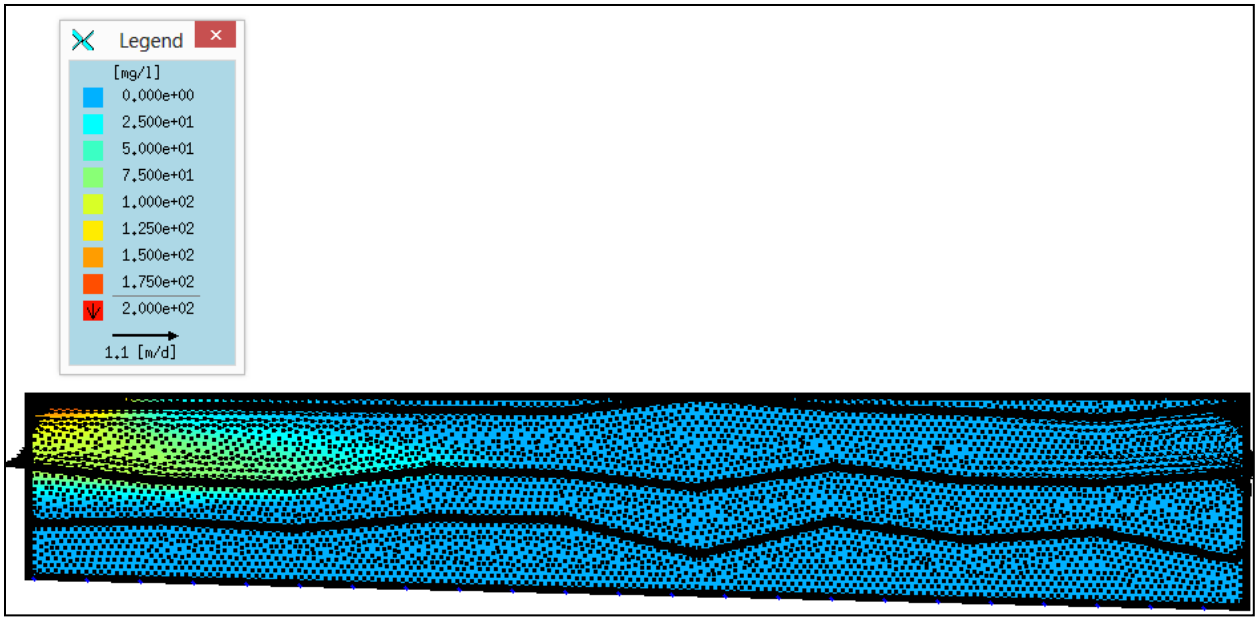

Figure 3.8b: Contaminant transport model showing the extent of plume migration with no precipitation (0 m/s) from top boundary simulated after 10 years for west-east model

The following case shows the extent of the contaminant plume and its concentration gradient in the layers after 10 years of simulation. The contaminant plume as seen in figure 3.8b occupies the first 40m of the upper sand aquifer and the upper weathered portion of the silt/sand aquitard with the concentration gradient varying from 200mg/L to 25mg/L in the horizontal direction. After 10 years of simulation majority of the upper sand aquifer, almost all of the silt/sand aquitard and the entire lower sand aquifer are free of contamination. There is not much difference in the extent of the contaminant plume for models with and without the influence of precipitation after 10 years; this may change as the time frame of observance is increased.

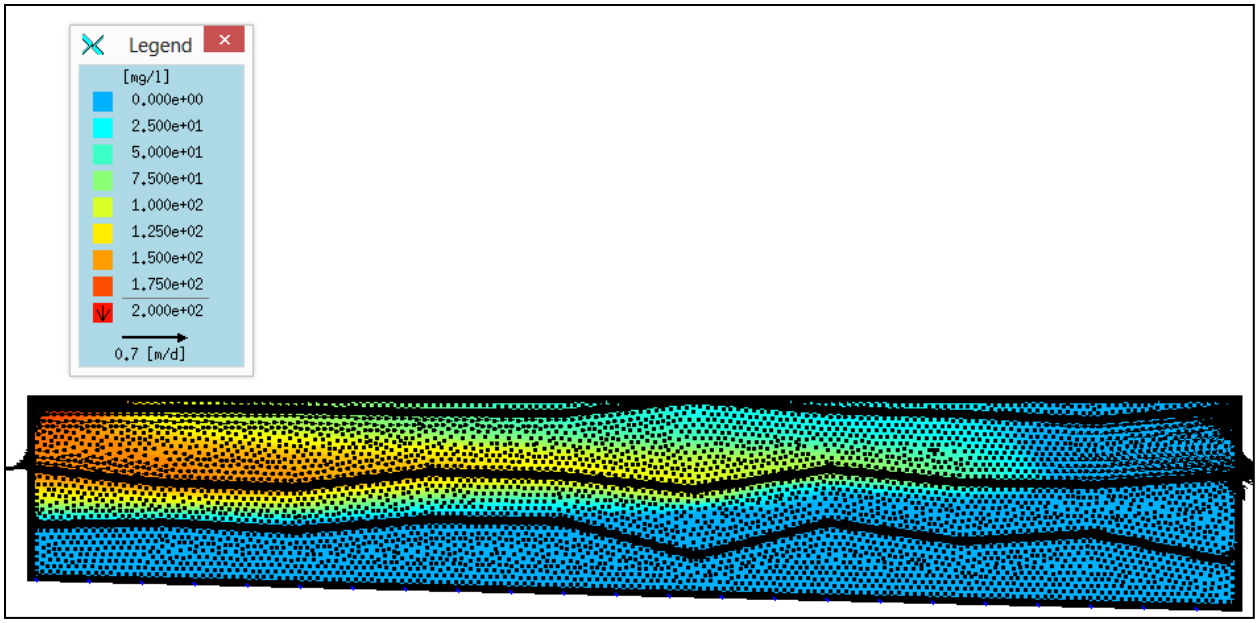

Figure 3.8c: Contaminant transport model showing the extent of plume migration with no precipitation (0 m/s) from top boundary simulated after 100 years for west-east model

The next case shows the extent of contamination in the layers after a period of 100 years. As can be seen from figure 3.8c, there is a clear horizontal trend in the movement of the contaminant plume which now occupies most of the upper sand aquifer and the upper weathered portion of the silt/sand aquitard. The concentration gradient in the upper aquifer ranges between 200mg/L in the western portion of the upper aquifer to about 20mg/L in the eastern portion of the upper aquifer. After 100 years of simulation the difference in concentration gradient of the contaminant plume is higher in the model with no precipitation compared to the model with regular precipitation (Figure 3.7c). There is not much difference in the horizontal extent of the plume in both models.

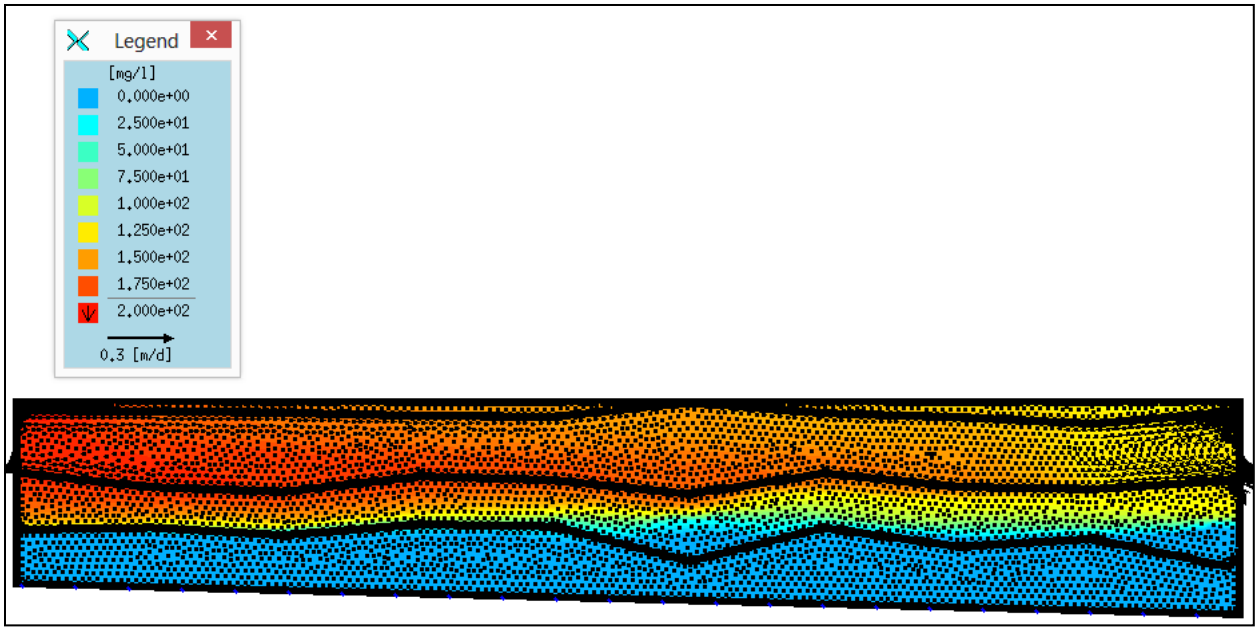

Figure 3.8d: Contaminated transport model showing the extent of plume migration with no precipitation (0 m/s) from top boundary simulated after 1000 years for west-east model

After 1000 years of simulation, figure 3.8d shows the entire upper sand aquifer and most of the silt/sand aquitard occupied by the contaminant plume. The difference in concentration gradient is still enormous compared to the 1000 years simulation of the model with regular precipitation. There is not much difference in the spatial extent of the contaminants in both models; however the lower sand aquifer is still free of contamination after 1000 years.

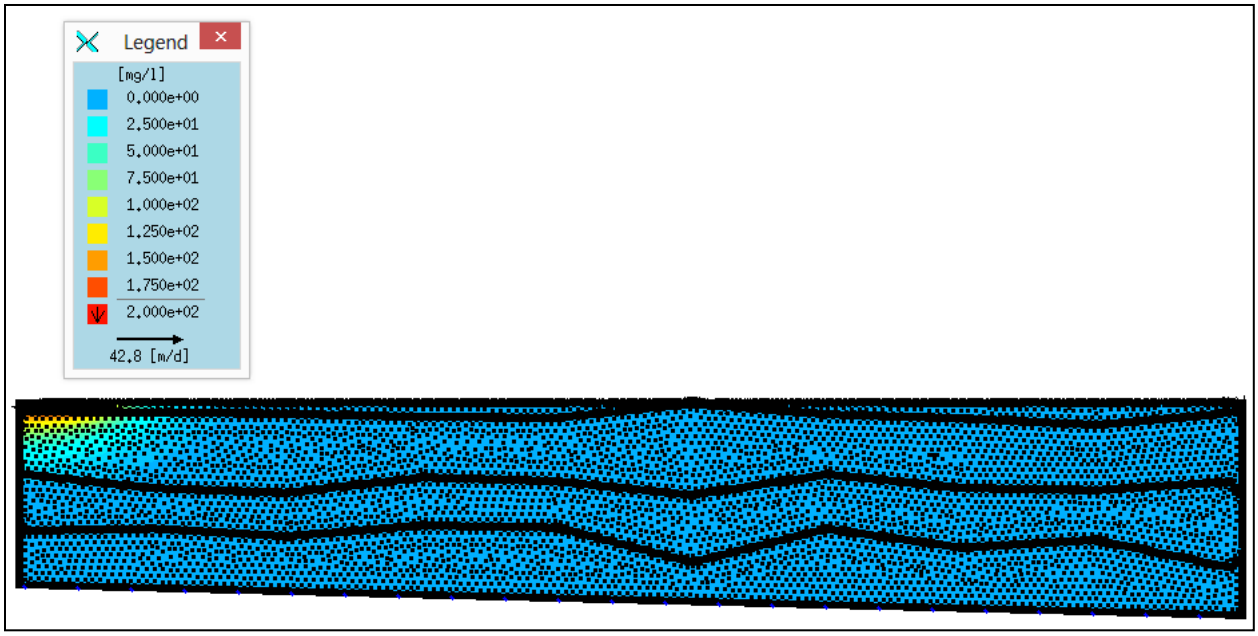

Figure 3.9a: Contaminant transport model showing the extent of plume migration with double precipitation (3.728E-08 m/s) rate from top boundary simulated after 1 year for west-east model

The next set of models show the pathway taken by contaminants using the same initial mass conditions but with double the infiltration rate from precipitation (wet period). The idea behind this simulation was to see the difference in concentration gradient and the extent of the plume in the layers compared to models with regular precipitation and no precipitation for 1, 10, 100, 1000 and 10,000 years. The first case shows the contaminant plume migration in the upper sand aquifer with double infiltration simulated after 1 year. As can be seen in figure 3.9a, there is a small vertical and horizontal component to plume migration in the aquifer. The concentration gradient is in the range of 20mg/L to 25mg/L in a short horizontal distance of 20-30m which means that the excess precipitation through the top boundary is influencing the concentration gradient of the contaminant plume thus affecting the speed of the diffusion and dispersion process.

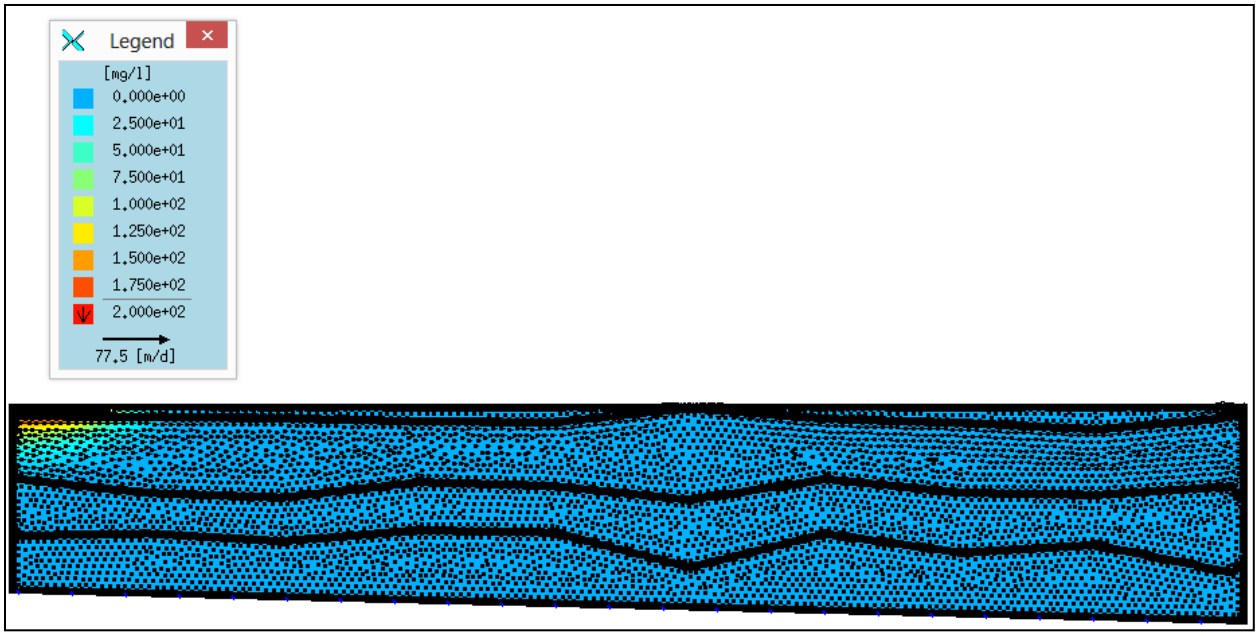

Figure 3.9b: Contaminant transport model showing the extent of plume migration with double precipitation (3.728E-08 m/s rate from top boundary simulated after 10 years for west-east model

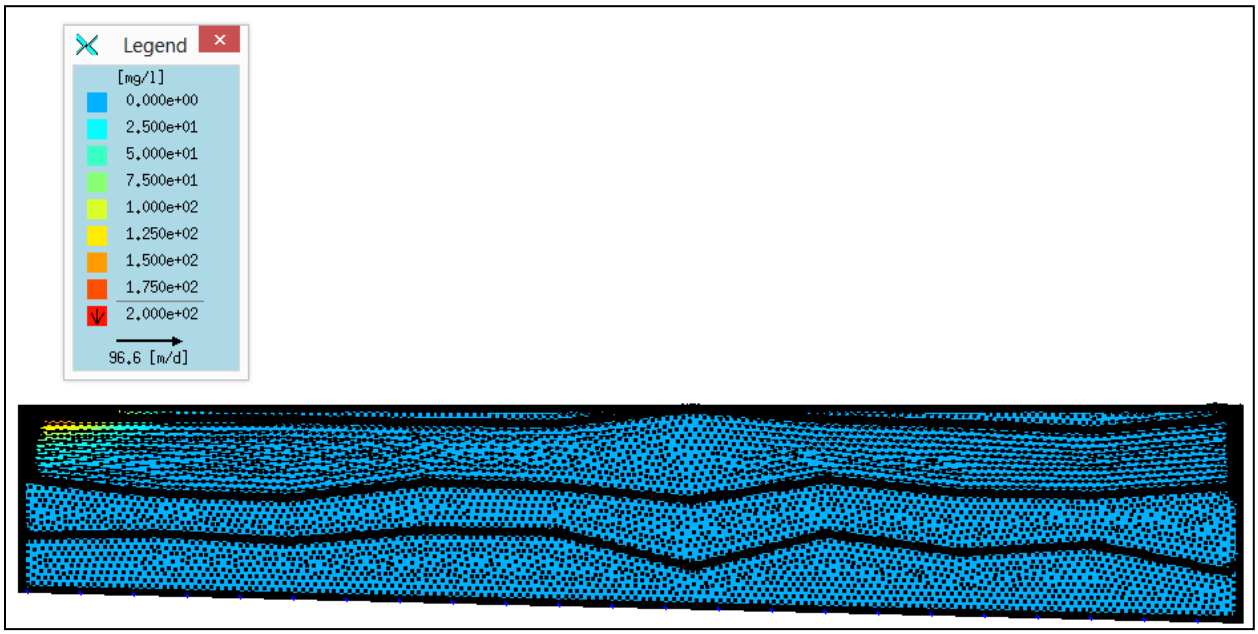

Figure 3.9c: Contaminant transport model showing the extent of plume migration with double precipitation (3.728E-08) rate from top boundary simulated after 100 years for west-east model

The next two simulations for 10 and 100 years (Figures 3.9b and 3.9c) were considered at once as it was difficult to determine the extent of the contaminants within the layers. The difference in concentration gradient between the source and the farthest point of plume's extent was too small for the software to detect. The legend that shows the concentration variation is predetermined by the software and the values of the colors changes automatically while the model is running, thus the user is unable to change the colors of a particular concentration to make them prominent in the model.

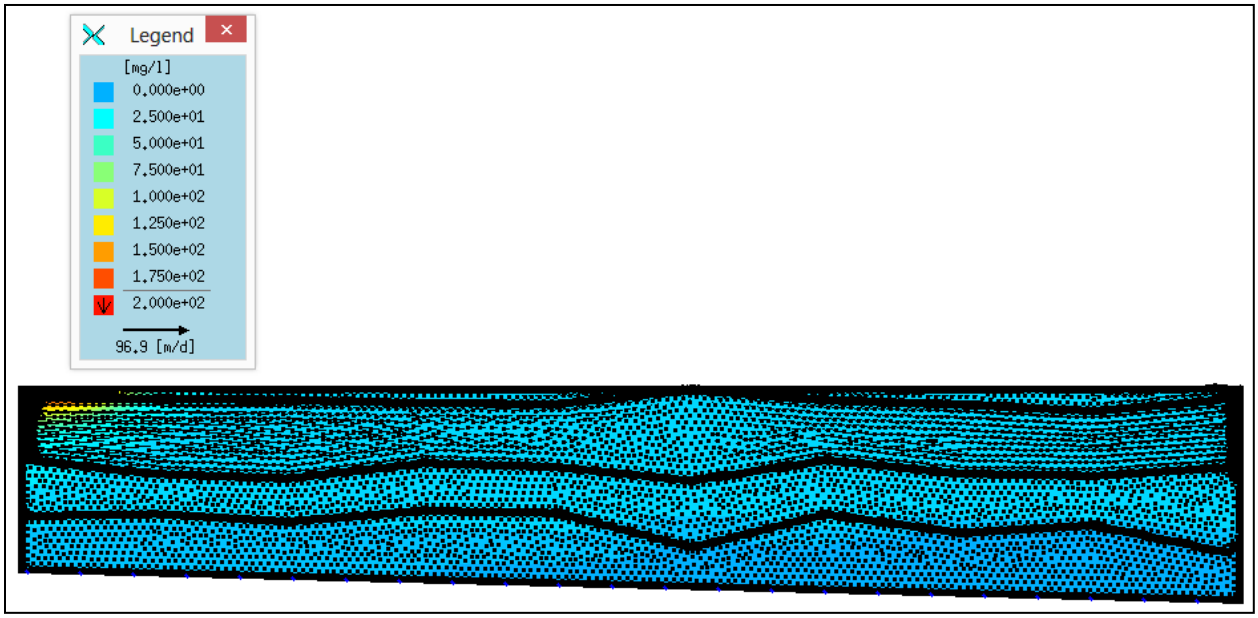

Figure 3.9d: Contaminant transport model showing the extent of plume migration with double precipitation (3.728E-08 m/s) rate from top boundary simulated after 1000 years for west-east model

However, for the case with 1000 years of simulation, the extent of the plume is now visible (Figure 3.9d) and although the concentration gradient is still low, the plume appears to occupy the entire upper sand aquifer and the silt/sand aquitard with a difference in concentration ranging between 200mg/L to 26mg/L. The low concentration gradient was caused by the excess fluid-flux from the top boundary due to double precipitation rates.

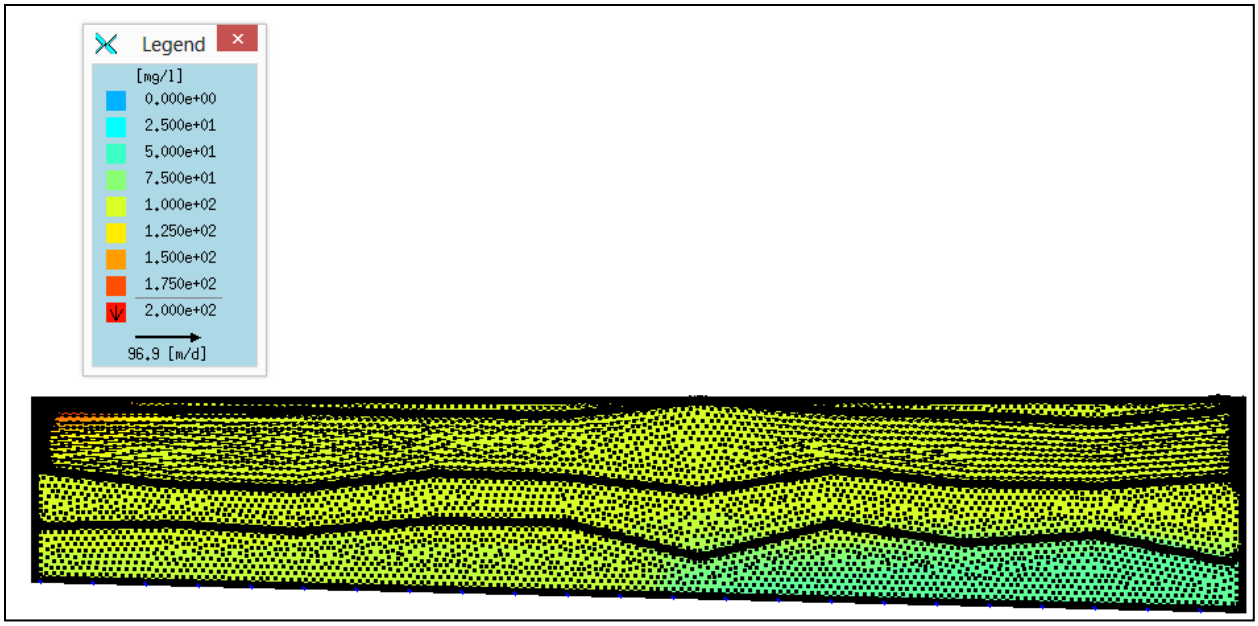

Figure 3.9e: Contaminant transport model showing the extent of plume migration with double precipitation (3.728E-08 m/s) rate from top boundary simulated after 10,000 years for west-east model

The final case for the west-east profile shows the extent of contamination in the layers after 10,000 years of simulation as can be seen in figure 3.9e. After 10,000 years, the entire model seems to be contaminated by the plume, with majority of the layers showing concentrations of 100mg/L and the eastern portion of the lower sand aquifer measuring at 50mg/L. Thus after 10,000 years the system still has not reached equilibrium and shows the effects of the contaminant plume originating from the waste located in the western portion of the upper aquifer.

3.4 Conclusions

The results from groundwater modeling give a good insight into the movement of contaminants and the implications of their extent in the future. The principal purpose of conducting groundwater modeling studies was to investigate the effect of regular (1.864E-08 m/s), no (0 m/s) and double precipitation (3.728E-08 m/s) through the top boundary on contaminant distribution at the landfill. Previous work at the landfill regarding the extent of contaminants has confined them to the upper sand aquifer and the upper weathered portion of the silt/sand aquitard. Based on the results shown above, the following conclusions can be made about the extent of contamination in various layers over time:

a) Models showing contaminant transport with regular precipitation (S-N) show both vertical and horizontal components to movement of the contaminant plume due to diffusion and dispersion effects. After 1000 years of simulation, the contaminants have completely occupied the upper sand aquifer with constant concentration and the majority of the upper weathered portion of the silt/sand aquitard with lower concentration. However, no evidence of the contaminants escaping into the lower sand aquifer was observed.
b) Models showing the contaminant transport with no precipitation (S-N) show a primarily vertical direction of plume migration at the edges of the model. After 1000 years of simulation, the contaminants have completely occupied the upper sand aquifer and the silt/sand aquitard at a higher concentration compared to the models with regular precipitation. This is because the contaminants were not diluted by the precipitation. However there was no difference seen in the spatial extent of the contaminants with or without the influence of regular precipitation.
c) Models showing contaminant transport with double precipitation show a primarily horizontal spread of the contaminants and within a 1000 years of simulation, the contaminants have found a way into the southern portion of the lower sand aquifer at a concentration of 132mg/L. Due to the excess precipitation, the contaminants although diluted were more mobile and as a result contaminated the lower sand aquifer during the same simulation time as the previous models.
d) The (W-E) models show the contaminant source in the western edge of the model with the plume direction primarily being horizontal. After 1000 years of simulation, the contaminant plume covers all of the upper sand aquifer and most of the silt/sand aquitard due to diffusion and dispersion effects.
e) The (W-E) models with no precipitation from top boundary show a higher concentration associated with the contaminant plume as it occupies the entire upper sand aquifer and most of the silt/sand aquitard. This is because the contaminants were not diluted by the water from

precipitation as seen in the previous models. However, there is not much difference in the spatial extent of the contaminants for both models with or without the influence of precipitation.

f) The (W-E) models with double precipitation show the extent of the contamination which has occupied all of the upper sand aquifer and the silt/sand aquitard with most of the lower sand aquifer at a lower concentration of 100mg/L. The contaminant plume is heavily diluted due to the excess precipitation when compared to the models with regular or no precipitation. Thus, with double precipitation contaminants do reach the lower sand aquifer between 1000-10,000 years but with lower concentration differences.

Bibliography

Anderson, M.P. and Woessner, W.W. (1992). *Applied Groundwater Modeling*. San Diego, California, USA: Academic Press.

Benson, R.C., Turner, M., Turner, P. and Vogelsang, W. (1988). In situ, time-series measurements for long-term groundwater monitoring. In: Collins, A.G. and Johnson, A.I. (Eds.), Ground-Water Contamination: field methods, Philadelphia, USA, 58-77.

Chargaff, E. (1978). *Heraclitean Fire: Sketches from a life before Nature*. The Rockefeller University Press, New York, USA, 252.

Darr, R.E. (1979). Ground-Water computer models-practical tools. *Ground Water*, 17(2), 174-176.

Derham, J. (1995). The Engineering of (a sustainable) landfill. The Role of Groundwater in Sustainable Development, Proceedings of the *15th Annual Groundwater Seminar, Portlaoise, International Association of Hydrogeologists*, 9.

Faust, C.R. and Mercer, J.W. (1980). Ground-Water Modeling: Recent Developments. *Ground Water*, 18(6), 569-577.

Fetter, C.W. (1994). *Applied Hydrogeology*. 3rd Edition, Macmillan College Publishing Company, New York, USA.

Friedman, R., Ansell, C., Diamond, S. and Haimes, Y.Y. (1984). The use of models for water resources management, planning and policy. *Water Resources Research*, 20(7), 793-802.

Gray, D.A., Mather, J.D. and Harrison, I.B. (1974). Review of groundwater pollution from waste disposal sites in England and Wales, with provisional guidelines for future site selection. *Quarterly Journal of Engineering Geology and Hydrogeology*, 7(2), 181-196.

Hamilton, D.A. (1982). *Groundwater Modeling: Selection, Testing and Use*, Volume 1, Michigan Department of National Resources, 199.

Konikow, L.F. and Bredehoeft, J.D. (1978). Computer model of two dimensional solute transport and dispersion in groundwater. *Techniques of Water-Resources Investigations of the United States Geological Survey*, Book 7, Chapter C2.

McDonald, M.G. and Harbaugh, A.W. (1984). A Modular three dimension finite-difference groundwater flow model. *Techniques of Water Resources Investigations of the United States Geological Survey*, Book 6, Chapter A1.

Porter, R. (2002). The Economics of Waste, Resources of the Future, Washington, D.C., USA.

Prickett, T.A. and Lonnquist, C.G. (1973). Aquifer simulation model for use on disk supported small computer systems. *Department of Registration and Education*, 73(114), 1.

Thomas, H.E. and Leopold, L.B. (1964). Groundwater in North America. *Science*, 143, 1001-1006.

Trescott, P.C., Pinder, G.F. and Larson, S.P. (1976). Finite-difference model for aquifer simulation in two dimensions with results of numerical experiments. Techniques of Water-Resources Investigations of the United States Geological Survey, Book 7, Chapter C1, 116.

Wang, H.F. and Anderson, M.P. (1982). *Introduction to Ground-Water Modeling: Finite Difference and Finite Element Methods*, W.H. Freeman, 256.

Chapter IV

Summary and Future Work

4.1 Summary

This study focused on delineating areas of underground leachate distribution at the landfill using non-invasive geophysical methods and to predict the movement of these contaminants through layers over an extended period of time using groundwater modeling. The DualEM 2S/4S instrument was utilized to determine the terrain conductivity variation at the site. Results from the EM terrain conductivity mapping suggested that the western portion of the site has a higher conductivity reading compared to the eastern portion. This difference in conductivity could potentially be due to the operation of the leachate collector system situated on the southeastern corner of the site which may dilute the waste in the eastern half.

The western portion of the site was further examined with the DC resistivity method using a Wenner-α array with 5m electrode spacing. The idea behind this survey was to determine both the contaminant distribution at depth and the subsurface geology of the site. Based on the electrode separation, the DOI was calculated to be 30m which allowed us to visualize the clay cap, upper sand aquifer, silt/sand aquitard and the upper portion of the lower sand aquifer. Based on the DC resistivity results, the waste was buried in the upper sand aquifer with most profiles showing strong evidence of horizontal plume migration from the waste towards the south (for the S-N resistivity profiles) and towards the east (for the W-E resistivity profiles). This direction of flow agrees well with the natural groundwater flow regime in the upper aquifer at the site. Few DC resistivity profiles show a small vertical component to plume migration which enters the upper weathered portion of the silt/sand aquitard however, due to the low hydraulic conductivity of the aquitard the contaminants are confined to this region and no evidence has been found of the contaminants entering the lower sand aquifer within the landfill. The clay cap is not continuous in most of the resistivity profiles which allows more infiltration of water/snow melt in some areas than others. Overlying the clay cap is a thin layer of sand and gravel (higher apparent resistivity than clay) which protects the clay cap from the elements of weather and helps in increasing its life span however, once the sand and gravel layer is removed by runoff from heavy rain or snow melt, the clay cap is exposed and deteriorates over time thus increasing the possibility of leachate springs. A few resistivity profiles show the leachate extending up to the surface where there is little to no capping material.

Based on the results of the geophysical surveys, two conceptual models outlining all the layers were designed and the source of contaminants were strategically placed on three locations (depicting the S-N profiles) and one location (depicting the W-E profiles) in the groundwater modeling software FEFLOW. Simulations were run for regular fluid-flux, no fluid-flux and double fluid-flux from top boundary to mimic normal, dry and wet periods respectively. The simulations were run for 1, 10, 100, 1000 and for one (W-E) model even up to 10,000 years to predict the pathway taken by the contaminants in the layers.

All groundwater model simulations for both (S-N) and (W-E) profiles simulated to 1000 years showed the contaminants had occupied the entire upper sand aquifer and most of the silt/sand aquitard and the one (W-E) model simulated to 10,000 years showed a major part of the lower sand aquifer was contaminated as well. However, these models were considered where there is a continuous release of contaminants from the waste not taking into account the degradation of the waste material itself. Obviously, no waste material would be existent for 10,000 years and the material of the aquifers and aquitard would adsorb some of the contaminants over time but this simulation was the worst case scenario which could happen. Even though the simulations of models made some predictions relating to the contaminant extent in the aquifers/aquitard, lateral or vertical inhomogenities in flow or material properties of the aquifer and aquitard can either accelerate or reduce the pace of contaminant propagation in these layers. The accuracy of these simulations can be assessed over time by conducting field measurements from monitoring wells and calibrating the results obtained to that of the simulation.

4.2 Future Work

The following are the recommendations and future work for this study:

1) The terrain conductivity measurements were conducted in a (S-N) and (N-S) direction using the flip option on the instrument. To improve the accuracy and resolution at depth of the conductivity measurements (W-E) and (E-W) profiles should also be conducted. This will help eliminate measurement artifacts and will enhance resolution at greater depths.
2) Different EM conductivity interpretation software should be used instead of the ArcMap GIS based software. The ArcMap software does not have the capability to perform processing techniques such as removal of instrument noise or setting constraints to maximum or minimum conductivity measurement limits. Other interpretation software such as ‘Surfer Contouring’ should be tried.
3) The apparent resistivity of the western portion of the site should be remeasured with using either a greater electrode spacing (10m) or a different array altogether (e.g. Schlumberger or Dipole-Dipole). The 10m electrode separation will provide a greater depth of investigation which will allow us to visualize the entire lower sand aquifer and possibly the underlying lower silt/sand aquitard. The Schlumberger array rates highest in terms of signal response after the Wenner array and in the sounding method, the Schlumberger method provides the highest resolution for horizontally layered structures. Also the Wenner and Schlumberger arrays are less prone to electrode effects and near-surface inhomogenities. The Dipole-Dipole array is beneficial in

mapping steeply dipping targets and due to the separate connection of wires between the current and potential dipoles, the effect of EM conduction is reduced.

4) The area south of the landfill (near the McDonald Pit and Stockwell Pit) should be investigated by running both EM conductivity and DC resistivity profiles around the area. This will assist in mapping the functionality of the CAZ zone which was setup in 2004 to prevent any off-site impacts of the contaminants. The area northwest of the site should also be investigated for off-site impacts and the integrity of the clayey barrier which was setup in 1998 due to greenhouse construction activities should be routinely tested.
5) Besides geo-electrical surveys, other geophysical methods should be utilized such as the seismic refraction method. The seismic refraction method will not assist in outlining the waste or leachate distribution but it will give an accurate response to sub-surface geology far more reliable than the DC resistivity or EM conductivity methods. This information can then be incorporated in the groundwater modeling simulation to improve the accuracy and reliability of the simulation.
6) Chemical modeling of contaminants such as adsorption and decay rates should also be considered to improve the accuracy of the prediction in determining the extent of contaminants in the layers. A 3D conceptual model should be designed and other species such as boron (B) and chloro-vinyl (CH_2-CHCl) should be incorporated into the modeling procedure.

VITA AUCTORIS

Name: Siddharth Dilip Joshi

Place of Birth: Mumbai, India

Year of Birth: 1986

Education: High School, International School of Choueifat, Abu Dhabi, UAE
2005
University of Windsor, Windsor, Ontario
2010, B.Sc.
University of Windsor, Windsor, Ontario
2013, M.Sc.

PUBLICATION

Joshi, Siddharth Dilip[1], Yang, Jianwen[1], Sereres, Clayton[2] and Tamr, Radwan[2] (2013)."Geo-Electrical Investigation of Underground Leachate Distribution at a Closed Landfill in Southwestern Ontario, Canada" *GSA 2013 - Abstracts with Programs*, Vol.45(4), 25.